

ADRIANA PACIFICO

PH.D. THESIS

**SEISMIC RISK ASSESSMENT OF ITALY AT
DIFFERENT TIME-SPACE SCALES**

Tutor: Prof. Iunio Iervolino

Co-tutor: Prof. Eugenio Chioccarelli

TABLE OF CONTENTS

LIST OF TABLES	IX
Chapter 1 – INTRODUCTION.....	10
1.1 Objective of the thesis.....	10
1.2 Outline of the thesis	11
Chapter 2 – SEISMIC SAFETY OF BUILDINGS AND OTHER COMMON RISKS IN ITALY	14
2.1 . Introduction.....	14
2.2 . The seismic reliability of code-conforming structures in Italy	15
2.3 . SEISMIC FATALITY RATES.....	20
2.3.1 Method 1.....	21
2.3.2 Method 2.....	22
2.4 . Oterh risks in italy.....	23
2.5 . Discussion and final remarks	24
Chapter 3 – DESING PROGRESS AND SEISMIC SAFETY IMPROVEMENT IN ITALY.....	25
3.1 . Introduction.....	25
3.2 . Assessing the seismic reliability of code- and old-code-conforming Italian buildings.....	26
3.3 . Fatality rates evaluation	30
3.3.1 Method 1.....	30
3.3.2 Method 2.....	30
3.3.3 Method 3.....	31
3.4 Results and discussions.....	32
3.5 . Final remarks.....	34
3.6 Acknowledgements.....	34
Chapter 4 – SEISMIC RISK AT NATIONAL SCALE FOR CODE- CONFORMING STRUCTURES IN ITALY	35
4.1 . Introduction.....	35
4.2 . Fragility functions of code-conforming RINTC structures.....	37
4.2.1 Reinforced-Concrete Structures	38
4.2.2 Unreinforced Masonry Structures	40

4.2.3	Base-Isolated Structures.....	44
4.3	. Methodology for computation of failure rates	45
4.4	Input data for nationwide code-conforming risk assessment.....	47
4.4.1	Probabilistic Seismic Hazard Analyses Based on MPS04	47
4.4.2	Hazard Classes and Building Replacement Criteria.....	48
4.4.3	Local Soil Classes at a Municipality Scale	50
4.4.4	Alternative Hazard Models	52
4.5	Results and discussions.....	54
4.5.1	Seismic Risk for Fixed-Base Structures Based on MPS04 Hazard	54
4.5.2	Alternative risk metric.....	55
4.5.3	Seismic Risk for Base-Isolated Structures Based on MPS04..	56
4.5.4	Seismic Risk for Fixed-Base Structures Based on MPS19	58
4.5.5	Seismic Risk for Fixed-Base Structures Accounting for Mainshocks-Aftershocks Contribution to the Hazard	60
4.6	Conclusions.....	61
4.7	Data sources	62
Chapter 5 – OPERATIONAL EARTQUAKE LOSS ASSESSMENT ON EXISTING ASSETS		63
5.1	. Introduction.....	63
5.2	. MANTIS-K.....	64
5.3	. MANTIS V.2	67
5.3.1	Loss forecasting referring to already damaged buildings	67
5.3.2	Loss forecasting accounting for more than one earthquake	71
5.3.3	Inventory update.....	71
5.4	. Case Study	73
5.4.1	Input models.....	74
5.5	. Results.....	82
5.5.1	MANTIS-K	83
5.5.2	MANTIS v2.0	84
5.6	. Conclusions and discussion	87

Chapter 6 – SUMMARY AND CONCLUSIONS.....	89
APPENDIX A	91
APPENDIX B.....	94
APPENDIX C	102
REFERENCES	112

LIST OF FIGURES

Figure 1. Left: Italian map of the seismic peak ground acceleration (PGA) on rock, which is exceeded at any site on average every 475 years (used by the code).8 Right: PGA (rock) hazard curves for the three sites at which the structures are designed.....	18
Figure 2. Left: average seismic failure rates for the considered code-conforming buildings as resulting from the RINTC project. Right: annual seismic fatality rates, computed with the HAZUS- (HZ) and the Zuccaro-Cacace-based (EMS) methods, in comparison with other risks in Italy. (Vertical bars provide the range of rates for each typology.)	20
Figure 3. Arithmetic averages of the fatality rates as a function of the design epochs. (White markers indicated that design of S for the ‘80-‘90 epoch also apply to previous epochs.).....	33
Figure 4. Fatality rates as a function of the design epoch and site. (White markers indicated that design of S for the ‘80-‘90 epoch also apply to previous epochs.).....	33
Figure 5. RC6 buildings: bare-frame (left), infilled-frame (center); pilotis-frame (right). (Adapted from [1]).....	39
Figure 6. Fragility functions of (a) RC3 and (b) RC6.....	40
Figure 7. Plan view of the URM buildings. Figures from (a) to (f) represent the “C” configurations (1-5 and 7 respectively), while figures from (g) to (l) represent the “E” configurations (2, 5 8 and 9 respectively).....	41
Figure 8. Fragility functions of two storeys URM buildings (left column) of L'Aquila (top row), Naples (mid row), and Milan (bottom row) and of three storeys URM buildings of the same sites (right column).....	43
Figure 9. Fragility functions of BI buildings of (a) L’Aquila and (b) Naples.....	45
Figure 10. (a) PGA hazard curves computed via PSHA for all the Italian municipalities adopting MPS04, (b) map of PGA_{475} together with the thirty-six seismic zones of [9], (c) hazard classification according to PGA_{475} of each municipality.	48

Figure 11. Probability of each structural typology per municipality.....	50
Figure 12. Soil class probabilities in the urbanized areas of Italian municipalities.	51
Figure 13. (a) Hazard classification of the Italian municipalities according to MPS19; (b) <i>PGA</i> hazard curves computed via PSHA adopting MPS19.	53
Figure 14. (a) Hazard curves of the three considered sites in term of $Sa(0.15s)$ and $Sa(0.5s)$ evaluated with PSHA (continuous lines) or SPSHA (dashed lines); (b) hazard increments due to SPSHA with respect to PSHA.	54
Figure 15. Maps of failure rates per municipalities considering (a) UPD and (b) GC evaluated adopting MPS04 and considering FB structures; (c) map of the ratios of the failure rates evaluated for UPD and GC.....	55
Figure 16. Maps of the expected number of failed buildings in one year per municipality considering (a) UPD and (b) GC.....	56
Figure 17. Maps of failure rates per municipalities considering (a) UPD and (b) GC evaluated adopting MPS04 source model and considering BI structures.	57
Figure 18. Ratio of the failure rates computed for BI and FB structures: (a) UPD, and (b) GC.....	58
Figure 19. Maps of failure rates per municipalities considering (a) UPD and (b) GC evaluated adopting MPS19 source model; map of the ratios of the failure rates computed according to MPS19 and MPS04: (c) UPD and (d) GC.....	59
Figure 20. Ratio of the failure rates computed via SPSHA and PSHA: (a) UPD and (b) GC.....	60
Figure 21. Map of considered municipalities grouped for the increasing distance from the mainshock; the stars represent the epicenters of the earthquakes of Table 7.	74
Figure 22. OEF-Italy weekly rate release from 05/04/09 to 10/04/09.....	76
Figure 23. Composition of the building stock according to the construction material.....	78

Figure 24. Soil probabilities in the municipalities within 100km from L’Aquila 2009 mainshock.80

Figure 25. ShakeMap, in term of PGA , $Sa(0.3s)$ and $Sa(1s)$, of the mainshock of 2009 L’Aquila sequence in the area around the epicenter, on the left; evaluated $E\left[Sa_{avg}(\mathbf{T})|Sa_{avg}(\mathbf{T}^*),m^*,r^*,\theta\right]$ for the urbanized areas, on the right.82

Figure 26. Outcomes of MANTIS-K system applied to 2009 L’Aquila seismic sequence.84

Figure 27. Outcomes of MANTIS v2.0 system applied to 2009 L’Aquila seismic sequence.85

Figure 28. Building portfolio damage state at the days of prevision.87

Figure 29. Example of capacity curve and definition of PLs . The subscripts y , c , p and u denote, in turn, the yielding-point, the capping-point, the residual-point and the ultimate-capacity-point.....94

Figure 30. MANTIS K percentage of buildings expected to remain pl_1 in the week follow the day of forecast per municipality.102

Figure 31. MANTIS-K percentage of buildings expected to reach pl_2 in the week follow the day of forecast per municipality.103

Figure 32. MANTIS K percentage of buildings expected to reach pl_3 in the week follow the day of forecast per municipality.104

Figure 33. MANTIS K percentage of buildings expected to reach pl_4 in the week follow the day of forecast per municipality.105

Figure 34. MANTIS K percentage of buildings expected to reach pl_5 in the week follow the day of forecast per municipality.106

Figure 35. MANTIS V2.0 percentage of buildings expected to remain pl_1 in the week follow the day of forecast per municipality.107

Figure 36. MANTIS V2.0 percentage of buildings expected to reach pl_2 in the week follow the day of forecast per municipality.108

Figure 37. MANTIS V2.0 percentage of buildings expected to reach pl_3 in the week follow the day of forecast per municipality. 109

Figure 38. MANTIS V2.0 percentage of buildings expected to reach pl_4 in the week follow the day of forecast per municipality. 110

Figure 39. MANTIS V2.0 percentage of buildings expected to reach pl_5 in the week follow the day of forecast per municipality. 111

LIST OF TABLES

Table 1. Structures for which seismic structural reliability has been evaluated in the RINTC project.....	17
Table 2. Summary of the analyzed structures per site, structural typology and design epochs.	28
Table 3. Fatality probabilities from HAZUS and association with RINTC-e structures.	31
Table 4. Parameters of RC fragility functions (IM in g).....	39
Table 5. Parameters of URM fragility functions (IM in g).	42
Table 6. Parameters of BI fragility functions (IM in g).	44
Table 7. Earthquakes with moment magnitude larger than 4.5 identified by a progressive number (ID), latitude and longitude, in degree, and M	73
Table 8. Parameters of building-classes capacity curves.	95
Table 9. Parameters of fragility functions.	96
Table 10. Parameters of state-dependent fragility functions.	98

Chapter 1 –INTRODUCTION

1.1 OBJECTIVE OF THE THESIS

Started in 2015, the *Rischio Implicito delle strutture progettate secondo NTC* project, hereafter RINTC project [1], aims to assess the seismic risk of structures ideally located in different Italian sites. In the first three years, the project focused on the study of structures designed following the prescription of the codes currently in force in Italy, i.e., *Norme Tecniche per le Costruzioni del 2008* [2] and its 2018 updating [3]. One of the main results of the project was that the implicitly accepted risk in the design is not uniform on the national territory regardless of the structure and site considered, although the design adopts seismic actions characterized by the same return period. It has been observed that the seismic risk, evaluated in terms of the failure rate of the structures, i.e. the mean annual number of earthquakes (mainshocks) that cause structural failure, is strictly dependent on the construction site, and in particular tends to grow with the hazard of the site [4,5]. Two main reasons can explain this phenomenon: the first concerns the minimum low limits which must be respected in the design and which cause oversizing of the structures in low seismicity sites; the second concerns a phenomenon whereby the earthquakes expected beyond the project intensity relative to 475 years are proportionally larger in sites with high seismicity (see [6] for details).

The thesis also discusses the assessment of seismic risk at a different time scale. The calculation of the seismic risk can refer to a shorter time window than the year taking into account information updated in real time. This requires that the geographic region of interest is monitored by a network of accelerometers whose data can be analyzed in almost-real time. Basing on the Italian Operational Earthquake Forecasting system, OEF-Italy [7], an Italian Operational Earthquake Loss forecasting (OELF) system, called MANTIS-K [8], has been developed. It provides the risk forecast in terms of expected losses in a short period, due to a seismic event. Losses are evaluated as the expected number of damaged buildings, deaths or injuries.

OEF-Italy provides, at least every day, the rate of earthquakes expected in the following week for a dense grid of point, treated as point seismic sources, covering the entire national territory. From these rates it is possible to derive the short-term hazard for a generic site of interest. OEF-Italy releases new rates

after each earthquake of a magnitude greater than or equal to 3.5 recorded, too. For each new OEF-Italy release, MANTIS-K provides the loss forecast. By integrating information on short-term hazard, vulnerability of the building stock and exposure, MANTIS-K provides an estimate of the expected losses in the week following the forecast.

1.2 OUTLINE OF THE THESIS

The objective of **Chapter 2** is to quantify the seismic risk in terms of fatality rates, i.e., to pass from the mean number of earthquakes that cause the structural failure of code conforming buildings (that come from RINTC project) to the mean number of seismic events in one year cause the death of an individual due to structural failure. This risk index has two advantages: it summarizes information on the different performance levels of the building and can be compared with the risk that the same individual has of dying from other causes, natural or not (e.g., diseases or road accidents). Although this evaluation is subject to assumptions and hypotheses, this comparison has shown that even in the most dangerous sites, the death rates are (on average) lower than the probabilities of death due to the other causes analyzed.

In **Chapter 3**, it is acknowledged that, since design codes of the design hazard have had a relatively continuous evolution, following the international development of earthquake engineering, most of the existing building stock, mainly composed of reinforced concrete or unreinforced masonry buildings, is very slowly renovated, so that these structures are designed with now obsolete or without any seismic provision. Considering that codes, even those at the state-of-the art, do not explicitly control the reliability implied by design, the safety achieved by the progress in seismic design has not been quantified systematically. This is the scope of this chapter that, resorting from the results of a large research project, quantified the seismic safety, by means of fatality rates computed according to three different methods, following the changes in codes in Italy. Although highly conventional and mainly useful for relative comparisons, the results clearly show the improvement of safety achieved by evolving seismic design, with the largest increment attributable to the current code, which is based on the same principles as Eurocode 8.

Chapter 4 still deals with the results of the RINTC project on the code-conforming structures. In fact, as mentioned, RINTC chose for the risk

assessment few sites, differ for the seismic hazard level; these results were extended to the whole country and ideal risk maps were produced, i.e., maps showing the risk to which structures in Italy would be subject if all existing residential buildings were replaced by buildings compliant with NTC. Furthermore, this work was repeated for different hazard models: (i) the one adopted in the definition of the designed seismic hazard in the NTC, i.e., the so-called MPS04 [9]; (ii) the new developed seismic hazard model for Italy, MPS19 [10]; (iii) a hazard model that takes into account the occurrence of seismic sequences (i.e., the possibility that the structural failure is due not to the main shock but to one of the following ones [11]). The results confirm the RINTC ones, i.e., the non-homogeneity of the seismic risk in the country and show that the MPS19 and MPS04 models provide results in the same order of magnitude; finally, if the occurrence of the seismic sequences is considered in the hazard assessment, the seismic risk it increases up to 80%.

In **Chapter 5**, deals with the development of an updated version of MANTIS-K, called MANTIS V.2, currently under development within the Real-time earthquake rIsk reduction for a ReSilient Europe project, called RISE. The main limitation of the currently available system is that the possibility of observing cumulative damage on structures is neglected. Especially in a seismic sequence, it is possible that an aftershock finds a structure already damaged by the mainshock or one of the previous shocks. The response of the already damaged structure should be different from what it would have had if it had been intact. It can be taken into account using the so-called state-dependent frailties as demonstrated in [12]. The methodology illustrated in [12] to consider the accumulation of damage on a single structure was extended to building classes and implemented in the new version of the forecasting system. The building classes considered are those of the European SERA project (Seismology and Earthquake Engineering Research Infrastructure Alliance for Europe, [13]) and the state-dependent fragilities were developed by [14] within the RISE project. MANTIS V.2 is able to update the damage status of the building stock after each recorded shock, in such a way as to have a forecast of the expected losses in the following week that does not neglect the possibility of observing the accumulation of damage on the buildings. This methodology was applied to a case study. In particular, the 2009 L'Aquila sequence was chosen. The same sequence was also analyzed with the MANTIS-K system in order to compare the estimate of expected losses, in terms of expected number of damaged

buildings, considering or not the accumulation of damage. The results show that not updating the state of damage to the building stock leads to an underestimation of losses, especially in the shocks follow the main one. In particular, in the considered sequence, the mainshock was preceded by minor events so the predictions of MANTIS-K and MANTIS V.2 before the main shock are not dissimilar. However, MANTIS-K assumes that buildings are undamaged when hit by aftershocks leading to a lower loss forecast than that of MANTIS V.2.

Chapter 2 – SEISMIC SAFETY OF BUILDINGS AND OTHER COMMON RISKS IN ITALY

The following paper have been derived from this Chapter:

- Iervolino I. and Pacifico A. (2021) *How seismically safe is safe enough? Earthquake Engineering and Structural Dynamics* 50(11): 3083-3089. DOI: 10.1002/eqe.3472.

2.1. INTRODUCTION

The Italian building code[15] is based on *capacity design* and has design seismic actions determined via *probabilistic seismic hazard analysis* (PSHA).[16] It has its roots in Eurocode 8[17] (EC8) and can be generally considered to be of state-of-the-art level, even if it does not entail quantification of the reliability implied by design, whose absence is commonplace in modern seismic codes.¹

An extensive research program in Italy, *Rischio Implicito – Norme Tecniche per le Costruzioni* or RINTC [5] (2015-2017) evaluated the seismic structural reliability of several code-conforming, residential and industrial, buildings located at three sites that can be considered as representative of low-, mid- and high-hazard in Italy. Hundreds of buildings from these typologies, with various configurations, were designed, modelled and analyzed. The seismic reliability metric adopted is the expected number of earthquakes that, in one year, cause a certain seismic performance that identifies failure; i.e., the *failure rate*. Two performances were considered, they are related to impeded usability and life-threatening failure. The computation of the failure rates followed the *performance-based earthquake engineering* (PBEE) paradigm[18], that entails integrating the structural *fragility* with the site's *hazard curves*.

The most relevant result of the project was that the reliability systematically tends to decrease as the hazard of the site can be considered more severe [5]. Further research attributed that to the effect of code-prescribed minima and gravity-load design in low-, and possibly mid-hazard sites, as well as the impact on the reliability of ground motions with return periods larger than those considered in design [19]. This may spark concerns, as the law rationally postulates homogeneous safety, measured – for example – via *fatality rates*, for

¹ An advancement to this approach is the so-called risk-targeted design, which, however, yet has to find its way in building codes.

similar buildings designed across the country. On the other hand, it may be argued that even spatially variable safety is still acceptable if compared to other risks. To contribute to this debate, in the simple study presented in the following, the fatality risk caused by the structural failure of code-conforming buildings is computed in a simplified manner and compared to other risks that building residents may be exposed to; e.g., some diseases or fatal accidents. Because the assessment of the fatality risk for code-conforming buildings requires significant working assumptions and a degree of conventionality, the rates were computed following two alternative approaches. To evaluate the other risks for the comparison, the death rates due to common causes were derived from national and local data of the *Istituto Nazionale di Statistica* (ISTAT).

The remainder of this note is structured so that in the next section the RINTC project is briefly recalled, followed by a description of the approaches adopted to evaluate the fatality rates. Subsequently, the risk related to some other death causes in Italy is computed and compared to the seismic fatality risk. Some conclusions end the short paper.

2.2. THE SEISMIC RELIABILITY OF CODE-CONFORMING STRUCTURES IN ITALY

As anticipated, a large set of buildings was designed according to the Italian current building code, modelled and analyzed to evaluate their seismic reliability. In particular, five structural typologies were considered so as to represent as much as possible residential and industrial standard modern Italian constructions. As these structures were extensively discussed in dedicated literature [20], here a brief summary is only given:

- unreinforced masonry structures (URM) – residential buildings of two- and three-story made of perforated clay units with mortar joints varying for the architectural configurations and wall thickness, either regular or irregular according to the definition provided by the code [21,22];
- reinforced concrete (RC) – three-, six-, and nine-story moment resisting frame buildings (MRF), regular in plan and elevation, with different configuration (bare-frame or BF, infilled-frame or IF, and pilotis-frame or PF) with or without shear walls (SW) [23];
- steel (S) – one story rectangular industrial buildings featuring moment resisting frames in the transverse direction and concentrically braced

frames placed in the outer spans of the frame in the longitudinal direction; four different configurations were considered varying, transverse and longitudinal bay widths [24];

- precast reinforced concrete (PRC) – single-story industrial buildings that have precast columns fixed at the base and connected, at the top, to longitudinal precast prestressed beams through dowel connections; four different configurations were considered varying transverse and longitudinal bay widths and the story height [25];
- base-isolated reinforced-concrete buildings (BI) – six-story infilled moment resisting frame building isolated considering three isolation systems, that is, double-curvature friction pendulums (FPS), high-damping rubber bearings (HDRB), and an hybrid system made of HDRB's and sliders (SLDR) [23,26].

These structures were designed in three Italian sites characterized by low-, mid- and high-hazard, that is at Milan (MI), Naples (NA) and L'Aquila (AQ), respectively (Figure 1, left) and for two different soil site conditions (i.e., A and soil C according to the EC8 classification).²

Design referred to code's *damage* and *life-safety* limit states, which correspond to ground motion intensity with 50 and 475 yr exceedance return period (Tr), respectively; Table 1, summarizes the structures analyzed.³

The seismic reliability of these structures was assessed considering the two performances levels, or damage states, defined in the project: usability-preventing damage (UPD) and global collapse (GC). The onset of UPD is based on a multi-criteria approach; if one of following conditions occurs the structure is considered failed: (i) light damage in 50% of the main non-structural elements (e.g., infills); (ii) at least one of the nonstructural elements reached a severe damage level; (c) first attainment of 95% of the maximum base-shear of the structure. The GC criterion is based on the deformation capacity (the roof displacement or the inter-story drift ratio) corresponding to 50% strength decay from the nonlinear static capacity curves of the structural model.

² The Italian code allows design URM of buildings even in high seismicity areas; however, simplified design methods for URM cannot be used for buildings with the number of story larger than three when the PGA with 475 yr return period is larger than 0.35g.

³ For some RC structures soil-structure-interaction (SSI) and model uncertainty (MU) was also considered, although it was found that both have a relatively minor impact on the reliability.

Table 1. Structures for which seismic structural reliability has been evaluated in the RINTC project.

	AQ – soil A	AQ – soil C	NA – soil A	NA – soil C	MI – soil A	MI C – soil C
URM 2-st.	4 – Configs.	6 – Configs.	3 – Configs.	4 – Configs.	4 – Configs.	3 – Configs.
URM 3-st.	3 – Configs.	-	4 – Configs.	6 – Configs.	4 – Configs.	4 – Configs.
RC 3-st. MRF	-	IF, BF, PF.	-	IF, BF, PF	-	IF, BF, PF.
RC 6-st. MRF	-	IF, BF, PF.	-	IF, BF, PF, IF-MU, BF-MU, PF-MU.	-	IF, BF, PF.
RC 9-st. MRF	IF, BF, PF.	-	-	IF, BF, PF.	-	IF, BF, PF
RC 9-st. SW	IF-SSI, BF-SSI, PF-SSI.	IF, BF, PF.	IF, BF, PF.	IF, BF, PF.	-	IF, BF, PF.
S	4 – Configs.	4 – Configs.	4 – Configs.	4 – Configs.	4 – Configs.	4 – Configs.
S w/ cladding	4 – Configs.	4 – Configs.	4 – Configs.	4 – Configs.	4 – Configs.	4 – Configs.
PRC	4 – Configs.	4 – Configs.	4 – Configs.	4 – Configs.	4 – Configs.	4 – Configs.
BI	-	HRDB, FPS, HDRB+SL DRS.	-	HRDB, FPS, HDRB+SL DRS	-	-

The seismic structural reliability was quantified via the failure rate, $\lambda_{f,DS}$, computed as:

$$\lambda_{f,DS} = \nu \cdot \int_{-\infty}^{+\infty} P[F_{DS} | IM = x] \cdot f_{IM}(x) \cdot dx. \quad (1)$$

where, $P[F_{DS} | IM = x]$ is the probability of failure corresponding to a certain damage state (DS), when $DS \equiv GC$ or $DS \equiv UPD$, given the value of a (non-negative) ground motion intensity measure (IM), that is, the seismic fragility of the structure; ν is the rate of earthquakes, above a minimum magnitude of

interest, affecting the construction site; $f_{IM}(x)$ is the probability density function of the IM at the site, given the occurrence of an earthquake among those the ν rate refers to. It is useful for the following to acknowledge that the integral in Eq. (1) is just the failure probability (i.e., reaching or exceeding the damage state DS), given an earthquake among those the ν rate refers to. Indicating such a probability as $P[F_{DS}|E]$, the equation can be written as $\lambda_{f,DS} = \nu \cdot P[F_{DS}|E]$. It is also noted that the product $\nu \cdot f_{IM}(x)$ is the absolute value of the derivative – multiplied by $d(im)$ – of the hazard curve for the site, computed via PSHA. The hazard curve provides, for any value of IM , say x , its annual rate of exceedance, $\lambda_{IM}(x)$ [27].

The seismic response of the structures was computed via *multi-stripe* nonlinear dynamic analyses or MSA [28] on three-dimensional nonlinear structural models. To this aim, the chosen IM was the pseudo spectral acceleration (with five percent viscous damping) at a vibration period close to the one fundamental of each structure; in fact the following periods, T , were considered: $T = \{0.15s, 0.50s, 1.00s, 1.50s, 2.00s, 3.00s\}$. The IM domain was discretized considering IM values taken from the hazard curve for the site at which the structure is designed; in fact, the IM values corresponding to ten exceedance return periods (from 10^1 to 10^5 years) were considered; i.e., 10, 50, 100, 250, 500, 1000, 2500, 5000, 10000 and 100000 years. Twenty (two-components) records for each IM level were selected according to the *conditional spectrum method* [29] as an input for MSA.

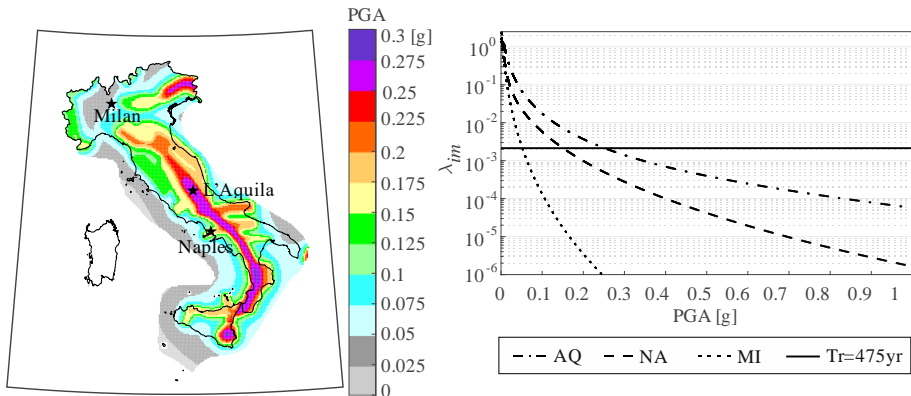


Figure 1. Left: Italian map of the seismic peak ground acceleration (PGA) on rock, which is exceeded at any site on average every 475 years (used by the

code).8 Right: PGA (rock) hazard curves for the three sites at which the structures are designed.

In the RINTC project the failure rates were computed with the fragility evaluated by means of the Shome & Cornell approach [30], and discretizing the integral in Eq. (1) at the IM values at which MSA was performed. Because the integral was truncated at the IM with 10^5 years return period, 10^{-5} was conservatively added to the rate from the integration, see [5] for a discussion on this issue. However, for the sake of the study herein presented (i.e., to improve with respect to the described integration procedure), the failure rates were re-computed. In fact, for each structure, a lognormal fragility functions were fitted to the MSA results from the project via the R2R-EU [31] software. Consequently, also the probabilistic seismic hazard had to be recalculated ad hoc. Thus, the hazard curves, for the three sites were computed using the REASSES software[32] implementing the branch 921 of hazard model that was used to build the official Italian hazard map [33] (i.e., that shown in Figure 1).

The resulting failure rates are given in Figure 2 (left) for both the considered performances. For representation purposes, for each typology, the rates are shown in terms of average taken across the failure rates of the analyzed buildings belonging to that typology. (In the figure, rates below 10^{-5} were set equal to 10^{-5} , as low failure rates are based on significant extrapolation of seismic hazard models.) One can see from the figure that the rates tend to decrease with the decreasing hazard for the site. The reason is twofold: first, the code-prescribed minimum design requirements and gravity-load design tend to dominate in low- and possibly mid- hazard sites (i.e., Milan and Naples) ensuring larger seismic reliability in comparison to the design for L'Aquila. The second reason is that the structures were designed against seismic actions with maximum return period of exceedance equal to 475 yr. However, it has been established that ground motions intensity beyond 475 years is disproportionately larger at L'Aquila with respect to Naples and Milan; i.e., the so-called *peak-over-threshold* [6] that can lead to lower seismic reliability in the high-hazard site. This can be seen in in Figure 1 (right), where the PGA (on rock) hazard curves show a significant difference in shape for return periods beyond 475 years.

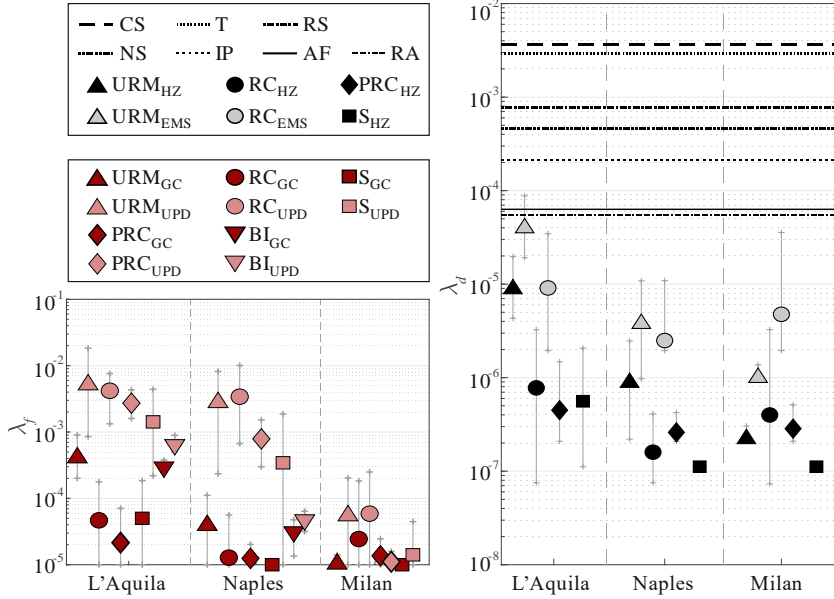


Figure 2. Left: average seismic failure rates for the considered code-conforming buildings as resulting from the RINTC project. Right: annual seismic fatality rates, computed with the HAZUS- (HZ) and the Zuccaro-Cacace-based (EMS) methods, in comparison with other risks in Italy. (Vertical bars provide the range of rates for each typology.)

2.3. SEISMIC FATALITY RATES

The fatality rates, λ_d , for the structures discussed above, can be interpreted as the expected number of earthquakes (above the minimum magnitude of interest) to cause fatality, and can be seen as the product of the probability of dying given the occurrence of the seismic event, $P[D|E]$, and the rate of earthquake occurrence at the construction site. Applying the total probability theorem, the fatality rate can be computed as:

$$\begin{aligned}
 \lambda_d &= \nu \cdot P[D|E] = \nu \cdot \sum_{i=1}^n P[D|DS_i] \cdot P[DS_i|E] = \\
 &= \nu \cdot \sum_{i=1}^n P[D|DS_i] \cdot \left(P[F_{DS_i}|E] - P[F_{DS_{i+1}}|E] \right) = \\
 &= \sum_{i=1}^n P[D|DS_i] \cdot \left(\nu \cdot P[F_{DS_i}|E] - \nu \cdot P[F_{DS_{i+1}}|E] \right) = \\
 &= \sum_{i=1}^n P[D|DS_i] \cdot \left(\lambda_{f,DS_i} - \lambda_{f,DS_{i+1}} \right)
 \end{aligned} \tag{2}$$

where n is the number of the considered damage states, $P[D|DS_i]$ is the probability of death given the reaching of the i -th damage state, and $P[DS_i|E]$ is the probability that the structure is in the i -th DS given earthquake occurrence, which can be computed as the difference of the failure probability related to the DS_i and DS_{i+1} states. The last equality in Eq. (2) shows what the computation is reduced to, by only considering the UPD and GC damage states and with $P[D|DS]$ left to be determined. Herein, $P[D|DS]$ has been calculated following two alternative methods.

2.3.1 Method 1

The first method is based on Tsang & Wenzel.[34] In this approach, $P[D|DS]$ are taken equal to the fatality rates given structural damage obtained from HAZUS.[35] In particular, $P[D|GC]$ is computed considering that GC corresponds to *complete structural damage* (CSD), according to the HAZUS terminology, and distinguishing between *indoor* (in) or *outdoor* (out) probability of death:

$$P[D|GC] = P[D|GC, indoor] \cdot P[indoor|GC] + P[D|GC, outdoor] \cdot \{1 - P[indoor|GC]\} \quad (3)$$

In the equation $P[indoor|GC]$ the probability of being indoor at the time of failure, and it is assumed to be equal to 0.9. The probability of death being indoor, is computer further splitting in the fact that GC leads to *collapse*⁴ or not:

$$P[D|GC, indoor] = P[D|GC, indoor, collapse] \cdot P[collapse|GC] + P[D|GC, indoor, nocollapse] \cdot \{1 - P[collapse|GC]\} \quad (4)$$

$P[collapse|GC]$ and $P[D|GC, outdoor]$ are taken from HAZUS, which provides these probabilities as function of the structural typology. (In fact, the

⁴ Note that the collapse as per the HAZUS terminology does not coincide with the *global collapse* according to the RINTC project.

fatality rates for the BI could not be computed because this typology is not covered in terms of required fatality model.)

HAZUS considers fatality for different injury severity levels; herein, *severity 3*, that is injuries that pose an immediate life-threatening condition if not treated adequately and expeditiously and *severity 4*, that is *instantaneously killed or mortal injure*, were considered. Therefore:

$$P[D|GC,indoor,collapse] = P[severity3|GC,indoor,collapse] + P[severity4|GC,indoor,collapse] \quad (5)$$

The same applies for $P[D|GC,in,nocollapse]$ and $P[D|GC,out]$. Finally, for $P[D|UPD]$, the same approach is followed, with UPD corresponding to moderate structural damage in HAZUS; in this case $P[collapse|UPD]=0$.

2.3.2 Method 2

The other method used to compute the fatality risk is based on the work of Zuccaro & Cacace [36] as adopted by Iervolino et al. [8] in the context of *operational earthquake loss forecasting*. In this model, the casualty probability given a DS is provided based on the vulnerability class the building is assigned to in accordance with the *European Macroseismic Scale* [37] (EMS). In this context, vulnerability class C and D were assigned to the URM and RC buildings, respectively. Moreover, it is also needed to associate the UPD and GC performances to those from EMS; in this case UPD was associated to DS3 and GC to DS5. (Because no industrial buildings or base-isolated structures are considered by EMS, it was not possible to apply this approach to STEEL, PRC and BI structures.) Because, according to this model, zero fatality probability is associated with damage levels equal to or lower than DS3, Eq. (2) can be further simplified as:

$$\lambda_d = P[D|GC] \cdot \lambda_{f,GC} \quad (6)$$

where $P[D|GC]$ can be expressed by Eq. (3) assuming $P[in|GC]=0.65$ and $P[D|GC,out]=0$.

The fatality rates computed with these two methods are interpreted herein as about equal to the annual probability of an individual continuously exposed to failure of a building of a given typology at a specific site.⁵

2.4. OTHER RISKS IN ITALY

For comparison, the annual fatality rates associated with different causes of death in Italy were also computed. To this aim, ISTAT data related to the 2012-2016 period were retrieved analyzed. The considered death causes are:

- (IP) infectious and parasitic diseases (tuberculosis, HIV, viral hepatitis, others);
- (T) tumors;
- (NS) diseases of the nervous system and sense organs (Parkinson's disease, Alzheimer's disease, others);
- (CS) diseases of the circulatory system (ischemic heart diseases, cerebrovascular diseases, others);
- (RS) diseases of the respiratory system (flu, pneumonia, chronic diseases of the lower respiratory tract, others);
- (AF) accidental falls;
- (RA) road accidents (in which car occupants or pedestrians died).

The fatality rates were obtained by dividing the number of deaths in Italy⁶ for a specific cause and year by the size of the resident population on January 1st of the year in question. Because the results among the considered years of analysis vary only mildly, only those referring to 2016 are considered in the following. These rates can be interpreted as the annual probability that a random member of the population dies for the considered cause.

The comparison of the seismic safety and the risk due to other causes is given in Figure 2 (right). In the figure, the seismic fatality rates provided are simply the arithmetic averages for the considered buildings, without any relative weighting of the various configurations and possible occupancies. The comparison is carried out in the hypothesis that a generic (random) individual is continuously exposed to the causes of death the lines refer to in the very same

⁵ The legitimacy of such an assumption depends on the way the conditional probabilities are formulated and computed in the two methods considered and could benefit from a refined modelling of individual exposure to building failure.

⁶ In fact, the analysis was also carried out at a local scale referring to the provinces of Milan, Naples, and L'Aquila, but the results were similar to those at the national level.

way the same individual is continuously exposed to the seismic risk, measured by the seismic fatality rate for the (code-conforming) building typology corresponding to a specific mark. Although this may be considered simplified and conventional, it can be argued that the seismic risk is generally lower than the other considered risks. This holds even if the fatality rates for the URM buildings at L'Aquila from the Zuccaro & Cacace approach, which provides larger rates than those based on Tsang & Wenzel, are comparable to the lowest rates from the other considered causes.

2.5. DISCUSSION AND FINAL REMARKS

This study compared the seismic safety of Italian code-conforming buildings at three different sites, by transforming the failure rates into fatality rates according to two different methods. Because computed fatality rates depend on the two performance levels for which reliability was available, the evaluation of the fatality rates must be considered simplified, if not conventional, and subject to the working assumptions; nevertheless, it could be of interest, given the bulk of the results from the RINTC project, about the reliability assessment of code conforming structures. Moreover, the Italian code has large similarities with the Eurocode 8 and can be considered of state-of-the-art level. The results show that the seismic structural safety of buildings tends to decrease as the seismic hazard for the site increases. Therefore, the seismic risk tends not to be uniform across the country.

This is a consequence of the minimum design requirements dominating at the low- and mid-hazard sites, as well as the fact that the ground motion with intensity larger than that considered in design is disproportionately larger at the most hazardous sites with respect to mid- and low- hazard sites. Nevertheless, the rough comparison with the fatality rates for some common causes building occupants are also exposed to, shows that the seismic risk tends to be – for the most of cases – lower than the others, even at the most seismically hazardous sites considered.

Although the comparison between fatality risk due to structural failure and those health-related requires must be done carefully, these results may contribute to the discussion on whether the seismic safety achieved by current standards can be considered acceptable and on the vision of the future of seismic codes, which is going towards risk-targeted design.

Chapter 3 – DESIGN PROGRESS AND SEISMIC SAFETY IMPROVEMENT IN ITALY

3.1. INTRODUCTION

The story of Italy is strewn with strong earthquakes that led, since the beginning of the XX century, to the continuous evolution of regulatory seismic design codes. The landmarking event was the 1908 Messina earthquake (magnitude, M , 7.1) which is estimated killed, in conjunction with a tsunami, some tens of thousands of people. The Italian seismic building code released in 1909 contained provisions about building height to be enforced in the areas hit by the earthquake. (In fact, the seismic classification of the territory, a prodromic design hazard assessment of the country, has been based – for a large part of the last century – on requiring seismic design only in the areas where recent earthquakes occurred.) The introduction of a design base shear was after the 1915 Avezzano earthquake (M 7). Another major step was the 1975 introduction of the response spectrum concept, and the related dynamic analysis as an alternative to the static one. In 1996, the limit state design and some indications to improve local and global ductility were introduced. A paradigm change occurred in 2003, after the S. Giuliano di Puglia earthquake (M 5.7), which caused the partial collapse of a school killing twenty-seven children and their teacher, causing a major societal concern. The seismic code then introduced followed the Eurocode 8 approach [38]. For the first time, the design hazard for the whole country, excepted Sardinia region, was based on the value of the peak ground acceleration (PGA), on stiff soil, with an exceedance return period of 475 years, evaluated by means of probabilistic seismic hazard analysis [16]. Most importantly the code was explicitly referring to capacity design principles and the behavior factor. Nevertheless, the 1996 code was still applicable and it required the 2008 L'Aquila earthquake (M 6.3) for the definitive enforcement of performance-based design criteria. This code, hereafter referred to as NTC, had a revision in 2018, yet without changing its main principles, and it is the one currently enforced. Many other steps, some also not necessarily representing progress, characterized the seismic design evolution in Italy and the interested reader can find details in a specific study and references therein, for a more comprehensive review [39].

The Italian building stock is mostly made of unreinforced masonry and reinforced concrete buildings, with the latter built in the post-World-War-II

period and the former being mostly older than that. Therefore, only a minority of the building heritage reflects current seismic design technology. This, in conjunction with a relatively high seismic hazard throughout the country, let Italy be considered one of the most exposed nations to seismic risk in Europe. On the other hand, none of the enforced codes, including the current one, generally enables the designer to explicitly control the seismic reliability implied by design. Therefore, a government funded large Italian research program *Rischio Implicito – Norme Tecniche per le Costruzioni esistenti* or RINTC-e [40].

This project followed one following especially on the current code, and named hereafter RINTC-n [5], the results of which enabled to compute, although in a highly conventional manner, the seismic fatality rates implied by state-of-the-art seismic design, as a measure of seismic safety achieved [41]. Among other results, it was found that for current-code-conforming structures, even if the design ground motion intensity has the same return period of exceedance at all sites in Italy, the resulting fatality rates tend to increase when the hazard of the construction also site increases. This is possibly due to: (i) the oversizing effects of the code-prescribed minima (including gravity-load design in low-to-moderate hazard regions), and (ii) the ground motion intensity with return periods larger than that considered in design, which tends to increase disproportionately at the high-hazard sites with respect to mid- and low-hazard sites [19].

The objective of the study herein presented is to measure the eventual improvement of seismic structural safety due to changes in design codes in Italy, via the results of the RINTC-e project. To this aim, the remainder of the paper is structured such that in the following section RINTC-e project and its results are briefly described. Then, the conventional methodology to compute the fatality rates is illustrated. Finally, the fatality rates are mapped with respect to the design technology progress and compared with those referring to current design. Some final remarks close the paper.

3.2. ASSESSING THE SEISMIC RELIABILITY OF CODE- AND OLD-CODE-CONFORMING ITALIAN BUILDINGS

RINTC projects considered five structural typologies: unreinforced masonry buildings, URM; reinforced concrete buildings, RC; precast reinforced concrete buildings, PRC; steel buildings, S; and base-isolated reinforced

concrete buildings, BI (not considered in this work) as described in the following. Because the RINTC-n structures were already described in other references [41], the following mainly refers to the RINTC-e project, being the core of this study. The analyzed structures are supposedly located in five Italian sites: L'Aquila (AQ), Catania (CT), Naples (NA), Rome (RM), and Milan (MI), in decreasing order of hazard as evaluated today and in previous assessment during the last century.

Four main design epochs were identified for URM residential buildings (or seismically upgraded) years: Pre-'20, '20-'45, '45-'87, Post-'87. In fact, URM buildings considered in the project were real buildings that can be further categorized as *historical* (e.g., stone or brick masonry for walls and vaults or timber floors) and modern (e.g., with artificial block masonry for walls and reinforced concrete floors) with three, four, five or seven story. For some of these structures retrofitting according to an old code or NTC, was also simulated [42,43].

For RC residential buildings, three epochs were considered: Pre-'70, '70s, '80-'90. RC structures are three or six story frames analyzed in three configurations: infilled frame (IF), *pilotis* frame (PF) and bare frame (BF). The design according to the old codes was simulated for all the sites considered. The RC structures can be further categorized as gravity-load design and seismic design, given that seismic design was not mandatory at all sites through the design epochs [44].

PRC structures are single story industrial buildings four of designed at the Milan site without accounting for seismic loads and referring to two relevant design epochs: '70s and '80-'90. These structures are characterized by different roof and cladding solution (precast elements with or without additional RC topping and infilled frames or precast cladding panels, respectively) and connection details (friction or dowel). Two of these buildings were also relocated in Naples, while the others were re-designed ad-hoc in Naples. Finally, the four buildings were re-designed in L'Aquila moreover one of those was also re-designed referring to Pre-'70 epoch [45].

S single story industrial buildings were designed according to the epoch '80-'90 in L'Aquila, Naples and Milan (the results for this design epoch can be extended to buildings designed since the '60s, to follow). The structural scheme is a frame (hinged or restrained) in the transverse direction frames, while some portals have a bracing system (L-shaped or square hollow section) in the

longitudinal direction. Three different configurations were considered: bare frame, trapezoidal sheeting cladding, and sandwich panels sheeting [46].

Table 2. summarizes the investigated configuration, each one corresponding to a structural model, at all sites.

Table 2. Summary of the analyzed structures per site, structural typology and design epochs.

Typology	Epochs	AQ	CT	NA	RM	MI
URM	Pre-'20	2 Configs.	2 Configs.	1 Config.	1 Config.	-
	'20-'45	3 Configs.	-	-	-	1 Config.
	'45-'87	2 Configs.	1 Config.	2 Configs.	-	1 Config.
	Post-'87	-	-	-	4 Configs.	-
	NTC	2 Configs.	-	2 Configs.	1 Config.	-
RC	Pre-'70	6 Configs.	6 Configs.	6 Configs.	-	6 Configs.
	'70s	6 Configs.	6 Configs.	6 Configs.	-	6 Configs.
	'80-'90	6 Configs.	6 Configs.	6 Configs.	-	6 Configs.
PRC	Pre-'70	1 Config.	-	-	-	-
	70s	2 Configs.	-	2 Configs.	-	2 Configs.
	'80-'90	2 Configs.	-	2 Configs.	-	2 Configs.
S	Pre-'70	-	-	-	-	-
	'70s	-	-	-	-	-
	'80-'90	12 Configs.	-	4 Configs.	-	4 Configs.

The seismic reliability assessment considered structural failure with respect to two performance levels, that is *usability preventing damage* (UPD) and *global collapse* (GC). In the RINCT-n, the former is mainly related to the seismic damage experienced by non-structural elements, such as in-fillings to reinforced concrete frames, while the latter is generally related to the horizontal displacement capacity corresponding to the fifty-percent drop of the base shear, determined by means of nonlinear static analysis. In the RINTC-e project the same definitions apply for the performances, yet more typology- and design-epoch-specific adjustments were needed to capture the failure modes of low-

and pre-code buildings, such as brittle failures in RC frames. Details can be found in the referenced specific papers.

The seismic reliability metric adopted by the RITNC project is the failure rate (λ_f) or the mean number of earthquakes (i.e., mainshocks of seismic sequences) that, in one year, cause failure:

$$\begin{aligned}\lambda_f &= \nu \cdot P[F|E] = \nu \cdot \int_{IM} P[F|IM=x] \cdot f_{IM}(x) \cdot dx = \\ &= \int_{IM} P[F|IM=x] \cdot |d\lambda_{im}(x)|\end{aligned}, \quad (7)$$

In the equation, ν is the rate of earthquakes above a minimum magnitude of interest, while $P[F|E]$ is the probability of failure given the occurrence of an earthquake above the minimum magnitude. According to the performance-based earthquake engineering (PBEE) framework [18], $P[F|E]$ can be evaluated as the integral of the failure probability conditional to the value of a ground motion intensity measure (IM), $P[F|IM=x]$, that is the *fragility curve* of the structure and the probability density function of IM in one earthquake f_{IM} . In fact, $\nu \cdot f_{IM}(x) = |d\lambda_{im}(x)|$, that is, the absolute derivative of the *hazard curve* for the site [27].

To assess the seismic structural fragility multi-stripe nonlinear dynamic analysis (MSA, [47]) of 3D numerical structural models, was carried out. Ten *IM* stripes, corresponding to ten exceedance return periods of the IM at the site (from 10 to 100,000 years), were considered. For each structure, the chosen *IM* is the pseudo-spectral acceleration (with five percent viscous damping) at a period close to the first-mode vibration period. Real ground motion record, as the analysis input, were selected according to a recent hazard consistent procedure [48]. Finally, for each structure a lognormal fragility function was calibrated on the MSA results. The hazard curves for the considered IM at the sites were computed based on probabilistic seismic hazard analysis considering an authoritative seismic source model for Italy. Details on both hazard and fragility are given in a dedicated reference [49].

3.3. FATALITY RATES EVALUATION

The fatality rate, λ_d , can be defined as the expected number of earthquakes in one year causing death due to the structural failure of the buildings. It can be evaluated as the fatality probability given the occurrence of a seismic event, $P[D|E]$, times the expected number of earthquakes in one year:

$$\lambda_d = v \cdot P[D|E] = P[D|UPD] \cdot (\lambda_{f,UPD} - \lambda_{f,GC}) + P[D|GC] \cdot \lambda_{f,GC} , \quad (8)$$

The fatality rates computed in this study follows a conventional approach where considering that only two fatality rates are available from the RINTC project, for the GC and UPD performances only, indicated as $\lambda_{f,GC}$ and $\lambda_{f,UPD}$, respectively [41]. This yields to the rightmost hand side of Eq. **Errore. L'origine riferimento non è stata trovata.**, where $P[D|GC]$ and $P[D|UPD]$ are the fatality probabilities conditional to the two structural performances, which were determined according to three different methods. Two of which were already used, for the RINTC-n buildings, in Iervolino & Pacifico[41], where further details can be found.

3.3.1 Method 1

In this method [34] the fatality probabilities are taken equal to the fatality rates given structural damage obtained from HAZUS [50]. $P[D|GC]$ is computed considering GC and UPD corresponding to *complete structural damage* (CSD), and *moderate structural damage*, in HAZUS, respectively. Because the fatality probabilities depend on the structural typology or *class*, the association of the buildings RINCT to the HAZUS classes is given in Table 3.

3.3.2 Method 2

This method [36] adopts the European Macroseismic Scale (ESM, [51]) that is, *vulnerability classes* (A to D, from the most vulnerable to the less one) to assign the casualty probability conditional to *damage states* (DS). Herein, UPD and GC are considered corresponding to DS3 and DS5 respectively. Note that because ESM deals with residential building only, it was not possible to apply this approach to S and PRC RINTC-e buildings [41].

3.3.3 Method 3

The FIB bulletin no. 80 [52] also provides fatality probabilities in case of structural failure. Those based on other technical work [53], recommended to be used for buildings, are of interest to this study. The conditional fatality probabilities are provided as function of the consequence classes of Eurocode [54] with respect to the loss of human life. The RINTC industrial and residential buildings were associated to CC2 and CC1, respectively.

Table 3. Fatality probabilities from HAZUS and association with RINTC-e structures.

RINTC-e structures description	HAZUS		ESM		fib80 bulletin	
	Class	Description	Vuln. class	Description	Cons. class	Cons. for life loss
URM two-story buildings (Massive stone)	URML	Low-Rise Unreinforced Masonry Bearing Walls	B	Masonry Massive stone	CC1	Low
URM two-story buildings (Manufactured stone units)	URML	Low-Rise Unreinforced Masonry Bearing Walls	C	Masonry Unreinforced with manufactured stone units	CC1	Low
URM with three- (or more) story buildings. (Massive stone)	URMM	Mid-Rise Unreinforced Masonry Bearing Walls	B	Masonry Massive stone	CC1	Low
URM with three- (or more) story buildings. (Manufactured stone units)	URMM	Mid-Rise Unreinforced Masonry Bearing Walls	C	Masonry Unreinforced with manufactured stone units	CC1	Low
RC-G three-story BF buildings	C1L	Low-Rise Concrete Moment Frame	C	RC frame without earthquake-resistant design (ERD)	CC1	Low
RC-S three-story BF buildings	C1L	Low-Rise Concrete Moment Frame	D	RC frame with moderate level of ERD	CC2	Low
RC-G six-story BF buildings	C1M	Mid-Rise Concrete Moment Frame	C	RC frame without earthquake-resistant design (ERD)	CC1	Low
RC-S six-story BF buildings	C1M	Mid-Rise Concrete Moment Frame	D	RC frame with moderate level of ERD	CC1	Low

RC-G three-story IF and PF buildings	C3L	Low-Rise Concrete Frame with URM Infill Walls	C	RC frame without earthquake-resistant design (ERD)	CC1	Low
RC-S three-story IF and PF buildings	C3L	Low-Rise Concrete Frame with URM Infill Walls	D	RC frame with moderate level of ERD	CC1	Low
RC-G six-story IF and PF buildings	C3M	Mid-Rise Concrete Frame with URM Infill Walls	C	RC frame without earthquake-resistant design (ERD)	CC1	Low
RC-S six-story IF and PF buildings	C3M	Mid-Rise Concrete Frame with URM Infill Walls	D	RC frame with moderate level of ERD	CC1	Low
PRC buildings	PC2L	Low-Rise Precast Concrete Frames with Concrete Shear Walls	-	-	CC2	Medium
S buildings	S2L	Low-Rise Steel Braced Frame Steel	-	-	CC2	Medium

3.4 RESULTS AND DISCUSSIONS

The resulting fatality rates are here presented and compared to those of current-code-conforming structures [41], when possible. It has to be noted that, in the RINTC projects 1E-05 has been set as lowest possible values of the failure rates to avoid significant extrapolations of hazard and fragility models, this has an impact on the shown fatality rates.

In Figure 3 the results, for each structural typology, are given as the arithmetic average (markers) of the rates computed for all the configurations at all sites, as a function of the design epoch, while the vertical bars represent the range of rates contributing to the corresponding mean. The red markers and related bars represent results for the current code [41]. The evolution, that is, the general improvement, of structural safety is evident, with a few exceptions. For PRC industrial buildings, different plan configurations and design choices in the '80-'90 structures make the trend slightly less clear [45]. As it pertains

to the conventional methods adopted: it appears that, for residential buildings, RC and URM, that Method 3 and Method 2, provides lower and larger rates (up to one order of magnitude), respectively. For the industrial buildings, PRC and S, the lowest fatality rates are from Method 1.

For a deeper understanding, Figure 4 shows the fatality rates for each considered structural typology, as a function of the design epoch and the construction site (only MI, RM and AQ are shown). To prevent the figure to be too cluttered, considering that a similar trend is observed for all the methods considered, only the results from Method 1 are reported.

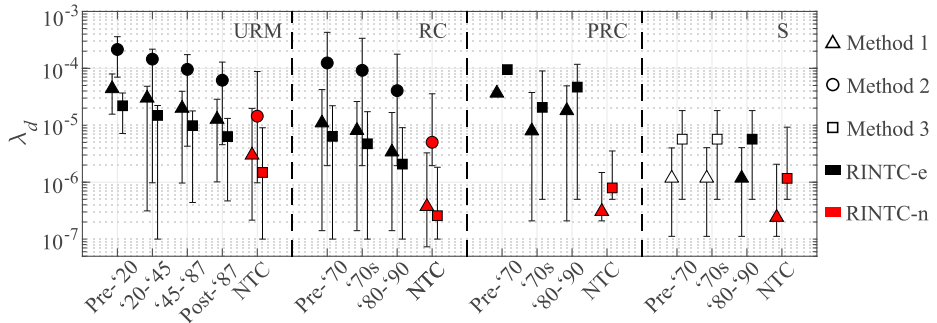


Figure 3. Arithmetic averages of the fatality rates as a function of the design epochs. (White markers indicated that design of S for the ‘80-‘90 epoch also apply to previous epochs.)

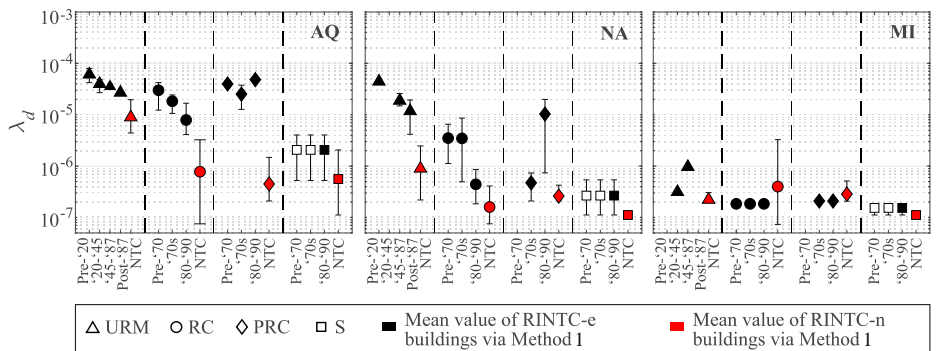


Figure 4. Fatality rates as a function of the design epoch and site. (White markers indicated that design of S for the ‘80-‘90 epoch also apply to previous epochs.)

Once again, the markers represent the averages, and the vertical bars are the ranges of rates contributing to each mean. For URM and RC, at L’Aquila and Naples, the same trend of Figure 3. In Milan, this trend cannot be appreciated because of the 1E-05 limit on the failure rates values; in other words, the hazard

is so low that the seismic safety in Milan is driven by gravity load design, and the failure rates, to be computed, require large fragility extrapolation, much beyond the results of the dynamic analyses of structural models [49].

3.5. FINAL REMARKS

This study presented analyzed the evolution of the seismic safety, measured in terms of fatality rates, corresponding to the development of design codes. The fatality rates are based on the failure rates from a large research project, computed for pre- and low-code Italian structures, residential and industrial somewhat representing the existing Italian building stock. The casualty probabilities to pass from the failure to the fatality rates were derived, in a highly conventional manner, by means of three methods: (1) one based on HAZUS [34]; (2) one based on EMS [36]; (3) and one based on fib80 bulletin [52].

It is found that, as somewhat expected, the fatality rates decrease with the development in time of the design technology, with the largest improvement due to the enforcement of the current code. The three methods considered provide results ranging in one order of magnitude. Moreover, most seismically hazardous sites, according to the current assessment, have larger fatality rates, while unreinforced masonry shows the largest rates. This is generally independent of the design epoch, which confirms previous findings for current-code-conforming structures.

The fatality rates computed herein have the advantage to represent a quantitative measure of structural safety; nevertheless, the way they were derived herein is highly simplified and conventional, such that these results are mainly for comparison and should be used with caution otherwise.

3.6 ACKNOWLEDGEMENTS

The study presented in this article was developed within the activities of the ReLUIS-DPC 2019–2021 research programs, funded by the *Presidenza del Consiglio dei Ministri – Dipartimento della Protezione Civile* (DPC). Note that the opinions and conclusions presented by the authors do not necessarily reflect those of the funding entity.

Chapter 4 – SEISMIC RISK AT NATIONAL SCALE FOR CODE-CONFORMING STRUCTURES IN ITALY

The following paper has been derived from this Chapter:

- *Pacifico A., Chioccarelli E., Iervolino I. (2022) Residential code-conforming structural seismic risk maps for Italy. Soil Dynamics and Earthquake Engineering 153. DOI:10.1016/j.soildyn.2021.107104*

4.1. INTRODUCTION

The evolution of structural seismic design in Italy has been such that code improvements were mostly motivated by seismic events causing serious losses. The first document in which horizontal forces were considered for structural design goes back to 1909 and was referred to the geographic area affected by the magnitude (M) 7.1 Messina earthquake of 1908. In the following hundred years, a number of structural design codes were enacted, and the portion of national territory associated to seismic actions slowly increased (see [55,56] for a comprehensive analysis). The whole Italian territory has been considered seismically prone only since 2003 [57]. However, practitioners were not obliged to design according to the new hazard classification of the sites until 2008, when the current Italian building code, *Norme Tecniche per le Costruzioni* or NTC08 [2], was published. (An updated version of the Italian building code, NTC18 [3], was recently published but the hazard classification of the territory was not modified.) It can be considered at the state of the art internationally and is somewhat similar to Eurocode 8 [17]. In the code, the design seismic actions are derived from probabilistic seismic hazard analysis or PSHA (e.g., [27]) for the construction site.

Comparing the code evolution with the construction age of the Italian building portfolio, some infer that most of the existing buildings are expected to be designed with inadequate or absent seismic provisions (e.g., [39]) resulting in significant seismic vulnerability and risk (e.g., [58–61]). However, also the design according to current code exposes structures to some implicit seismic risk [5]. Indeed, the probability that a structure exceeds a defined performance (i.e., failure), in a given time interval, is not explicitly controlled by practitioners.

On this basis, in 2014, a large Italian national research project, *Rischio Implicito delle Strutture progettate secondo le NTC* or RINTC ([1,20]), had the

goal of quantifying the annual failure rate (numerically close to the annual failure probability) of code-conforming structures in Italy. Among others, residential fixed-based (FB) buildings considered in the project are reinforced concrete (RC) buildings of three, six and nine storeys (w/o infillings), and unreinforced masonry structures (URM) of two and three storeys. Moreover, residential six-storey RC base-isolated (BI) structures were also considered. The structures are supposedly located in three Italian sites chosen to be representative of different levels of design seismic hazard (low, medium, and high) according to the most recent probabilistic assessment [62]. Referring to each site and to specific soil conditions (to follow), each structure was first designed in accordance with NTC08 (or its 2018 update); then, the failure rate was computed with respect to ad-hoc defined performance levels. The results of the project showed that, although the design seismic actions (i.e., design ground motion intensity) have the same exceedance return period over the country, the structural reliability significantly changes across the sites. This is for reasons that further research showed attributable to inherent features of the code and of the seismic hazard of the considered sites beyond the exceedance return period of the seismic actions considered for design [19].

The aim of the work described herein is to depict the seismic risk in Italy in an ideal scenario where the existing (residential) buildings are substituted by the code-conforming structures of the RINTC project. To this end, the seismic risk is quantified, at the municipality scale, by the mean number of earthquakes that in one year cause structural failure of a randomly selected building of the municipality of interest; that is, still an annual failure rate leading to the annual expected number of buildings experiencing structural failure in the considered municipality. Thus, failure rate must be a function of the seismic hazard of the site evaluated by means of PSHA (including the soil conditions), the seismic vulnerability of the structural typologies and the proportion among different structural typologies in the municipality, that is, the exposure.

Several maps of the municipality rates, which represent the result of the study, are derived based on different options for hazard and vulnerability characterization. In particular, three hazard models are considered: (i) the current official hazard for Italy, that is, the one on which design actions in the Italian code are based on (defined as MPS04; [62]); (ii) a more recent model, named MPS19, derived by a large research effort [10]; (iii) hazard computed via the so-called sequence-based PSHA, SPSHA, [63] that also accounts for aftershocks'

contribution, something neglected in classical hazard analysis (including both MPS04 and MPS19). As pertaining to structural vulnerability, a substitution criterion is defined to replace the existing residential buildings with fixed-base code-conforming URM and RC buildings, with different number of floors and architectural configurations. Moreover, an alternative scenario in which all the existing buildings are all substituted by base-isolated six-storey RC buildings is considered.

The remainder of this paper is structured such that the buildings of RINTC project are described together with the fragility functions that are derived for the purposes of this study. Then, the methodology for the computation of the failure rates at municipality scale is presented. After introducing all the input models required for risk assessment, results considering four scenarios are discussed. The first two scenarios are those of PSHA based on MPS04 and combined with structural vulnerabilities of FB and BI structures. Then, results associated to PSHA based on MPS19 and structural vulnerability of FB structures are provided. Finally, failure rates of FB structures are computed in the case of SPSHA, referring to MPS04. Some final remarks close the paper.

4.2. FRAGILITY FUNCTIONS OF CODE-CONFORMING RINTC STRUCTURES

In the RINTC project, a large set of residential buildings was designed according to the current Italian building code [2,3], to be ideally located in a few Italian sites: L'Aquila (AQ), Naples (NA), and Milan (MI), representative of high, medium, and low seismic hazard in the country, respectively. Different soil conditions were considered at the sites: soil class A (rock) and C (soft soil) according to the classification of the code. Each structure was designed referring to damage and life-safety limit states as defined in NTC08. On the other hand, structural reliability, was assessed in the project referring to two different performance levels (PL) that are named usability-preventing damage (UPD) and global collapse (GC). UPD is reached if one of following conditions occurs: (i) light damage in 50% of the main non-structural elements; (ii) at least one of the non-structural elements reaches a severe damage level leading to significant interruption of use; (iii) attainment of 95% of the maximum base-shear of the structure. GC, generally, corresponds to the deformation capacity associated to a 50% post-peak deterioration of the total base shear of the

building (some adjustments of these criteria apply to specific typologies accounting for their peculiarities; see [5,64]).

In the RINTC project, for each building, multiple-stripes nonlinear dynamic analyses, (MSA) [65] were performed on three-dimensional structural models at ten ground motion intensity measure (IM) levels (i.e., values) corresponding to ten exceedance return periods from 101 to 105 years. For each IM value, twenty two-component horizontal records were selected according to the conditional mean spectrum method [29]. In particular, each analysis was performed associating the two horizontal components of each record to the two main orthogonal directions of the structure and measuring the maximum response (i.e., in terms of either the roof displacement ratio or the maximum inter-storey drift ratio). The IM adopted for the MSA is the largest (between the two horizontal components) 5% damped pseudo-spectral acceleration at a period, T , close to the first vibration period of each model; it is indicated hereafter as $Sa(T)$.

In the following, the results of the dynamic analyses performed in the project are used to compute, for each structure (st) and for both the considered performance levels, the probability that PL is reached or exceeded given a value of IM , $P[PL^{(st)} \geq pl|im]$, that is the lognormal fragility function of the structure:

$$P[PL^{(st)} \geq pl|im] = \Phi \left[\frac{\ln(im) - \mu^{(st)}}{\sigma^{(st)}} \right], \quad (9)$$

where $\{\mu^{(st)}, \sigma^{(st)}\}$ are parameters retrieved via the R2R-software [31], neglecting estimation uncertainty [66]. In the following, the considered structures and their fragilities are described; further details are given in [49].

4.2.1 Reinforced-Concrete Structures

RC structures are moment resisting frame buildings of three (RC3) and six storeys (RC6) characterized by regularity in plan and elevation. While in the RINTC project bare-, pilotis-, and infilled-frames are designed, modelled, and analyzed [23] (Figure 5), hereafter only the infilled configurations of three- and six-storey are considered; i.e., the most common configuration. Such structures are all designed for class C soil at the three sites. Fragility functions, modelled

as per Eq.(9), refer to $Sa(0.15s)$ for the RC3 and $Sa(0.5s)$ for RC6. In Table 4, considered RC structures are listed and, for each of them, the parameters of fragility functions are reported for both performance levels.

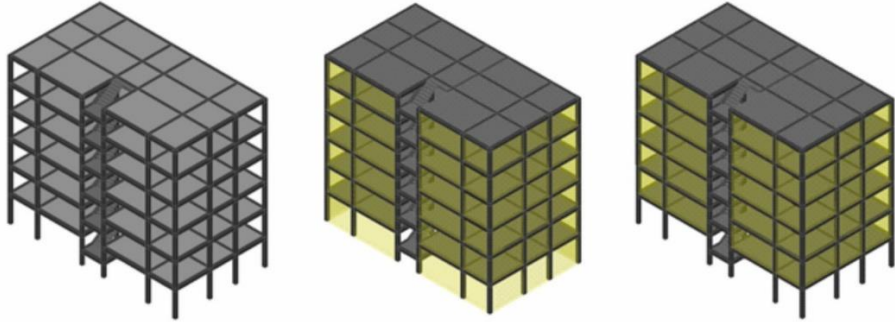


Figure 5. RC6 buildings: bare-frame (left), infilled-frame (center); pilotis-frame (right). (Adapted from [1])

In Figure 6 the fragility functions are represented: black lines refer to GC and gray lines to UPD. (Although some IM values in the figure may appear unlikely, they are given to completely represent the curves and it should be noted that their effects on results of this study are negligible; see Section 4.5.1.)

Table 4. Parameters of RC fragility functions (IM in g)

Site	N. of storeys	UPD		GC	
		μ	σ	μ	σ
AQ	3	-0.44	0.41	1.79	0.66
AQ	6	-0.33	0.39	1.50	0.67
NA	3	-0.08	0.51	1.41	0.32
NA	6	-1.11	0.49	1.33	0.23
MI	3	0.06	0.51	0.30	0.32
MI	6	-0.55	0.29	0.40	0.31

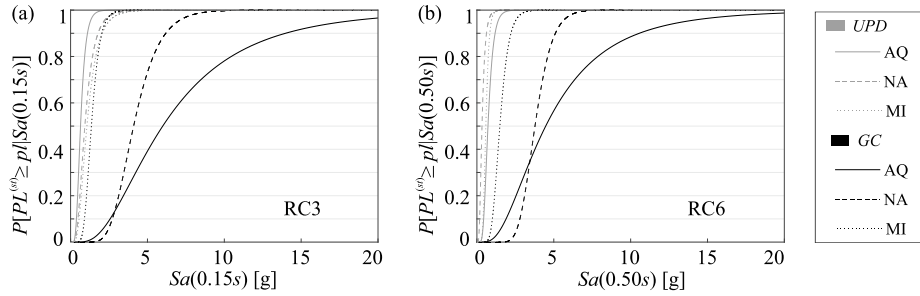


Figure 6. Fragility functions of (a) RC3 and (b) RC6.

4.2.2 Unreinforced Masonry Structures

For the three considered sites, two- and three-storey URM buildings (URM2 and URM3, respectively) made of perforated clay units with mortar joints were designed, modelled, and analyzed, within the RINTC project [22]. While buildings with both regular and irregular plan configurations were studied, here only those regular, according to the NTC08 criteria, are considered. They are characterized by different architectural configurations: the buildings associated to a letter E are examples of real modern URM buildings while those identified by a C are conceived as structural variations of regular wall arrangements. In both C and E classes, different thicknesses of structural walls are considered: C buildings are represented by six structural configurations from C1 to C5 and C7; E buildings are four, named as E2, E5, E8 and E9 (see [21] for further details).

Figure 7 shows the different plan views of the URM structures considered herein. The two-storey building in L'Aquila has five alternative architectural configurations whereas, in the same site, three configurations for the three-storey building are considered. In Naples, the two-storey and three-storey building have two and four configurations, respectively. Finally, in Milan, three and four configurations are associated to the two-storey and three-storey building, respectively.

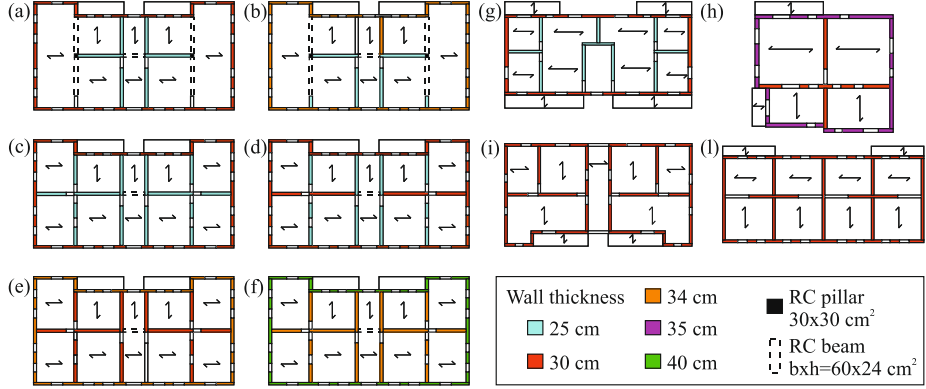


Figure 7. Plan view of the URM buildings. Figures from (a) to (f) represent the “C” configurations (1-5 and 7 respectively), while figures from (g) to (l) represent the “E” configurations (2, 5 8 and 9 respectively).

All the considered URM buildings were designed on class C soil (not to be confused with one of the configurations) apart from the three-storey buildings of L’Aquila for which design for C soil is not available; these cases (i.e., three architectural configurations) were substituted by the buildings designed on class A soil (the RINTC project has shown that the seismic vulnerability does not change dramatically with the soil class [5]).

Fragility functions are computed for each architectural configuration. Thus, considering the k -th architectural configuration pertaining to a given structural typology, the conditional failure probability, $P\left[PL^{(st,k)} \geq pl|im\right]$, is computed via Eq. (9). Then, the fragility function for each structural typology at a specific site, $P\left[PL^{(st)} \geq pl|im\right]$, is computed combining $P\left[PL^{(st,k)} \geq pl|im\right]$, as per Eq. (10):

$$P\left[PL^{(st)} \geq pl|im\right] = \sum_k P\left[PL^{(st,k)} \geq pl|im\right] \cdot w_{st,k}, \quad (10)$$

where $w_{st,k}$ weighs how much a specific architectural configuration is representative of the actual building portfolio (assuming that these configurations completely cover the building stock). Indeed, a value of $w_{st,k}$ was associated to each URM configuration basing on expert judgement (S. Cattari, personal communication) so that the sum of the weights for all the architectural configurations of the same structural typology equals to one.

The first vibration period of all the URM structures is close to 0.15s, thus the adopted IM for fragility functions is $Sa(0.15s)$. Table 5 shows, for each considered URM structure, the μ and σ parameters for both performance levels, along with the assigned $w_{st,k}$. Figure 8 shows the URM fragilities.

Table 5. Parameters of URM fragility functions (IM in g).

Site	N. of storeys	Architectural configuration	$w_{st,k}$	UPD		GC	
				μ	σ	μ	σ
AQ	2	E2	0.20	-0.04	0.21	0.60	0.34
	2	E5	0.20	-0.32	0.26	0.56	0.43
	2	E8	0.20	-0.25	0.20	0.61	0.32
	2	E9	0.20	-0.11	0.18	0.28	0.26
	2	C3	0.20	-0.55	0.31	0.51	0.28
AQ	3	E2	0.33	-0.24	0.42	0.42	0.53
	3	E8	0.33	-0.26	0.38	0.47	0.51
	3	C1	0.33	-1.05	0.22	0.23	0.46
NA	2	C1	0.44	-0.72	0.24	0.95	0.42
	2	C4	0.56	-0.57	0.31	0.95	0.35
NA	3	E2	0.27	-0.06	0.57	0.88	0.24
	3	E8	0.27	-0.12	0.51	0.86	0.32
	3	C3	0.27	-0.87	0.28	0.69	0.45
	3	C5	0.20	-0.86	0.24	0.73	0.42
MI	2	E2	0.41	0.06	0.16	0.30	0.12

	2	C1	0.18	-1.16	0.09	0.45	0.08
	2	C7	0.41	-0.83	0.13	-0.18	0.08
MI	3	E2	0.27	-0.38	0.20	-0.41	0.08
	3	E8	0.27	-0.64	0.15	-0.39	0.13
	3	E9	0.27	-0.76	0.10	-0.63	0.094
	3	C2	0.18	-0.86	0.31	-0.06	0.12

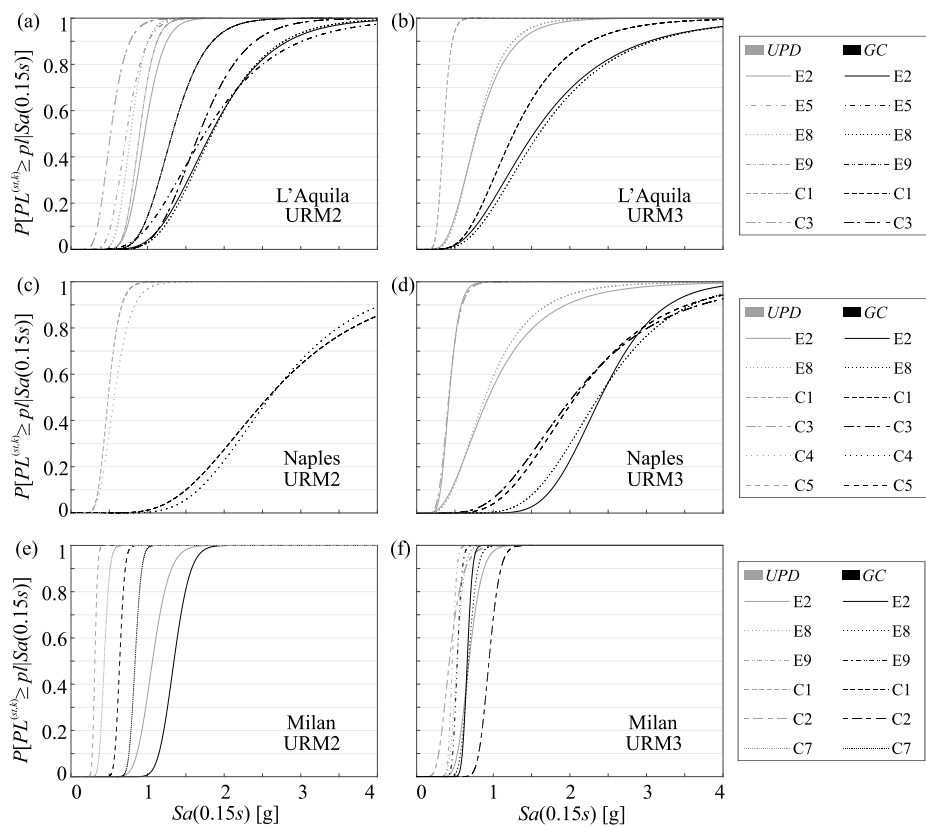


Figure 8. Fragility functions of two storeys URM buildings (left column) of L'Aquila (top row), Naples (mid row), and Milan (bottom row) and of three storeys URM buildings of the same sites (right column).

4.2.3 Base-Isolated Structures

For the mid- and high-hazard sites, that is Naples and L'Aquila, respectively, residential six-storey infilled RC, base-isolated, buildings were also designed on class C soil. Indeed, it was assumed that BI structures are unlikely in low seismic hazard class. Three isolation systems were studied: (i) double-curvature friction pendulums (FPS); (ii) high-damping rubber bearings (HDRB); (iii) and hybrid system of HDRB and sliders (HDRB+Sld).

The UPD failure criteria are the same of RC FB structures, whereas for GC needs to consider failure of both the isolation system and the superstructure. The superstructure failure criterion is the same of the RC buildings, while the failure of the base isolation was defined based on the specific device's responses described in [67].

For each isolation system, fragility functions were computed according to Eq. (9). The resulting curves at the same site were combined via Eq. (10) in which the alternative isolation systems were treated as the alternative architectural configurations of URM buildings. To this end, the weight of each isolation system was computed on the basis of the reconstruction data following the 2009 L'Aquila earthquake (M6.3); indeed, a large number of buildings were isolated with these three systems in the following percentages: 2% with HDRB, 41% FPS and 57% HDRB+Sld (D. Cardone, personal communication). Thus, the weights adopted in Eq. (10) are 0.02, 0.41 and 0.57, for HDRB, FPS and HDRB+Sld, respectively.

All the BI structures are characterized by first vibration periods close to 3s, thus the selected IM is $Sa(3.0s)$. Table 6 reports the fragility parameters for both performance levels together with the weight associated to each isolation system. In Figure 9 the fragility functions of AQ and NA are represented.

Table 6. Parameters of BI fragility functions (IM in g).

Site	Isolation system	$w_{st,k}$	UPD		GC	
			μ	σ	μ	σ
AQ	FPS	0.57	-1.51	0.37	-1.44	0.25
	HDRB	0.02	-1.77	0.44	-1.21	0.29

	HDRB+Sld	0.41	-1.55	0.35	-1.31	0.19
	FPS	0.57	-1.43	0.18	-1.47	0.09
NA	HDRB	0.02	-1.54	0.17	-1.22	0.14
	HDRB+Sld	0.41	-1.61	0.2	-1.5	0.24

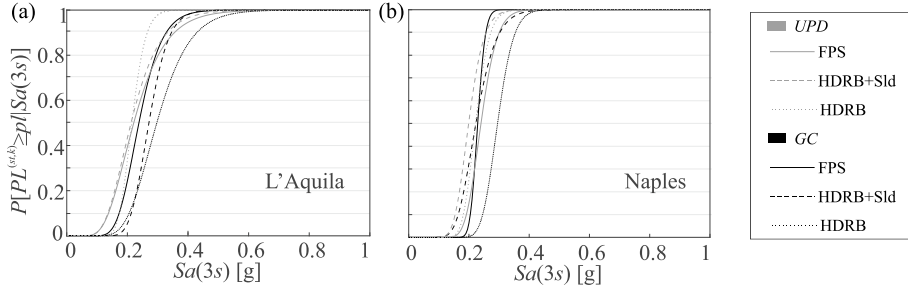


Figure 9. Fragility functions of BI buildings of (a) L'Aquila and (b) Naples.

4.3. METHODOLOGY FOR COMPUTATION OF FAILURE RATES

This section describes how fragility functions computed by the results of the RINTC project are used to derive ideal risk maps for Italy; i.e., assuming that all structures are code conforming. PSHA allows computing the rate of mainshocks (i.e., the maximum magnitude earthquake within each sequence) causing the exceedance of $IM = im$ for a known soil class, that is $\lambda_{E,im|\theta}$. The plot of $\lambda_{E,im|\theta}$ versus the possible im values is the so-called hazard curve. For a building of a given structural typology and located on a known soil class, the rate of mainshocks causing the building to fail, that is, to reach or exceed a performance level ($PL \geq pl$), $\lambda_{E,pl|st,\theta}$, can be computed via Eq. (11) in which it is assumed that the fragility is not dependent on the soil condition of the construction site and $|d\lambda_{E,im|\theta}(z)|$ is the absolute value of the differential of the hazard curve at $IM = z$:

$$\lambda_{E,pl|st,\theta} = \int_{im} P[PL^{(st)} \geq pl | z] \cdot |d\lambda_{E,im|\theta}(z)| \quad (11)$$

If the site is representative of a municipality (e.g., the center of its area) and the fragility function represents the structural typology the building belongs to, Eq.

(11) can be (approximately) applied to compute the failure rate of the buildings of the municipality belonging to the considered structural typology. The soil condition at the base of each building should be known, but usually this information is not available. However, it may be possible to compute $P[\theta_i]$, that is the probability that a generic building of the considered structural typology is located on each possible soil condition, i . Applying the total probability theorem, it results:

$$\lambda_{E,pl|st} = \sum_i \left\{ \int_{im} P[PL^{(st)} \geq pl|z] \cdot \left| d\lambda_{E,im|\theta_i}(z) \right| \right\} \cdot P[\theta_i] \quad (12)$$

If the probability that a building of the municipality belongs to a given structural typology, $P[st]$, can also be computed, the rate of earthquakes causing the generic building (i.e., randomly selected) to reach or exceed a performance level, $\lambda_{E,pl}$, can be computed via Eq. (13), where it is assumed that soil condition and structural typology are independent random variables:

$$\begin{aligned} \lambda_{E,pl} &= \sum_{st} \lambda_{E,pl|st} \cdot P[st] = \\ &= \sum_{st} \sum_i \left\{ \int_{im} P[PL^{(st)} \geq pl|z] \cdot \left| d\lambda_{E,im|\theta_i}(z) \right| \right\} \cdot P[\theta_i] \cdot P[st] \end{aligned} \quad (13)$$

The rate computed in the previous equation is a risk metric that, with a probabilistically consistent approach, accounts for several sources of uncertainties related to: (i) earthquake source and propagation, (ii) soil site conditions, (iii) building structural typology, (iv) structural damage given ground motion intensity. Moreover, according to the classical hypotheses of performance-based earthquake engineering [18], $\lambda_{E,pl}$ approximately leads to the expected number of failed buildings in the municipality in a small time interval $(t, t + \Delta t)$, $E[N_{pl}(t, t + \Delta t)]$:

$$E[N_{pl}(t, t + \Delta t)] \approx N_B \cdot \lambda_{E,pl} \cdot \Delta t, \quad (14)$$

in which N_B is the total number of buildings of the municipality. (The computed rate, practically, has not any other meaning that its use in this last equation, that is, to compute the expected value of damaged buildings.)

In fact, earthquakes are typically clustered in both time and space and, for each cluster, the mainshock is typically defined as the largest magnitude earthquake. Factually, PSHA neglects the hazard contribution of earthquakes preceding and following the mainshock within each cluster, that are identified as foreshocks and aftershocks, respectively. On the other hand, the so-called sequence-based PSHA, SPSHA, [11] allows to quantify the seismic threat accounting for the effect of aftershocks in PSHA. SPSHA allows to compute the rate of mainshock-aftershocks sequences that cause at least one exceedance of the chosen IM threshold for the soil class and the site of interest, $\lambda_{im|\theta}$. Such a rate can be used to replace $\lambda_{E,im|\theta}$ in Eq. (13), so that it provides the rate of sequences causing the generic building to reach or exceed a performance level, that is λ_{pl} . (In this context, seismic damage accumulation on the structures is neglected; see [12] for a discussion on this topic.)

4.4 INPUT DATA FOR NATIONWIDE CODE-CONFORMING RISK ASSESSMENT

4.4.1 Probabilistic Seismic Hazard Analyses Based on MPS04

The current official probabilistic hazard assessment (also at the basis of the design seismic actions in the current Italian building code) considers thirty-six seismic source zones for the country (except Sardinia Island) as described in [9] (see Figure 10b) and adopts a logic-tree constituted by sixteen branches [62]. Among them, the branch named 921, is the one adopted herein because it provides close results to those of the whole logic-tree. Such a branch defines the seismicity of each seismic zone via the mean annual number of mainshocks per magnitude bins, the so-called activity rates (e.g., [63]), and requires the implementation of the ground motion prediction equation (GMPE) of [68]. The IMs for which PSHA is implemented here are the pseudo-spectral accelerations adopted for fragility functions, that is $T = \{0.15s, 0.5s, 3s\}$, and the peak ground acceleration, PGA. Being the three seconds spectral period outside the definition range of the chosen GMPE, when such a period is of concern, the GMPE of [69] is adopted. (All these modelling choices are in accordance with the hazard evaluation involved in the record selections for nonlinear dynamic analyses in RINTC project.)

For each municipality, PSHA was performed according to the described models (i.e., reproducing branch 921 of the MPS04 model); the resulting hazard curves are identified hereafter as $\lambda_{E,im|\theta}^{04}$, to distinguish from results obtained when the MPS19 model is adopted; consequently, the failure rates are identified as $\lambda_{E,pl}^{04}$. Hazard analyses were performed via the REASSESS software [70]. An example of the hazard curves computed for each municipality is reported in Figure 10a referring to PGA and rock soil conditions. In the same figure, the hazard curve computed for Milan, Naples, and L’Aquila are identified together with the exceedance rate corresponding to a return period (T_r) equal to 475 years (yr): this is a reference value for design of new structures and is also involved in the definition of the substitution criterion of existing structures discussed in the following section. Figure 10b shows the seismic zones of [9], the location of the reference cities, and the values of PGA on rock corresponding, for each municipality, to $T_r = 475\text{yr}$, that is PGA_{475} . Both figures provide results of the PSHA for all the municipalities, except Sardinia (i.e., 337 municipalities) that, according to the source model, is outside the definition range of the GMPE.

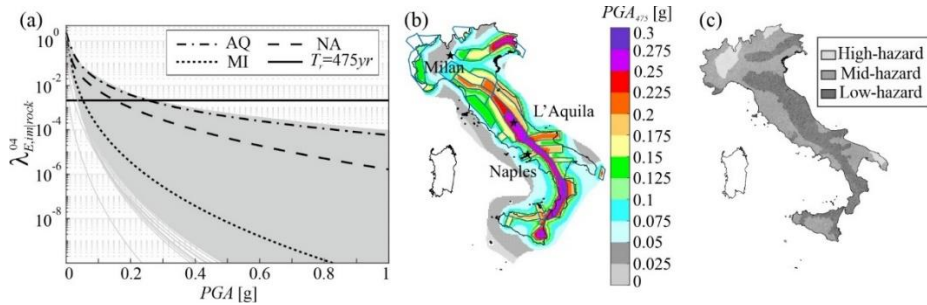


Figure 10. (a) PGA hazard curves computed via PSHA for all the Italian municipalities adopting MPS04, (b) map of PGA_{475} together with the thirty-six seismic zones of [9], (c) hazard classification according to PGA_{475} of each municipality.

4.4.2 Hazard Classes and Building Replacement Criteria

For the purposes of this work, RINTC data are incomplete in the sense that the studied sites and structural typologies cannot be directly representative of the whole Italian territory and building portfolio. Thus, some criteria to replace the

existing buildings with the code-conforming structures from RINTC are adopted.

The Italian municipalities were first grouped in three arbitrarily defined hazard classes, i.e., high-, mid-, and low-hazard. The value of PGA_{475} of each municipality (Figure 10b) was chosen for such a classification. The values of PGA_{475} of Naples (i.e., 0.15g) and Milan (0.05g) were taken as the limits of the classes, and sites characterized by a PGA_{475} lower than Milan were defined as low-hazard, sites with PGA_{475} lower than Naples (and larger than Milan) were considered a mid-hazard and sites with PGA_{475} larger than Naples were high-hazard. The resulting classification is represented in Figure 10c: the municipalities in low-hazard class are about 16% of the total (excluding Sardinia), whereas those in mid- and high-hazard are about 47% and 36%, respectively.

Following such a classification, it was assumed that the RINTC buildings designed in L'Aquila, Naples, and Milan were representative of buildings designed in any municipality belonging to the high-, mid- and low-hazard class, respectively. It should be noted that, among the high hazard class, few Italian municipalities (259 over more than 8000) are characterized by PGA_{475} larger than the one computed for L'Aquila, that is, the fragilities associated to these sites were in fact computed for structures designed for a site with lower PGA_{475} .

Data on the existing residential building stock were retrieved by IRMA [71]. They include, for each municipality, the number of reinforced concrete and masonry buildings of one, two, three, or more than three storeys. To be able to substitute the existing building typologies with the available one, some simple criteria were adopted: the RC buildings with three storeys, or less, are substituted by RC3, while RC buildings with more than three storeys are substituted by RC6; the masonry buildings with one or two storeys are substituted by URM2, and the three-storey masonry buildings are substituted by URM3. Finally, masonry buildings with more than three storeys are substituted by RC6; i.e., assuming that new-design URM buildings with more than three storey are unlikely.

The probability that a new building belongs to one of the considered structural typology, $P[st]$ from Eq. (15), where st corresponds to RC3, RC6,

URM2, URM3, is computed as the number of buildings of that structural typology (N_{st}) divided by the total number of buildings in the considered municipality (N_{TOT}):

$$P[st] = \frac{N_{st}}{N_{TOT}}, \quad st = \{RC3, RC6, URM2, URM3\}. \quad (15)$$

Figure 11 shows, for each municipality and for each structural typology, the values of $P[st]$ after the application of the described substitution criterion. As shown, the probability associated to URM2 is, generally, the largest whereas the one associated to RC6 is the lowest, with significant values concentrated in the major Italian cities. RC3 and URM3 have non negligible probability with a scattered distribution over the country.

Regarding the substitution with code-conforming BI buildings, the analyses only refer to medium and high-hazard classes being, as previously mentioned, BI buildings considered unlikely for the low-hazard class. Moreover, according to the available fragilities (see Section 4.2), the substitution criterion is that each existing building, regardless the construction material or the number of the storeys, is replaced by a six-storey BI building.

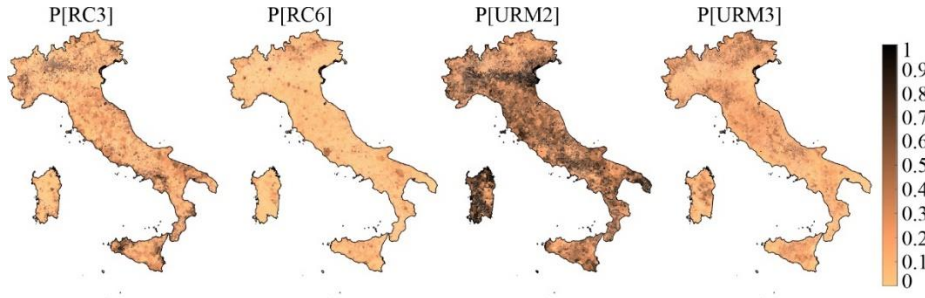


Figure 11. Probability of each structural typology per municipality.

4.4.3 Local Soil Classes at a Municipality Scale

In [72] it is provided a database of local soil characterizations for a grid of about one million points covering the whole Italian territory. For each point, the soil class (from A to D) according to NTC08 is defined. The latter can be converted into the soil classes of the GMPEs considered in the analyses. Indeed, both [68] and [69] GMPEs refer to three soil classes that are rock, stiff and soft soil. Soil conditions that, according to the Italian code, are identified as A correspond to

the rock category, whereas soil conditions B correspond to stiff soil and soil conditions C and D correspond to soft soil class of the GMPEs.

To quantify the probability that the building of a given municipality is located on a specific soil class, required by Eq. (13), soil data can be combined with the data provided by the Italian *Istituto Nazionale di Statistica* (ISTAT) that identify the urbanized areas (see the *Data sources* section for further details) of each municipality, intended as the areas associated to city centers and built areas (other areas are classified as productive sites and sparse houses). More specifically, the grid of soil classes from [72] was superimposed to the map of the urbanized areas and, in each municipality, $P[\theta_i]$ was computed as the number of grid points of a given soil class, N_{θ_i} , divided by the total grid points within the urbanized areas, N_{urb} :

$$P[\theta_i] = \frac{N_{\theta_i}}{N_{urb}}, \quad \theta_i = \{rock, stiff, soft\}. \quad (16)$$

The resulting probabilities are reported in Figure 12. The largest probabilities are associated to stiff soil in most of the municipalities; soft soil covers a non-negligible number of urbanized areas and is predominant in the north-eastern municipalities and along the coasts; finally, rock soil is significant only in a few areas (the effect on results of soil conditions is discussed in [73]).

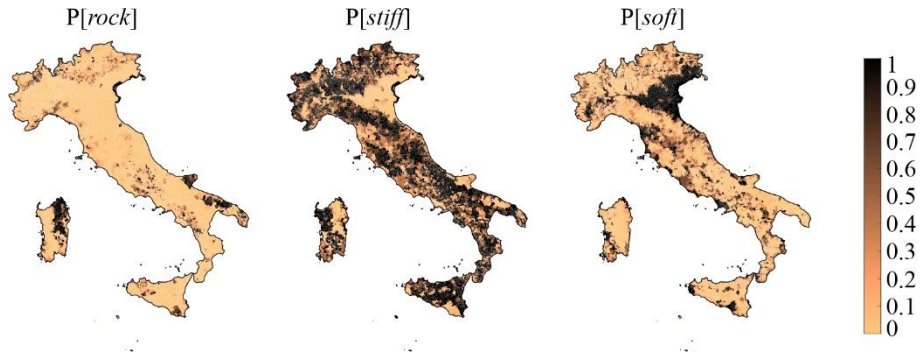


Figure 12. Soil class probabilities in the urbanized areas of Italian municipalities.

4.4.4 Alternative Hazard Models

4.4.4.1 Probabilistic seismic hazard analyses based on MPS19

A recent hazard model for Italy, MPS19, was developed by a large community of researchers, led by the *Istituto Nazionale di Geofisica e Vulcanologia* (INGV) [10]. MPS19 entails a fairly complicated logic tree composed by about six-hundreds branches. To facilitate the reproducibility of the results, a weighted average grid-seismicity model was provided in [74]. It is a grid of about eleven thousand point-sources covering and surrounding the whole country. For each point of the grid, the mean annual number of earthquakes per magnitude bin (i.e., the activity rates) and a probabilistic distribution of the style-of-faulting is provided. In the following, the hazard curves computed via PSHA and based on the grid-seismicity model from MPS19, that is $\lambda_{E,im|\theta}^{19}$, will be used to compute the corresponding failure rates, $\lambda_{E,pl}^{19}$. It should be noted that, in this case, the adopted GMPE is that of [75], which entails a different definition of the IM with the respect to [68], adopted in MPS04. Indeed, the latter refers to the largest (horizontal) spectral component, while the former provides the geometric mean of the two horizontal spectra components. Since in RINTC project, fragility functions were derived in terms of the largest component, when MPS19 substitutes MPS04, [76] conversion was adopted to convert the hazard curves from geometric mean to largest component; this allows to consistently combine hazard results and fragility functions.

Moreover, due to the hazard modification, when $\lambda_{E,pl}^{19}$ is of concern, the substitution criteria described in Section 4.4.2 was re-applied in accordance with the new hazard results. Since the RINTC structures were designed according to MPS04, the value of PGA_{475} of Naples and Milan computed with MPS04 were maintained as limits of the hazard classes. The difference with respect to the previous case is that the value of PGA_{475} computed in each site and identifying its hazard class is derived by MPS19. The resulting classification is reported in Figure 13a, which shows minor differences with respect to the equivalent classification of Figure 10c. The percentage of municipalities classified in low-hazard reduces from 15% to 7% when the source model changes from MPS04 to MPS19; the number of the sites falling in the mid-hazard class increases from 48% to 65% while the sites associated to the high-hazard decrease from 37% to 28%. Figure 13b shows the hazard

curves in PGA computed implementing MPS19 together with the hazard curves of L'Aquila, Naples, and Milan computed implementing MPS04 (in the legend AQ^{04} , NA^{04} , MI^{04} , respectively). The black horizontal line represents the 475 years exceedance return period (i.e., the one adopted for hazard classification). As shown, the hazard curves derived by the grid model are comparable with those from MPS04 in the range of low and medium return periods (i.e., up to about 500yr). Major differences appear when the return period increases. (It is also to note the systematic lower heterogeneity of the curves when passing from MPS04 to MPS19.)

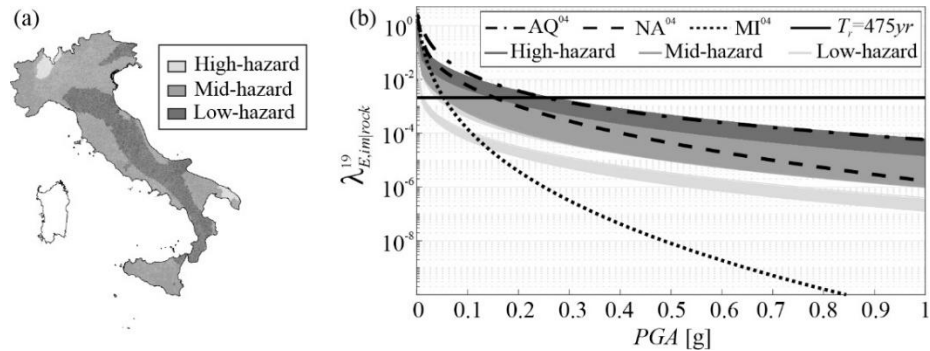


Figure 13. (a) Hazard classification of the Italian municipalities according to MPS19; (b) PGA hazard curves computed via PSHA adopting MPS19.

4.4.4.2 Sequence-based probabilistic seismic hazard analyses based on MPS04

As early mentioned, SPSHA [11] includes the effect of aftershocks, along with that mainshocks, in the hazard assessment. In [63] the hazard increments due to SPSHA with respect to PSHA were computed referring to the MPS04 source model, showing that, for a given return period, the value of the intensity measure computed via SPSHA (im_{SPSHA}) can be up to 30% larger than the corresponding value computed via PSHA (im_{PSHA}). Herein, still referring to the MPS04 source model, the SPSHA/PSHA comparison is extended to structural risk.

Because SPSHA requires a larger effort than PSHA, it was decided in this study – as an approximation – to perform SPSHA only for the site of L'Aquila, Naples, and Milan, to compute the hazard increases for these sites, and to adopt such increments to increase the PSHA hazard curves at the all the other Italian sites. Figure 14a shows the hazard curves computed for L'Aquila, Naples, and

Milan on rock site conditions and considering the spectral ordinates of interest for the structural typologies, that is $Sa(0.15s)$ and $Sa(0.5s)$ (the models here adopted for SPSHA are the same described in [63]). Then, for each site and spectral ordinate, the hazard increments with respect to PSHA, that is the im_{SPSHA}/im_{PSHA} ratio, was computed as a function of the return period; see Figure 14b (the ratios computed at given site, considering different spectral periods, may intersect; see [63]). The hazard increments computed in L'Aquila, Naples, and Milan were used to scale the corresponding hazard results computed for the municipalities in high-, medium-, and low-hazard class, respectively. The resulting hazard curves are used to compare the failure rates considering the effect of aftershocks with those considering mainshocks only (see the following sections).

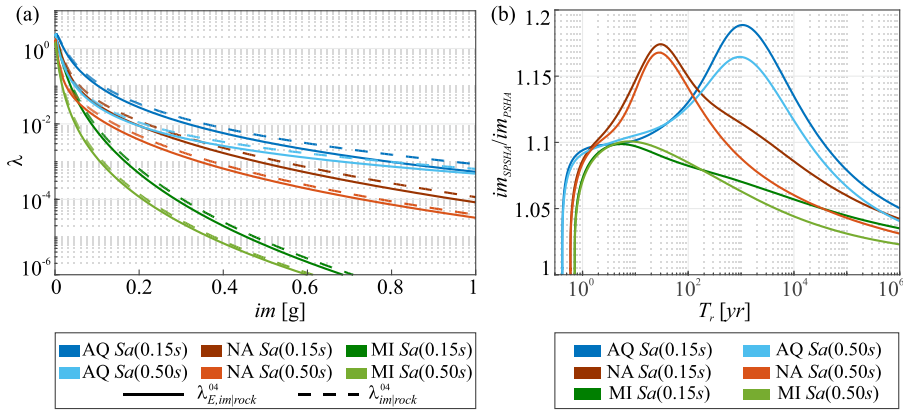


Figure 14. (a) Hazard curves of the three considered sites in term of $Sa(0.15s)$ and $Sa(0.5s)$ evaluated with PSHA (continuous lines) or SPSHA (dashed lines); (b) hazard increments due to SPSHA with respect to PSHA.

4.5 RESULTS AND DISCUSSIONS

4.5.1 Seismic Risk for Fixed-Base Structures Based on MPS04 Hazard

This section discusses the results of Eq. (13) when hazard curves are computed via PSHA based on MPS04 and in the hypothesis of substituting the existing residential buildings with the FB code-conforming ones. Figure 15a represents the failure rates of each Italian municipalities considering UPD ($\lambda_{E,UPD}^{04}$), whereas Figure 15b refers to GC ($\lambda_{E,GC}^{04}$). It is worth noting that, hereafter, failure rates lower than $1E-05$ are substituted by $1E-05$ to avoid significant

extrapolations of hazard and fragility models, acknowledging the approach of [5]. This value was chosen based on the maximum return period at which MSA is performed (see Section 4.2).

UPD failure rates vary between $1\text{E-}05$ to $6.62\text{E-}03$ and 51% of the municipalities are characterized by rates larger than $1\text{E-}03$; 30% of sites have rates within $1\text{E-}04$ and $1\text{E-}03$; about the 20% of municipalities have rates lower than $1\text{E-}04$. A comparison between Figure 15a and Figure 10c shows the effect on results of the hazard classes. More in details, all the sites belonging to the low hazard class show $\lambda_{E,UPD}^{04}$ lower than $5\text{E-}05$, whereas 95% of the municipalities in the high hazard class have rates higher than $1\text{E-}03$.

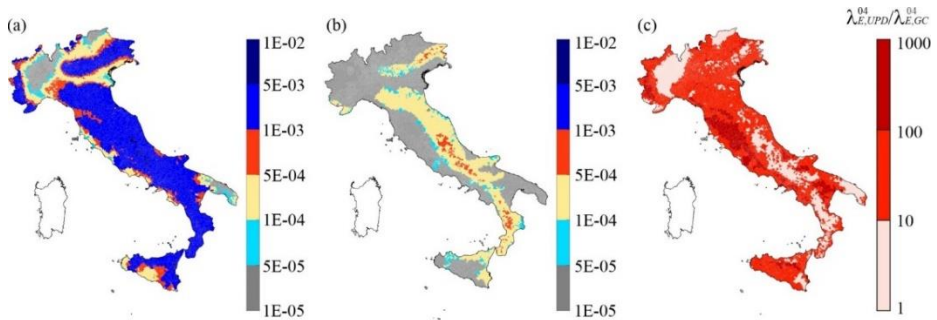


Figure 15. Maps of failure rates per municipalities considering (a) UPD and (b) GC evaluated adopting MPS04 and considering FB structures; (c) map of the ratios of the failure rates evaluated for UPD and GC.

GC failure rates range between $1\text{E-}05$ and $8.91\text{E-}04$. Most of the sites (64%) presents a failure rate lower than $5\text{E-}05$ and values higher than $5\text{E-}05$ are associated to the municipalities belonging to high-hazard regions. The largest failure rates are computed in municipalities of central and southern Apennines, reflecting the hazard of the region. With respect to UPD, GC failure rates are up to two orders of magnitude lower as shown by the map of ratios, $\lambda_{E,UPD}^{04} / \lambda_{E,GC}^{04}$, reported in Figure 15c. In 60% and 8% of the municipalities the ratio is between $1\text{E+}01$ and $1\text{E+}02$, and higher than $1\text{E+}02$, respectively. For the remaining 32% of the sites, the same order of magnitude for the two failure rates is computed; results in these sites are controlled by the lower bound of $1\text{E-}05$.

4.5.2 Alternative risk metric

The hypotheses characterizing the ideal scenarios discussed in this study are not available in literature and a comparison of the results of this work with other

similar studies is not directly possible. However, it may be useful to provide risk maps in a comparable representation with respect to available studies dealing with the national seismic risk of existing structures. These risk maps are often presented in two scales (e.g., [77,78]): (i) the percentage and (ii) the absolute number of failed buildings per municipality in a given time interval (usually, one year). Thus, it should be noted that, in accordance with Eq. (14), all the maps of failure rates shown here can also be interpreted as maps of the annual number of failed buildings in each municipality divided by the total number of buildings of the same municipality. In any case, the rates in Figure 11 are also converted into the mean annual number of failed buildings per municipality, that is, from Eq. (14) assuming Δt equal to one year, see Figure 16.

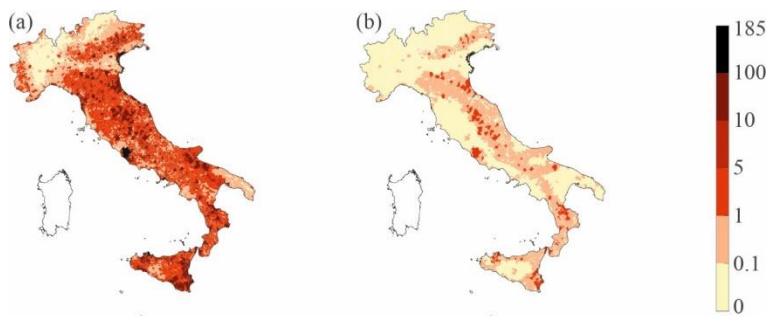


Figure 16. Maps of the expected number of failed buildings in one year per municipality considering (a) UPD and (b) GC.

When the UPD performance level is considered, Figure 16a, for the 26% of the municipality the expected value of failed building is lower than 0.1, it ranges between 0.1 and 1 for the 32% of municipalities whereas it is between 1 and 5 for the 34% of the municipalities; finally, the expected number of failed buildings is larger than 5 in 8% of the municipalities. Figure 16b presents the expected value of buildings at GC. In most of the municipalities (73%), the expected number of failed buildings ranges between 0 and 0.1. Among the remaining municipalities, that mostly belong to the high-hazard class, this expected number ranges between 1 and 5 in 26% of the considered sites, and it is larger than 5 only in 1% of the municipalities.

4.5.3 Seismic Risk for Base-Isolated Structures Based on MPS04

This section discusses the case in which all the existing buildings (except those in the low-hazard class) are replaced with RC BI structures; seismic hazard is

evaluated via PSHA based on MPS04. The resulting maps of failure rates for UPD and GC are reported in Figure 17a and Figure 17b, respectively. As shown, the two maps are similar; this is because UPD refers to the response of superstructure that is typically not affected by damages as long as the isolation system does not fail. However, the failure of the isolation system corresponds to GC. Only for UPD, few municipalities (0.38%) have failure rates larger than $5E-04$; for both performance levels, more than 70% of the municipalities have rates lower than $5E-05$.

In Figure 18, the two alternative substitution criteria are compared providing, for each municipality, the ratio between the values of the failure rates related to BI and FB structures; UPD and GC are considered in Figure 18a and Figure 18b, respectively. Reddish color is assigned when the failure rate associated to BI structures is larger than the one computed for FB structures; green is the opposite case. When comparison refers to UPD, 100% of sites are green: failure rates for BI structures are one and two orders of magnitude lower than FB structures for 67% and 23% of the sites, respectively. For GC, the failure rate associated to the FB structures are larger than those associated to the BI structures for 85% of the municipalities. On the other hand, in 15% of the sites, GC rates for BI are larger than FB and the ratio of failure rates is between 1 and 10, whereas such a rate is larger than 10 only for 0.2% of the cases. These results, although possibly counterintuitive, are in accordance with the findings of other authors (e.g., [79,80]).

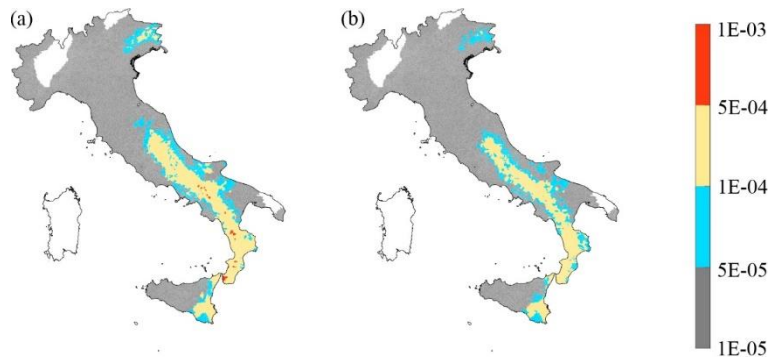


Figure 17. Maps of failure rates per municipalities considering (a) UPD and (b) GC evaluated adopting MPS04 source model and considering BI structures.

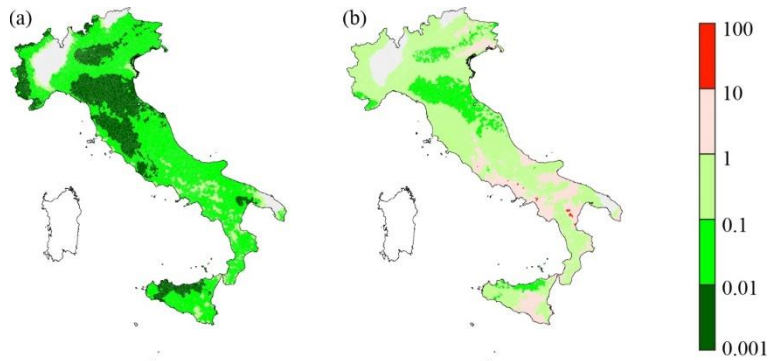


Figure 18. Ratio of the failure rates computed for BI and FB structures: (a) UPD, and (b) GC.

4.5.4 Seismic Risk for Fixed-Base Structures Based on MPS19

In this section, the results of Eq. (13) when hazard curves are computed via PSHA based on MPS19 and considering FB code-conforming buildings, are discussed. When UPD is concerned, the failure rates range from $1\text{E-}05$ to $8.1\text{E-}03$. Less than the 0.1% of the municipalities have UPD failure rates lower than $1\text{E-}04$; in the 39% of the sites, mostly belonging to the low-seismicity class, they are from $1\text{E-}04$ to $1\text{E-}03$, whereas, in most of the sites, (61%) failure rates are larger than $1\text{E-}03$. As regards GC failure rates, they are mostly between $1\text{E-}05$ in $1.3\text{E-}03$; the largest values are in north-eastern and central Italy.

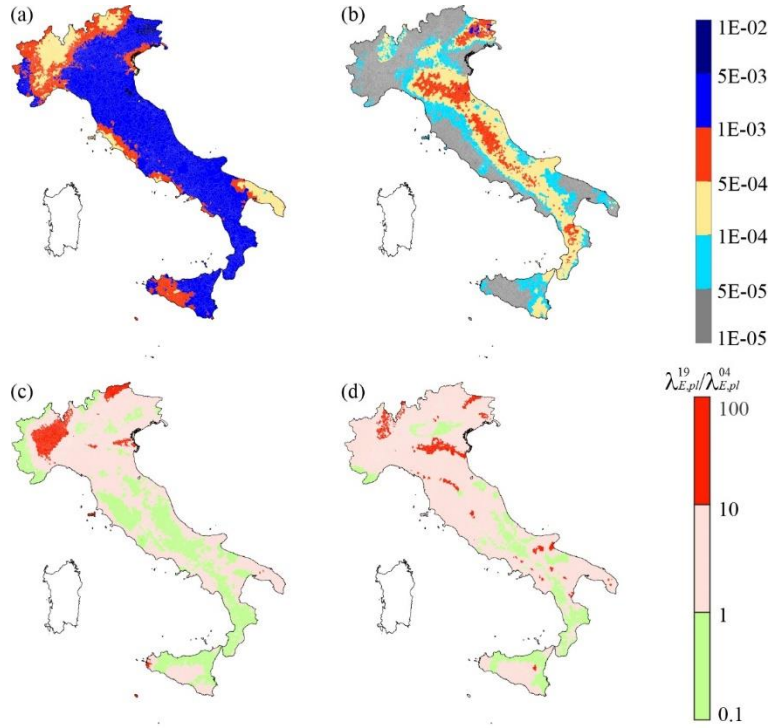


Figure 19. Maps of failure rates per municipalities considering (a) UPD and (b) GC evaluated adopting MPS19 source model; map of the ratios of the failure rates computed according to MPS19 and MPS04: (c) UPD and (d) GC.

The discussed results are also presented in the form of maps of the ratios between failure rates based on MPS19 and those based on MPS04. Figure 19c refers to UPD $\left(\lambda_{E,UPD}^{19}/\lambda_{E,UPD}^{04}\right)$, whereas Figure 19d refers to GC $\left(\lambda_{E,GC}^{19}/\lambda_{E,GC}^{04}\right)$. In both figures, reddish color is adopted for the cases in which MPS19 produces failure rates larger than MPS04, green otherwise. For UPD, most of the case, that is 87% of the municipalities, show failure rates resulting from the two source models of the same order of magnitude. MPS19 provides failure rates one order of magnitude larger than MPS04 in the low hazard class of the Northern Italy and in few sites of the Po Valley and Sicily (i.e., 13% of the sites). Overall, UPD failure rates from MPS19 are larger than MPS04 for the 72% of the Italian municipality (excluding Sardinia); such sites correspond, mostly, to the low and medium hazard classes according to MPS04. Conversely, in the 28% of sites, mostly belonging to the high-hazard class, MPS19 provides UPD failure rates lower than MPS04. As regards GC, Figure

19b shows that failure rates are of the same order of magnitude regardless the adopted source model in the 94% of the municipalities. In 84% of sites, the MPS19 failure rates are larger than the MPS04; in the remaining 16% of sites, mostly located along the Apennines and in Sicily, MPS19 rates are lower than MPS04.

4.5.5 Seismic Risk for Fixed-Base Structures Accounting for Mainshocks-Aftershocks Contribution to the Hazard

This section discusses the risk assessment when the contribution of mainshock-aftershocks sequences is considered via SPSHA based on MPS04. The failure rates are computed referring to UPD and GC, that is λ_{UPD}^{04} and λ_{GC}^{04} . Results are shown, for each municipality, in term of comparison with respect to those from PSHA (Figure 15). As expected, all the ratios are larger than one: UPD ratios varies between 1.25 and 1.50 in most of the municipalities (89%); all the values lower than 1.25 are associated to municipalities (10% of the total) belonging to the low-hazard class whereas in the 1% of the municipalities, all belonging to the high-hazard class, ratios are higher than 1.50 (up to 1.60). As regards to GC, the ratios increase up to almost 1.80. In the low-hazard class and in most of the mid-hazard class, the ratios of the failure rates are between 1.0 and 1.25, (58% of the Italian municipalities). They are between 1.25 and 1.50 in 17% of the sites that correspond to the Calabrian arc and some municipalities of the northeastern Italy. In the other municipalities, all belonging to the high-hazard class, the ratios vary between 1.50 to 1.80. In conclusion, the aftershocks' effect to the seismic hazard may almost double the GC failure rates.

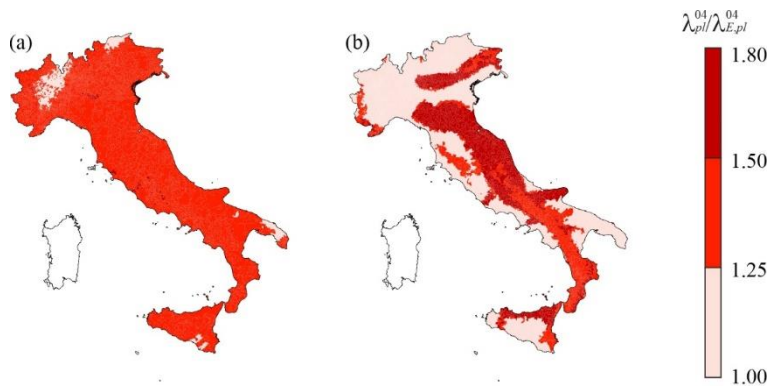


Figure 20. Ratio of the failure rates computed via SPSHA and PSHA: (a) UPD and (b) GC.

4.6 CONCLUSIONS

This study herein presented evaluated the ideal seismic risk of Italy at municipality scale; i.e., assuming that all the residential buildings are replaced with code-conforming structures. For each municipality, the risk is quantified via the mean number of mainshocks (or mainshock-aftershocks seismic sequences), that in one year, cause failure of a randomly selected building of the municipality of interest. Considered structural performances are usability-preventing damage (UPD) and global collapse (GC). Structures designed, modelled, and analyzed in the RINTC project for three Italian sites (i.e., L'Aquila, Naples, and Milan), were adopted to represent code-conforming buildings of the municipalities in high-, mid- and low-seismic hazard classes, respectively. These classes were identified according to the value of the PGA_{475} computed for each Italian municipality. Different risk modelling options were considered, and the main conclusions from them are listed hereunder.

- When PSHA is based on the current reference Italian hazard model (MPS04) and fixed-base buildings are considered, it is shown that, although the design actions are characterized by the same exceedance probability, the failure rates are largely different among different structural typologies and sites. This generalizes the results of the RINTC project. UPD failure rates, over the country, vary between $1E-05$ and $6.62E-03$; 51% of the municipalities are characterized by failure rates larger than $1E-03$ while all the others are lower. Referring to the GC, failure rates range from $1E-05$ to $8.91E-04$ and the most of Italian municipalities (64%) shows a failure rate lower than $5E-05$. The replacement criterion was proven to be significant for such results; indeed, failure rates show relatively low variability within each seismic hazard class. In terms of annual expected number of failed buildings per municipality, the results show that, in most of the sites (i.e., 34%), the number of buildings expected to exceed UPD is between 0.1 and 1. As regards GC, the expected number of failed building ranges between 0.1 and 1 at 73% of the Italian municipalities.
- Considering base-isolated buildings replacing all the existing structures, with MPS04 hazard, the UPD and GC failure rates are comparable in each Italian municipality. As expected, they are lower than the counterpart computed for FB structures. This happens at 100% of sites for UPD, for which rates differ of one or two orders of

magnitude. In the case of GC, it occurs at 85% of the sites whereas, in the remaining 15%, BI structures provide larger rates than FB.

- When PSHA is based on a recent Italian hazard model (MPS19) the UPD risk of FB code-conforming buildings shows that failure rates are higher than those due to MPS04 at 72% of the municipalities (mostly corresponding to the low-, mid-seismic hazard classes). Such a percentage increases to 84% of the sites in the case of GC failure rates.
- When the effect of mainshock-aftershocks sequences is considered (i.e., in the case of SPSHA based on MPS04) the SPSHA/PSHA ratios of UPD failure rates for FB buildings vary from 1.25 to 1.50 in 89% of the municipalities. The analogous ratios, in the GC case, reach 1.80 in the high-hazard regions.

It must be finally remarked that all the results herein presented follow some (arbitrary) choices made for the hazard and the vulnerability characterization. Moreover, the limited available information lead to assume stochastic independency between soil conditions and structural typologies and the definition of substitution criteria based on the hazard classification of the Italian municipalities. Nevertheless, the provided maps may help to provide insights on the seismic risk in Italy inherent to the current building code.

4.7 DATA SOURCES

In addition to the cited references, data used in this study were accessible from the following source (last accessed 03/08/2021): *Istituto Nazionale di Statistica (ISTAT)* (<https://www.istat.it/it/archivio/222527>)

Chapter 5 – OPERATIONAL EARTHQUAKE LOSS ASSESSMENT ON EXISTING ASSETS

5.1. INTRODUCTION

Operational earthquake forecasting (OEF) is a recently developed branch of seismology that allows to constantly update the short-time estimates of seismicity in a region in which the earthquake activity is continuously monitored [81]. Although the efficacy of the OEF for seismic risk management and mitigation is currently under debate within the scientific community (e.g., [82,83]), the possibility of using the information provided by the OEF system for real-time risk assessment and mitigation is worth of investigation.

In Italy, because of the work of the *Istituto Nazionale di Geofisica e Vulcanologia*, a system for operational earthquake forecasting, named OEF-Italy [84], exists. It acquires information from the national monitoring network that continuously records the seismic activity in the country. Such information is used to probabilistically forecast the weekly expected number (i.e., rates) and locations of earthquakes with magnitude above a threshold occurring in the monitored area. On the basis of data provided by OEF-Italy, a system for operational earthquake loss forecasting (OELF), named MANTIS-K was developed [8]. MANTIS-K combines the weekly seismicity rates with vulnerability and inventory models for the Italian building stock to obtain weekly forecasts of seismic risk (consequences) metrics, that is, the expected number of collapsed buildings, fatalities, injuries, and displaced residents. However, MANTIS-K has some limitations that may affect the accuracy of the loss forecasting. The system, in its current formulation, adopts vulnerability and inventory models that do not change in time, that is, OEF rates are the only input that change among the loss forecasting computed at different times. This does not appear as an issue in *peace* conditions (i.e., when no earthquake has recently occurred in the area), but it may affect results right after the occurrence of a damaging earthquake (i.e., during a seismic crisis). Indeed, in such a case, MANTIS-K accounts for the fact that the estimated seismicity in the area increases (e.g., [85]) but it is not able to model that the structures in the area may have already been damage by previous seismic events. However, seismic crises are the cases in which the social relevance of the OELF results is the highest. Thus, to overcome such limitations, an upgraded version of the system, named MANTIS v2.0, is currently under-development in the context of the

ongoing research project RISE (Real-time earthquake rIsk reduction for a ReSilient Europe). In particular, profiting from the structural reliability model developed for accounting seismic damage accumulation on single structures [86], this document discusses how the MANTIS-K framework can be modified to account for evolutionary vulnerability models, that is seismic damage accumulation on the existing building portfolio.

The paper is structured such that MANTIS-K system is briefly recalled. Then the improved methodology at the base of MANTIS v2.0 is described together with the involved ground-motion and vulnerability models. It follows an application of the updated software to a case study, i.e., a past Italian earthquake sequence that allows to identify some of the differences between the two versions of the software. Final conclusions close the paper.

5.2. MANTIS-K

OEF-Italy system, continuously in time (t), analyses data of the recorded seismicity history of the country, $H(t)$, provided by the national monitoring network. Thus, referring to a grid of point-like seismic sources covering the whole Italian territory and some sea, OEF-Italy provides, for each source identified by coordinates $\{x, y\}$, the expected number per unit time (Δt , equal to one week) of earthquakes above magnitude four ($M4+$) i.e., $\lambda(t, x, y)$ that is the weekly rate of earthquake for the $\{x, y\}$ source. According to [8], knowing the rates associated to the whole grid of seismic sources, it is possible to retrieve the expected value of earthquakes per unit time that, in a given area (e.g., a municipality) identified by coordinates $\{w, z\}$, makes the building of a structural typology of interest, (k), to fail, that is, to reach a defined performance level, $PL^k = pl_j$. Indeed, it is assumed that a finite number, say n , of performance levels, PL , can be used to discretize all the possible (infinite) damage conditions of the structure: pl_1 identifies the undamaged state, pl_n the conventional collapse, pl_j , with $j = 2, \dots, n-1$, intermediate damages condition between the undamaged and the collapse state (increasing the value of j , the level of damage increases). The sought rate of earthquake causing

failure of one building of the structural typology k and located in $\{w, z\}$, $\lambda_{PL=pl_j}^k(t, w, z)$, can be computed via Eq. (17)

$$\lambda_{PL=pl_j}^k(t, w, z) = \iint_{x, y} \lambda(t, w, z) \cdot \sum_{ms} P[PL^k = pl_j | ms] \cdot \int_m P[MS = ms | m, R(x, y, w, z)] \cdot f_M(m) \cdot dm \cdot dx \cdot dy \quad (17)$$

in which $P[PL^k = pl_j | ms]$ is the probability that the building of the k -th structural typology reaches pl_j given the occurrence of a certain macroseismic, MS , intensity level, ms , in one earthquake; $R(x, y, w, z)$ is the distance between the point-like seismic source $\{x, y\}$ and the site of interest $\{w, z\}$; $f_M(m)$ is the probability density function of the magnitude of the earthquakes (assumed to be independent on the seismic source) conditional to the earthquake occurrence on the source; $P[MS = ms | m, R(x, y, w, z)]$ is the probability of observing ms at $\{x, y\}$ given an earthquake of magnitude m at distance $R(x, y, w, z)$ and it is usually provided by a model of macroseismic propagation. Eq. (17) is the one at the base of MANTIS-K.

However, $\lambda_{PL=pl_j}^k(t, w, z)$ can be also computed replacing MS with the ground motion intensity measure, IM , as per Eq. (18):

$$\lambda_{PL=pl_j}^k(t, w, z, \theta_q) = \iint_{x, y} \lambda(t, w, z) \cdot \int_{im} P[PL^k = pl_j | IM = im] \cdot \int_m f_{IM|M, R, \theta_q}(m, R(x, y, w, z), \theta_q) \cdot f_M(m) \cdot dm \cdot dx \cdot dy \quad (18)$$

In the equation, $f_{IM|M, R, \theta_q}(m, R(x, y, w, z), \theta_q)$ and $P[PL^k = pl_j | IM = im]$ substitute $P[MS = ms | m, R(x, y, w, z)]$ and $P[PL^k = pl_j | ms]$ of Eq. (17), respectively. $f_{IM|M, R, \theta_q}(m, R(x, y, w, z), \theta_q)$ is the probability density function (pdf) of IM at the site $\{w, z\}$ given an earthquake of magnitude $M = m$

generated at the $\{x, y\}$ point-like source. Such a pdf can be provided by a ground motion prediction equation (GMPE). The latter usually includes other covariates such as local soil conditions (and others not explicitly reported here) that are represented by soil classes, the number of which depends on the considered GMPE. Here the soil class is indicated as θ_q with $q = 1, \dots, Q$, being Q the number of soil classes considered in the adopted GMPE. The soil class is often deterministically known; on the other hand, the case in which θ_q has to be considered as a random variable is discussed in the following (see Eq. (20)). $P[PL^k = pl_j | IM = im]$ is the probability that a structure of the k -th structural typology reaches pl_j given that $IM = im$ at the construction site (such a probability is assumed independent on θ_q); it can be retrieved by the so-called fragility functions of the structural typology that provide the conditional probability that the structure reaches or exceeds pl_j given $IM = im$, that is $P[PL^k \geq pl_j | IM = im]$. Thus, knowing the fragility functions of the structural typology of interest for pl_j and pl_{j+1} , the sought $P[PL^k = pl_j | IM = im]$ can be computed according to Eq. (19):

$$\begin{aligned} P[PL^k = pl_j | IM = im] &= \\ &= P[PL^k \geq pl_j | IM = im] - P[PL^k \geq pl_{j+1} | IM = im] \end{aligned} \quad (19)$$

If the local soil conditions are not the same for all the buildings of the k -th structural typology and/or they are not deterministically known, the random variable representing the soil class at the site of the generic building of the structural typology can be considered defining its probability mass function, $P[\theta_q]$. In such a case, $\lambda_{PL=pl_j}^k(t, w, z)$ can be computed knowing the conditional pdfs of IM for all the soil classes and applying Eq. (20):

$$\lambda_{PL=pl_j}^k(t, w, z) = \sum_{q=1}^Q P[\theta_q] \cdot \lambda_{PL=pl_j}^k(t, w, z, \theta_q) \quad (20)$$

Although, Eq. (17) and Eq. (20) provide, in principle, the same result, the latter is introduced here because the use of IM is a preliminary condition for the

formulation of MANTIS v2.0, as will be clearer in the next section. However, before discussing such an improvement, the way in which the number of damaged buildings can be computed should be recalled.

Assuming that, in the small time interval, $(t, t + \Delta t)$, the process of earthquake occurrence can be approximated by a homogeneous Poisson process (HPP), if the number of building of the k -th structural typology at $\{w, z\}$ site is available, $N_B^k(w, z)$, the expected number of failed buildings in $(t, t + \Delta t)$, that is $N_{B, pl_j}^k(t + \Delta t, w, z)$, can be approximately computed via Eq. (21):

$$N_{B, pl_j}^k(t + \Delta t, w, z) \approx N_B^k(w, z) \cdot \lambda_{PL=pl_j}^k(t, w, z) \cdot \Delta t \quad (21)$$

5.3. MANTIS V.2

The upgraded version of the OELF system is formulated to account for the evolution, over time, of the structural damage conditions. This implies that loss forecasting must account for the possible structural damage accumulation due to the occurrence of more than one earthquake in the forecasting period. Moreover, the upgraded system has to estimate the possible damage due to the occurred earthquakes and, consequently, forecast the performance level of buildings that, at the time of computation, are already at an intermediate performance level. In the following, the loss forecasting referring to a building inventory constituted by already damaged buildings is discussed first. Then, the possible structural damage accumulation due to the occurrence of more than one earthquake in the forecasting time window is analysed. Finally, the adopted strategy for updating the inventory to account for the damage evolution in the sequence is described.

5.3.1 Loss forecasting referring to already damaged buildings

In order to account for damage accumulation, MANTIS v2.0 some hypotheses about the structural damage evolution over time have to be introduced. More specifically, it is assumed that, for each building of the considered structural typology, the probability to pass from pl_i with $i = 1, \dots, n-1$ to another (worse) performance level, pl_j with $j > i$, due to one earthquake does not depend on the damage history of the structure, but it only depends on pl_i and on the intensity of the earthquake at the site of the structure, that is im . This

hypothesis, usually accepted in structural engineering contexts, allows one to adopt a Markovian approach to model the evolution of seismic structural damage. Moreover, discretizing the time in intervals of fixed width, a Markov-chain approach can be adopted in analogy with [86]. However, it should be noted that, in the cited paper, the damage accumulation process was developed for single structures whereas here it is extended to all the buildings of the k-th structural typology.

Under these hypotheses, it is possible to compute the probability that a structure, located at the $\{w, z\}$ site, passes from pl_i to pl_j ($j > i$) given the occurrence of a generic earthquake (an earthquake of unknown magnitude and location), $P_{i,j}^{(k)}(t, w, z)$ as per Eq. (22):

$$P_{i,j}^k(t, w, z) = \sum_{q=1}^Q P[\theta_q] \cdot \int_{im} P[PL^k = pl_j | pl_i, IM = im] \cdot \int_x \int_y \frac{\lambda(t, w, z)}{\nu(t, w, z)} \cdot \int_m f_{IM|M,R,\theta_q}(im|m, R(x, y, w, z), \theta_q) \cdot f_M(m) \cdot dm \cdot dx \cdot dy \cdot d(im) \quad (22)$$

In the equation $P[PL^k = pl_j | pl_i, IM = im]$ is the probability the structure makes a transition from pl_i to pl_j for a given value of IM . Such a probability can be evaluated, via Eq. (23), as the difference between two probabilities, both conditional on the value of the intensity measure and the performance level pl_i in which the structure is before the earthquake occurrence; such conditional probabilities are those of reaching or exceeding pl_j and pl_{j+1} , respectively and are defined as state-dependent fragility functions [86]. Finally, $\lambda(t, x, y)/\nu(t, w, z)$ is the probability that, given that an earthquake affects the $\{w, z\}$ site, it is generated by the $\{x, y\}$ source; $\nu(t, w, z)$ is the rate of the earthquakes affecting the $\{w, z\}$ site and can be computed as:

$$\nu(t, x, y) = \iint_{x,y} \lambda(t, x, y) \cdot dx \cdot dy .$$

$$P[PL^k = pl_j | pl_i, IM = im] = P[PL^k \geq pl_j | pl_i, IM = im] - P[PL^k \geq pl_{j+1} | pl_i, IM = im] \quad (23)$$

A matrix collecting all the transition probabilities of the same structural typology at $\{w, z\}$ site given the occurrence of an earthquake, $[P^k(t, w, z)]$, can be defined as in Eq. (24) (for the sake of simplicity, the dependency on $\{w, z\}$ and time is neglected for the terms within the matrix):

$$[P^k(t, w, z)] = \begin{bmatrix} 1 - \sum_{j=2}^n P_{1,j}^k & P_{1,2}^k & \cdots & \cdots & P_{1,n}^k \\ 0 & 1 - \sum_{j=3}^n P_{2,j}^k & \cdots & \cdots & P_{2,n}^k \\ \cdots & \cdots & \cdots & \cdots & \cdots \\ 0 & \cdots & 0 & 1 - P_{(n-1),n}^k & P_{(n-1),n}^k \\ 0 & \cdots & \cdots & 0 & 1 \end{bmatrix}. \quad (24)$$

The matrix has $n \times n$ dimension and the element at row i and column j is the probability that, due to a generic earthquake, one structure of the k -th typology, that is in pl_i before the earthquake, goes to pl_j due to the earthquake occurrence. Thus, $[P^k(t, w, z)]$ is an upper triangular matrix because the structures cannot improve their damage condition due to an earthquake occurrence. Finally, the n -th state is the so-called *absorbing state*, from which the structures cannot escape, thus $P_{n,n}^k = 1$.

The unit time transition probability matrix for the structural typology, $[P_E^k(t, t + \Delta t, w, z)]$, collects the transition probabilities from one damage state to another in Δt . It can be computed assuming that, in the unit time, the process of earthquake occurrence can be approximated by a HPP (in analogy with what was discussed for MANTIS-K). Thus, if $\nu(t, x, y)$ is small (i.e., the probability of more than one earthquake in Δt is negligible), the matrix $[P_E^k(t, t + \Delta t, w, z)]$ can be approximated via Eq. (25):

$$\begin{aligned}
& \left[P_E^k(t, t + \Delta t, w, z) \right] \approx \nu(t, x, y) \cdot \left[P^k(t, w, z) \right] + \{1 - \nu(t, x, y)\} \cdot [I] = \\
& = \begin{bmatrix} 1 - \sum_{j=2}^n \nu \cdot P_{1,j}^k & \nu \cdot P_{1,2}^k & \cdots & \cdots & \nu \cdot P_{1,n}^k \\ 0 & 1 - \sum_{j=3}^n \nu \cdot P_{2,j}^k & \cdots & \cdots & \nu \cdot P_{2,n}^k \\ \cdots & \cdots & \cdots & \cdots & \cdots \\ 0 & \cdots & 0 & 1 - \nu \cdot P_{(n-1),n}^k & \nu \cdot P_{(n-1),n}^k \\ 0 & \cdots & \cdots & 0 & 1 \end{bmatrix}, \quad (25)
\end{aligned}$$

where $\nu(t, x, y)$ approximates the probability of one (or more) earthquake occurrence in the unit time, $\{1 - \nu(t, x, y)\}$ approximates the probability of no earthquake in the unit time and $[I]$, the identity matrix, accounts for the fact that, when no earthquake occurs, the structural typology does not change its performance level.

Once $\left[P_E^k(t, w, z) \right]$ is known, the expected number of buildings in each damage state at time $(t + \Delta t)$ can be computed knowing the number of buildings in each damage state at time t (see Section 2.2.3). More specifically, being $\mathbf{N}_B^k(t, w, z)$ the vector collecting the number of the buildings of the k -th structural typology located in $\{w, z\}$ in each performance level at the time t as per Eq. (26):

$$\mathbf{N}_B^k(t, w, z) = \left\{ N_{B,pl_1}^k(t, w, z), N_{B,pl_2}^k(t, w, z), \dots, N_{B,pl_n}^k(t, w, z) \right\}, \quad (26)$$

the vector collecting the expected number of buildings in each performance level at $(t + \Delta t)$, $\mathbf{N}_B^k(t + \Delta t, w, z)$, is provided by Eq. (27):

$$\mathbf{N}_B^k(t + \Delta t, w, z) = \mathbf{N}_B^k(t, w, z) \cdot \left[P_E^k(t, w, z) \right]. \quad (27)$$

Indeed, in Eq. (27), the transition probabilities from a starting damage state to an arriving one are multiplied by the corresponding number of buildings in the starting damage state. Eq. (27) in MANTIS v2.0 substitutes the corresponding Eq. (21) implemented in MANTIS-K.

5.3.2 Loss forecasting accounting for more than one earthquake

Depending on the seismic history, the rates of OEF may result in a value of $v(t, w, z)$ that corresponds to a non-negligible probability of more than one earthquake in Δt . In this case, the approximation introduced in Eq. (25) is not acceptable, but the application of the described Markovian approach remains possible if the original unit time, i.e. one week, is partitioned into smaller intervals such that, in each of them, the probability of more than one earthquake is negligible. Thus, the way in which the original Δt has to be partitioned depends on the distribution of the number of expected earthquakes over time. Once the length of the new time intervals is defined, Eq. (25) can be applied for each of them and the transition probability matrix referred to one week can be computed proofing of the Markov-chain properties. The resulting transition probability matrix will account for the possible damage accumulation due to multiple forecasted earthquakes in one week.

5.3.3 Inventory update

After the occurrence of each earthquake, it may be important to assess the damage condition of the building stock. To this aim, let us assume that the observed IM at the $\{w, z\}$ site, im^* , is known; the probability that the building in the k -th structural typology passed from pl_i to pl_j due to im^* , $P_{i,j}^{k*}(w, z)$, can be derived by the already introduced state-dependent fragility functions, as
$$P\left[PL^k = pl_j \mid pl_i, IM = im^*\right].$$

In fact, the value of im^* is known if an accelerometric station provides the recorded ground motion at $\{w, z\}$ site. If such a data is not available, it is possible to compute a distribution of the intensity measure of interest at $\{w, z\}$ conditional to the earthquake magnitude, m^* , the distance between the earthquake and the site, r^* , the soil class, θ_q , and possibly information from ground motion recorded at other sites, χ , that is $f_{IM|M,R,\theta,\chi}(im \mid m^*, r^*, \theta_q, \chi)$ [87,88]. Thus, it is sufficiently general to assume that, although the im^* value is unknown in $\{w, z\}$, $P_{i,j}^{k*}(w, z)$ can be obtained via Eq. (28):

$$P_{i,j}^{k*}(w,z) = \sum_{q=1}^Q P[\theta_q] \cdot \left\{ \int_{im=0}^{+\infty} P[PL^k = pl_j | pl_i, IM = im] \cdot f_{IM|M,R,\theta_q,X}(im | m^*, r^*, \theta_q, \chi) \cdot d(im) \right\}. \quad (28)$$

A transition probability matrix given the occurrence of the earthquake of m^* magnitude and r^* distance can be defined by collecting the values of $P_{i,j}^{k*}(w,z)$ for both i and j varying between 1 and n , as per Eq. (29):

$$[P^{k*}(w,z)] = \begin{bmatrix} 1 - \sum_{j=2}^n P_{1,j}^{k*} & P_{1,2}^{k*} & \cdots & \cdots & P_{1,n}^{k*} \\ 0 & 1 - \sum_{j=3}^n P_{2,j}^{k*} & \cdots & \cdots & P_{2,n}^{k*} \\ \cdots & \cdots & \cdots & \cdots & \cdots \\ 0 & \cdots & 0 & 1 - P_{(n-1),n}^{k*} & P_{(n-1),n}^{k*} \\ 0 & \cdots & \cdots & 0 & 1 \end{bmatrix}. \quad (29)$$

Moreover, if more than one earthquake occurs in the Δt , say $n_E = \{1, \dots, N_E\}$, a transition probability matrix per event can be defined, $[P_{n_E}^{k*}(w,z)]$, in accordance with Eq. (29). The cumulative effect of the N_E earthquakes can be computed by multiplying the corresponding transition probability matrices. Thus, the vector collecting the estimated number of buildings in each damage state, $\mathbf{N}_B^k(t, w, z)$, can be obtained from the equivalent vector estimated at the previous time interval in the same site, $\mathbf{N}_B^k(t - \Delta t, w, z)$, via Eq. (30):

$$\mathbf{N}_B^k(t, w, z) = \mathbf{N}_B^k(t - \Delta t, w, z) \cdot \prod_{n_E=1}^{N_E} [P_{n_E}^{k*}(w, z)]. \quad (30)$$

The computed $\mathbf{N}_B^k(t, w, z)$ is an input value for the operational earthquake loss forecasting, Eq. (27), as discussed in Section 5.3.1.

5.4. CASE STUDY

In this work, L'Aquila 2009 seismic swarm is retrospectively analysed with MANTIS v2.0. The characteristics of the seismic sequence are described hereafter together with the models adopted for MANTIS- v2.0 implementation. The discussion of results is reported in Section 5.5.

The mainshock (moment magnitude, M , 6.1) of the swarm struck the region at 01:32 a.m. of the 06/04/2009 and, from January 2009 to June 2010, a sequence of twenty-four earthquakes with moment magnitude larger than 4.0 occurred, within 50 km from the mainshock epicentre [89]. Among them, those with moment magnitude larger than 4.5 were eight (excluding the mainshock), all of them occurred after the mainshock in a short time interval ranging between the 06/04/2009 and 10/04/2009. Table 7 reports the coordinates of the epicentres and the magnitudes of the mainshock and of the eight $M4.5$ subsequent earthquakes.

Table 7. Earthquakes with moment magnitude larger than 4.5 identified by a progressive number (ID), latitude and longitude, in degree, and M .

Date [dd/mm HH:MM]	ID	Latitude [°]	Longitude [°]	M
06/04 01:32	1	42.342	13.380	6.1
06/04 02:37	2	42.360	13.328	5.1
06/04 03:56	3	42.335	13.386	4.5
06/04 23:15	4	42.463	13.385	5.1
07/04 09:26	5	42.336	13.387	5.1
07/04 17:47	6	42.303	13.486	5.5
07/04 21:34	7	42.372	13.374	4.5
09/04 00:53	8	42.489	13.351	5.4
09/04 19:38	9	42.504	13.350	5.2

The results of the OELF procedure are discussed considering a time window of five days ranging from the 05/04/2009 (i.e., one day before the mainshock) to 10/04/2009. It is (arbitrarily) assumed that earthquakes with magnitude lower than 4.5 produced negligible damages of the existing buildings. Thus, the updating of the building portfolio is performed considering the same earthquakes listed in Table 7. The OELF results are computed for all the municipalities that are within 100km from the epicentre of the mainshock

grouped in four sets characterized by increased distance from the mainshock. More specifically, as shown in Figure 21, the first set is constituted by the two municipalities within 10 km from the mainshock, the second set consists of 66 municipalities within 40 km; the third and the fourth sets are constituted by 283 and 598 municipalities that are within 70 km, and 100 km from the mainshock, respectively. In Figure 21 the epicentres of the considered earthquakes are also reported with the same ID defined in Table 7.

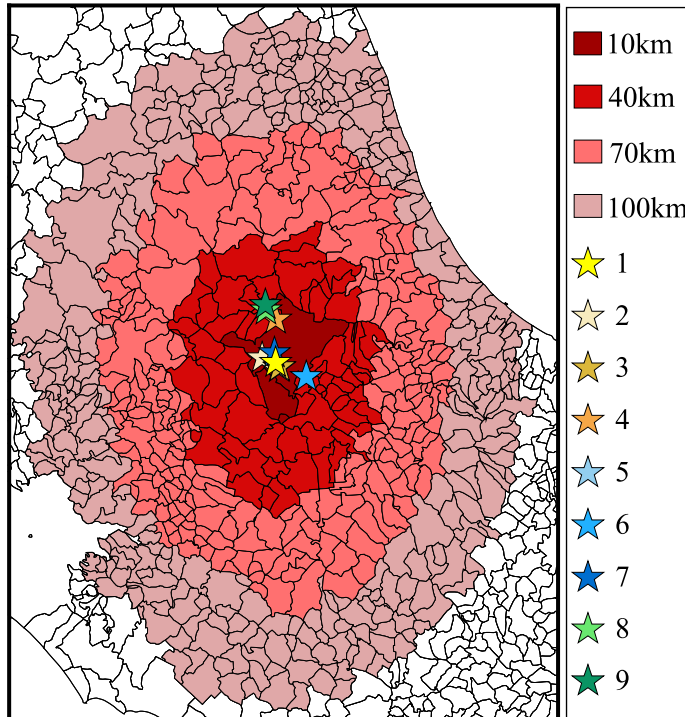


Figure 21. Map of considered municipalities grouped for the increasing distance from the mainshock; the stars represent the epicenters of the earthquakes of Table 7.

5.4.1 Input models

Models implemented in the development of MANTIS v2.0 are described in the following. In Section 5.4.1.1 the adopted hazard models are reported; in the following sections the fragility and exposure models are provided. Section 5.4.1.4 deals with the local soil model to evaluate the soil probabilities. Finally, in Section 5.4.1.5 the damage assessment model, involved in the inventory updated is explained.

Moreover, these models will be involved in Eq. (20) too, that is in MANTIS-K system (replacing those described in [8]), for the consistency of the comparison of the results between the two systems.

5.4.1.1 Hazard models

The short-term hazard modelling relies on the OEF-Italy forecasted rates $\lambda(t, x, y)$. The numerical values of the OEF rates released by OEF-Italy at midnight of the six days of interest are represented in Figure 22. As already discussed in literature [84], rates from OEF significantly increase right after strong earthquakes: in the considered cases, the maximum value of $\lambda(t, x, y)$ in the region of the sequence at 05/04 and 06/04 is about 5E-3, whereas, at 07/04 (i.e., the first forecasting after the mainshock) it increases up to 5E-2.

For each point-like seismic source, the pdf of the generated magnitude, $f_M(m)$, is derived from the Gutenberg–Richter relationship [90] with unbounded maximum magnitude and b-value equal to one. At the site of interest $\{w, z\}$, the conditional distribution of the intensity measure $f_{IM|M,R,\theta_q}(im|m, R(x, y, w, z), \theta_q)$ is computed proofing of the GMPE of [75] and the spectral correlation model of [91] spatial correlation model.

To be consistent with the fragility models (described in the next section), the geometric mean of the pseudo-spectral accelerations, $Sa(T)$, over a range of spectral periods is chosen as intensity measure [92]. Such an intensity measure, denoted as $Sa_{avg}(\mathbf{T})$, is defined by Eq. (31):

$$Sa_{avg}(\mathbf{T}) = \sqrt[L]{\prod_{l=1}^L Sa(T_l)}, \quad (31)$$

The vector \mathbf{T} collects the twenty-three vibration periods considered in [75] GMPE: $\mathbf{T}=\{0, 0.04, 0.07, 0.1, 0.15, 0.2, 0.25, 0.3, 0.35, 0.4, 0.45, 0.5, 0.6, 0.7, 0.8, 0.9, 1, 1.25, 1.5, 1.75, 2, 2.5, 2.75\}$ s, where $Sa(0s)$ represents the peak ground acceleration or *PGA*. Since the chosen GMPE does not directly provide the conditional distribution of $Sa_{avg}(\mathbf{T})$, the way in which such a distribution can be computed is discussed in APPENDIX A.

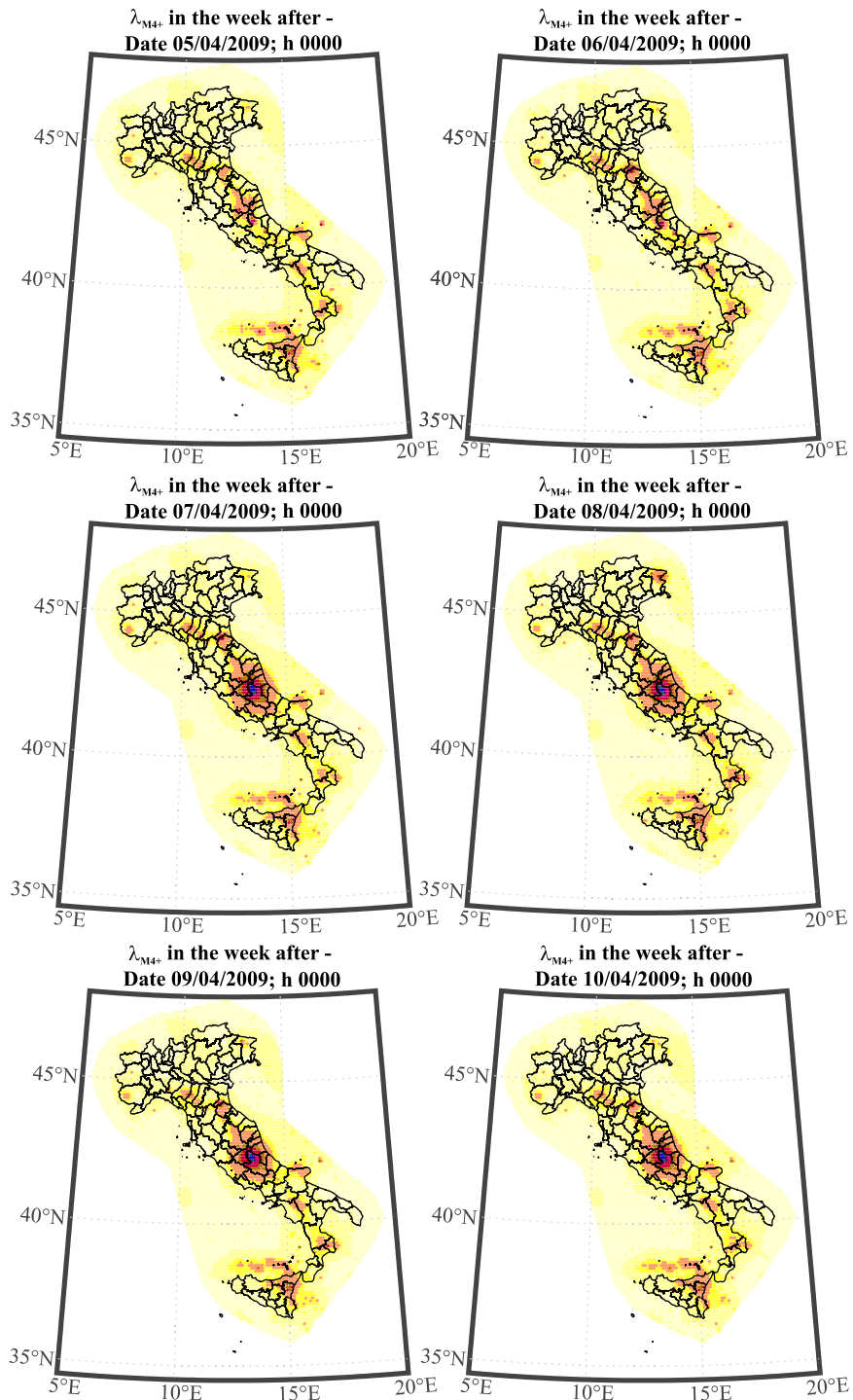


Figure 22. OEF-Italy weekly rate release from 05/04/09 to 10/04/09.

5.4.1.2 Fragility models

In a recent European research project, SERA (Seismology and Earthquake Engineering Research Infrastructure Alliance for Europe), a building taxonomy and the corresponding structural models representative of the European existing structures was developed [13]. They consider four main characteristics: (i) primary construction material (e.g., reinforced concrete (CR), unreinforced masonry made up by clay brick masonry (CL99), dressed stone masonry (STDRE), rubble stone masonry (STRUB), confined masonry (MCF), steel, etc.), (ii) typology of the lateral load resisting system (e.g., wall, moment frame, infilled frame, etc.), (iii) height expressed in terms of number of stories, (iv) seismic capacity-related properties (e.g., ductility and/or design lateral force), which depend on the evolution of seismic design in the country. Hereafter, the models associated to the Italian residential buildings are considered; that is, ten unreinforced masonry structures characterized by three stone typologies, five reinforced masonry structures, and eighteen reinforced concrete infilled frame structures with design lateral force coefficient, α , equal to 0 or 5. Masonry building typologies are characterized by a number of stories between one and five, whereas the height of reinforced concrete structures varies between one a six stories. Further details about the structural configuration are provided in APPENDIX B.

Each structural typology is modelled via equivalent single-degree-of-freedom systems or ESDoF (e.g., [64]) characterized by piece-wise linear backbone curves and a pinched hysteretic behavior exhibiting degradation of strength and of (unloading and reloading) stiffness under cyclic loading. Moreover, four damage thresholds were also defined in the SERA project on the basis of [93] and [94] identifying five performance levels: undamaged, slight damage, moderate damage, extensive damage and collapse. Finally, [14] developed fragility functions and state-dependent fragility functions for each structural typology and performance level; the adopted intensity measure is $Sa_{avg}(\mathbf{T})$ as defined in Eq. (31). Resulting state-dependent fragility functions are lognormal distributions, $\Phi[\bullet]$, with η and β parameters, as per Eq. (32):

$$P[PL^k \geq pl_j | pl_i, IM = im] = \Phi\left[\frac{\ln(im) - \eta}{\beta}\right]. \quad (32)$$

The values of η and β parameters for all the structural typologies are reported in APPENDIX B.

5.4.1.3 Exposure models

SERA project provides, for several European countries, the composition of the residential building stock at municipality scale. Thus, for each Italian municipalities, the number of the buildings of the k -th structural typology, N_B^k of Eqs. (21) and (26), is available.

Figure 23 depicts the composition of the building stock of the considered sets of municipalities. As it regards the CR structures, they have been divided according to the value of the design lateral force coefficient, thus $\alpha \neq 0$ and $\alpha = 0$ denote the absence or the presence of the seismic design, respectively. Residential buildings of the two municipalities within 10 km from the mainshock, are 15373; 63% of them are STRUB structures, 27% are RC structures with seismic design, 8% are MCF structures and there are no RC structures without seismic design. If the municipalities within 40 km, 70 km and 100 km are considered, the total number of residential buildings is 85458, 274445 and 685898 respectively. The percentage of the STRUB structures remains quite constant for all the considered municipalities, equal to about 75%; on the other hand, the percentage of RC structures with seismic design for municipalities within 40 km, 70 km and 100 km is 18%, 15%, 11% respectively. Referring to the set of 598 municipalities, 9% of the residential buildings is constituted by RC structures without seismic design, while this structural typology represents only 3% of the building portfolio when municipalities within 70 km are considered. Finally, the percentage of RC structures without seismic design becomes negligible when municipalities within 40 km are considered. In other words, the figure shows that, as expected, a large majority of Italian residential buildings are masonry buildings and RC structures are mostly located in the largest towns that, in the considered area, are represented by L'Aquila.

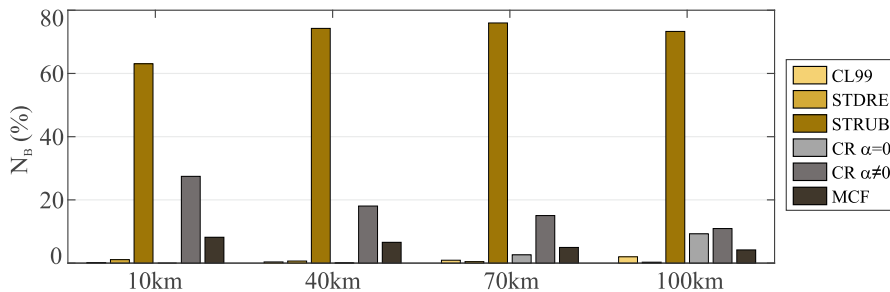


Figure 23. Composition of the building stock according to the construction material.

5.4.1.4 Local soil models

To apply Eqs. (20) and (22), the $P[\theta_q]$ probability has to be computed, at the municipality scale, for each soil class. More specifically, such a probability is computed referring to the *urbanized areas* of each municipality. They are derived by the data of the Italian *Istituto Nazionale di Statistica* (ISTAT) that classifies the Italian municipalities in four classes: *city centres*, *built areas*, *industrialized areas* and *sparse buildings areas*. The first two are considered as urbanized area (an analogous procedure was adopted in [95]). To compute $P[\theta_q]$, the grid of soil classes provided by [72] is superimposed, in area of interest, to the map of urbanized areas. Thus, for each municipality, defining the total number of points within the urbanized areas, N_{urb} , and the number of points of a specific soil classes, N_{θ_q} , $P[\theta_q]$ is computed as per Eq. (33), where $\theta_1, \theta_2, \theta_3, \theta_4$ correspond in turn to soil classes A, B, C, D of [75] GMPE:

$$P[\theta_q] = \frac{N_{\theta_q}}{N_{urb}}, \quad q = \{1, \dots, 4\}. \quad (33)$$

In Figure 24 the values of $P[\theta_q]$ are reported per municipality. In accordance with the findings of [95], soil class B is the most representative of the urbanized areas. A low percentage of soils C and A is present, while soil class D is generally low.

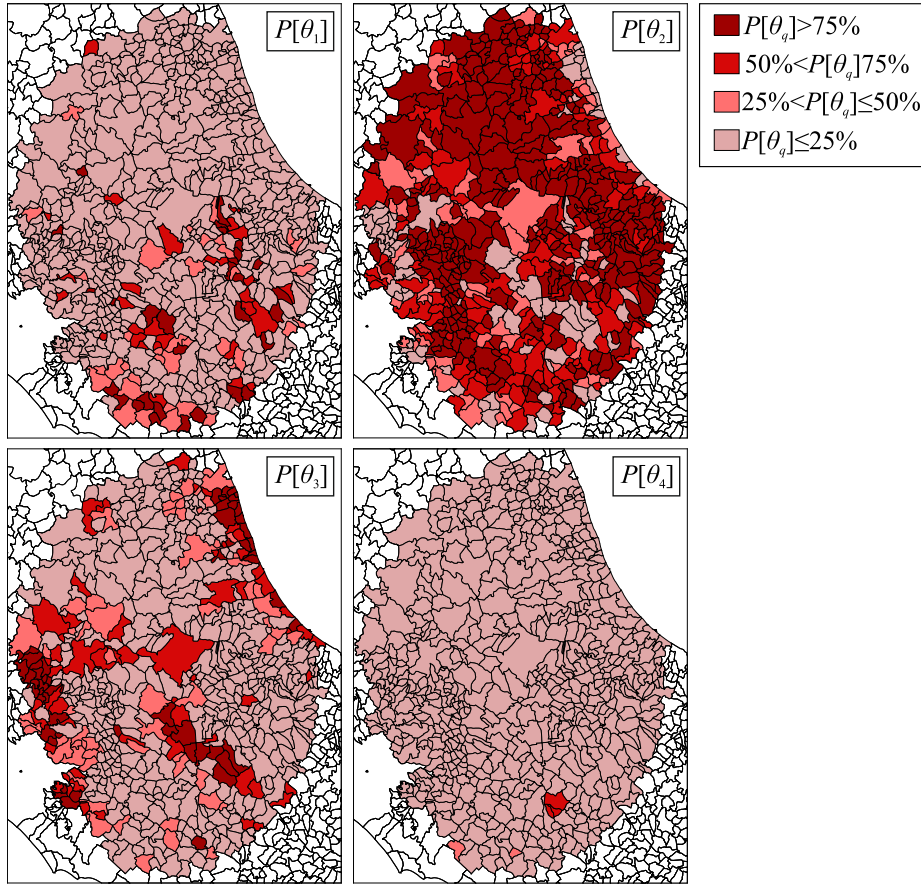


Figure 24. Soil probabilities in the municipalities within 100km from L'Aquila 2009 mainshock.

5.4.1.5 Damage assessment models

To update the building portfolio as per Eq. (28), the ground motion intensity of the occurred earthquakes is required for all the sites of interest $\{w, z\}$. The required IM is the $Sa_{avg}(\mathbf{T})$ defined as per Eq. (31). Although the latter is usually not directly available (it can be directly computed only if an accelerometric station recorded the effect of the earthquake in the site of interest), this information can be retrieved from ShakeMaps [88] that, starting from the data recorded by the Italian seismic network and the source type model

of [87]⁷, provides the expected values (and sigma) of some *IMs* (*PGA*, *Sa*(0.3*s*), *Sa*(1*s*), *Sa*(3*s*) and peak ground velocity, *PGV*) for a grid of points covering a large area around the earthquake source. As an example, the ShakeMap in terms of *PGA*, *Sa*(0.3*s*) and *Sa*(1*s*), delivered after the mainshock of the L'Aquila sequence and available at <http://shakemap.ingv.it/shake4>, are reported in the left panels of Figure 25.

Indeed, it is possible to demonstrate that, in each point of the grid, ShakeMap data can be used to retrieve the mean, and standard deviation of the logarithms of the Sa_{avg} evaluated over the periods \mathbf{T} , conditioned to the occurrence of the Sa_{avg} evaluated over the periods $\mathbf{T}^* = \{0, 0.3, 1\}$ s (i.e., the data of the ShakeMap). The mean, $E\left[\ln Sa_{avg}(\mathbf{T}) | \ln Sa_{avg}(\mathbf{T}^*), m^*, r^*, \theta\right]$, depends on the magnitude of the occurred earthquake m^* , the Joyner-Boore distance r^* and the local soil condition θ ; the standard deviation, $\sqrt{\text{VAR}\left[\ln Sa_{avg}(\mathbf{T}) | \ln Sa_{avg}(\mathbf{T}^*)\right]}$, only takes into account for the Sa_{avg} evaluated over the periods of the vector \mathbf{T}^* (see APPENDIX A for further details).

Assuming a lognormal distribution, for each grid point of the ShakeMap, the conditional probability $f_{IM|M,R,\theta,\chi}(im | m^*, r^*, \theta, \chi)$, presented in Eq. (28), can be computed. However, in accordance with Eq. (34), a transition probability for the each municipality, $P_{i,j}^{k*}(w, z)$, is required. To obtain such a value, assuming that multiple ShakeMaps values say, $n_p = \{1, \dots, N_p\}$, are available for the municipality, Eq. (28) can be applied in each of the N_p points of the ShakeMaps providing different values of $P_{i,j}^{k*}(w, z)_{n_p}$ due to different soil conditions (in principle, each point is also characterized by a different value of r^* but such an effect is considered to be minor). Thus, the value of $P_{i,j}^{k*}(w, z)$ the whole municipality, can be computed as:

⁷ Has to be highlighted that the soil characterization provided by the ShakeMap are consistent with [72] ones. Indeed, the latter is an upgraded of the work of Istituto Superiore per la Protezione e la Ricerca Ambientale [87], ShakeMap are basing on.

$$P_{i,j}^{k*}(w,z) = \sum_{n_p=1}^{N_p} P_{i,j}^{k*}(w,z)_{n_p} \cdot \frac{1}{N_p}. \quad (34)$$

The evaluated $E[Sa_{avg}(\mathbf{T})|Sa_{avg}(\mathbf{T}^*),m^*,r^*,\theta]$ are reported in Figure 25, on the right. The yellow star represents the epicentre of the earthquake, i.e., the point of coordinate $\{x^*,y^*\}$.

Finally, $P_{i,j}^{k*}(w,z)$ can be used for the construction of $[P^{k*}(w,z)]$ of Eq. (29).

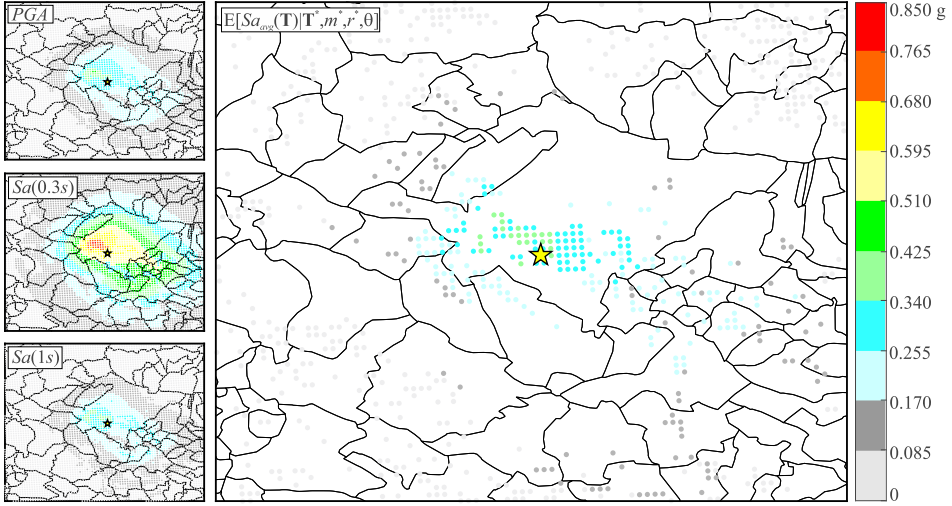


Figure 25. ShakeMap, in term of PGA , $Sa(0.3s)$ and $Sa(1s)$, of the mainshock of 2009 L'Aquila sequence in the area around the epicenter, on the left; evaluated $E[Sa_{avg}(\mathbf{T})|Sa_{avg}(\mathbf{T}^*),m^*,r^*,\theta]$ for the urbanized areas, on the right.

5.5. RESULTS

Both MANTIS-K and MANTIS v2.0 systems are (retrospectively) applied to L'Aquila 2009 seismic swarm. Forecasted losses computed at midnight of each day from 05/04/2009 to 10/04/2009 are presented and discussed referring to the percentages of damaged buildings. Although both the systems provide results at the municipality scale, in the following sections, the quantitative comparison between MANTIS-K and MANTIS v2.0 refers to results for larger areas, that is, all the municipalities within 10, 40, 70 and 100 km from the mainshock

epicentre. The maps showing numerical values for each municipality within 100 km from the mainshock are graphically reported in APPENDIX C.

5.5.1 MANTIS-K

Figure 26 shows results of MANTIS-K. In the figure, the panels from a) to d) shows the aggregated results for municipalities within 10, 40, 70 and 100 km from the epicentre of the mainshock; the results are in terms of the forecasted number of buildings in each *PL* as a function of the day of analysis. Due to the discussed limitation of the first formulation of the OELF system, the differences between the results of different days are only due to the characteristics of the OEF rates. Thus, regardless the extension of the considered area, the expected losses are negligible in the days before the mainshock (98% of undamaged buildings), i.e., the 5th and the 6th of April. Indeed, as also shown in Figure 22, before the occurrence of the mainshock, the OEF rates in the considered area were in accordance with those provided in other Italian areas characterized by large seismicity in long term conditions. This is a known characteristic of the OEF models (e.g., [8,96]).

Results associated to the 7th of April, i.e., when the OEF-Italy rates increase due to the occurrence of the M6.1 earthquake, strongly depend on the considered area. If the two municipalities within 10km are taken into account, only the 12% of the structures are forecasted to be undamaged, the 43% are expected to collapse, the 23%, 14%, and 8% belong to the intermediate performance levels, i.e., *PL*₂, *PL*₃ and *PL*₄ respectively. By enlarging the area up to 40 km, 70 km or 100 km, the percentage of the expected undamaged buildings passes to 20%, 36%, and 51% respectively; the 31%, 33%, and 29% of the buildings are expected to be in *PL*₂; the 16%, 12% and 9% of the buildings are expected to be in *PL*₃; the 8%, 5%, and 4% of the buildings are expected to be in *PL*₄, and the collapsed buildings are the 24%, 14%, and 8%.

The results computed on the 8th of April are comparable with those computed the day before because the OEF-Italy rates are very close on these two days, as shown in Figure 22. Since the rates forecasted by OEF-Italy on the 9th of April are lower, the percentage of the buildings expected to collapse decreases of with respect to the 08/04. Consequently, an increment of the expected number of undamaged buildings is observed (24%, 32%, 47% and 60% for the municipalities within 10, 40, 70 and 100km, respectively). The expected values of losses forecasted on the 10th of April are influenced by another increment of the OEF rates.

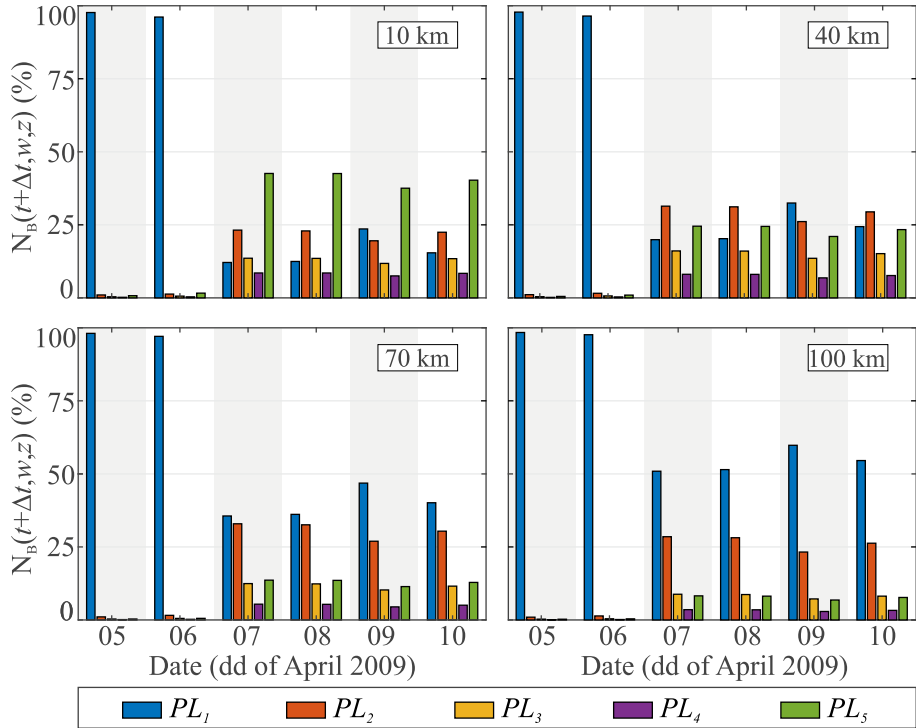


Figure 26. Outcomes of MANTIS-K system applied to 2009 L'Aquila seismic sequence.

5.5.2 MANTIS v2.0

In this section the results of MANTIS v2.0 are reported considering the same seismic sequence. In accordance with Figure 26, Figure 27 shows the expected number (in percentage) of buildings in each damage condition for the municipalities within 10, 40, 70 and 100 km from the epicentre of the mainshock. Similarly, to the already discussed results of MANTIS-K, when results refer to the rates of the 5th and the 6th of April, a few buildings are expected to collapse (about 1% in the municipalities closest to the mainshock epicentre). The results of the 7th of April depend on the considered area: the percentages of the expected undamaged buildings are 4%, 25%, 47% and 61% for the municipalities within 10 km, 40 km, 70 km and 100 km from the mainshock, respectively. Still referring to the 7th of April, the expected percentages of buildings in the intermediate *PLs* provided by MANTIS v2.0 are lower than the counterpart evaluated via MANTIS-K and the percentage of the buildings expected to collapse by MANTIS v2.0 are always larger than those evaluated by neglecting damage cumulation (76%, 42%, 22% and 13% for 10

km, 40 km, 70 km and 100 km, respectively), as expected. More specifically, the differences between the forecasted percentages of collapsed buildings according to MANTIS-K and MANTIS v2.0 are 33%, 18%, 8%, and 5% for municipalities within 10, 40, 70 and 100km. Thus, differences between results of the two systems are more significant in the epicentral areas and tend to be negligible increasing the extension of the area of interest.

Results of MANTIS v2.0 for the days from the 8th to the 10th of April, are in good accordance with those of the 7th of April.

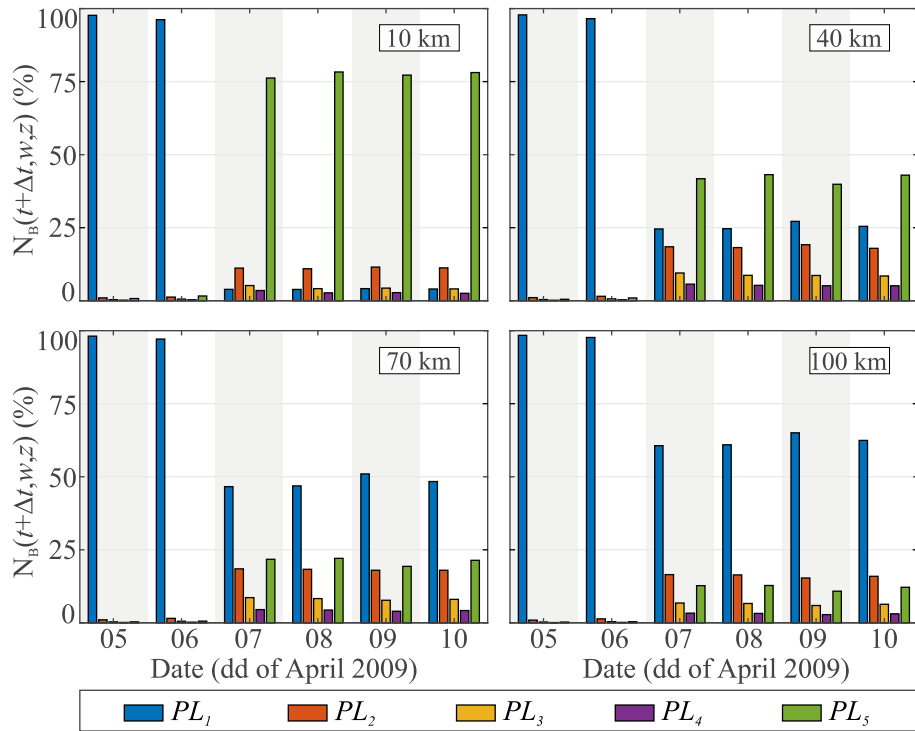


Figure 27. Outcomes of MANTIS v2.0 system applied to 2009 L'Aquila seismic sequence.

To deepen the comparison between the two version of MANTIS, Figure 28 shows the percentage number of buildings in each *PL* computed by MANTIS v2.0 in accordance with the available information about the already occurred earthquakes, i.e., by applying Eq. (30). Thus, it should be underlined that, although the format of Figure 28 is the same of Figure 26 and Figure 27, the values reported in Figure 28 are not the results of an operational forecasting; they represent the estimated damage conditions of the building portfolio that

MANTIS v2.0 adopts to compute the forecasting losses in the subsequent week. Thus, since the system does not account for structural retrofitting, the percentage numbers of collapsed buildings cannot reduce in any of the subsequent days of Figure 28.

As shown, in the municipalities closest to the epicentres of the sequence, a larger percentage of buildings is estimated to be damaged after the earthquakes occurred on 06/04: 15% of the buildings are estimated to be in PL_2 , 8% in PL_3 , 5% in PL_4 , 65% in PL_5 (i.e., collapsed), and only the 6% of the buildings result as undamaged. This implies, for example, that the value of 76% of collapsed buildings with 10km forecasted by MANTIS v2.0 on the 7th of April (see Figure 27) is obtained considering that 65% of the buildings are estimated to be already collapsed at 00:00 of the day and the remaining 11% of buildings are expected to collapse in the subsequent week. It is worth noting that the buildings expected to collapse in the same week by MANTIS-K are 43%%. This could sound counterintuitive since MANTIS-K neglect both the damage cumulation and the building portfolio update. In fact, MANTIS-K forecasted the 43% of collapsed buildings assuming that 100% are undamaged at the computation time. Two main causes can be adduced to explain the issue. Firstly, MANTIS v2.0 account that 65% of buildings are collapsed at the computation time and, consequently, only 35% of the buildings can collapse in the subsequent week; with respect to such a 35%, 11% is the expected value of collapsed buildings. On the other hand, the approximation introduced in MANTIS-K, that neglect the possibility to observe more than one earthquake in the time of forecast, makes not completely comparable the results of the two systems. Referring to the same area, the variations of the estimated collapsed buildings due to the occurred earthquakes from the 8th to the 10th of April is minor (only one M 5.4 earthquake occurred in that time interval).

Increasing the considered area, the percentage of undamaged buildings increases up to 91%, that is associated to the case of municipalities within 100km from the epicentres; thus, MANTIS v2.0 performs forecasts on an almost undamaged building portfolio, and the differences between the outcomes of MANTI-K and MANTIS v2.0 are mainly due to the possibility of damage accumulation in the subsequent week.

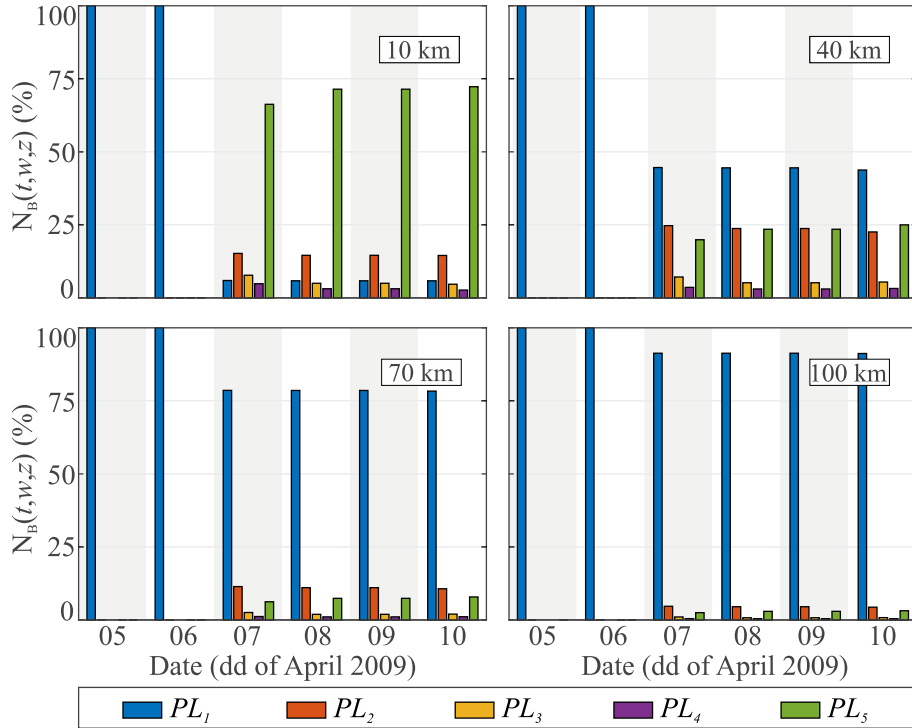


Figure 28. Building portfolio damage state at the days of prevision.

5.6. CONCLUSIONS AND DISCUSSION

MANTIS-K, an Italian system for operational earthquake loss forecasting, was formulated to convert the weekly seismic rates provided by an operational earthquake forecasting system into weekly seismic risk metrics. However, MANTIS-K, in its original formulation, is not able to account for structural damage accumulation and this limitation could lead to underestimate the forecasted losses during a seismic sequence. Thus, with the aim of upgrading the existing Italian OELF system, a new version, named MANTIS v2.0, is under-development.

Starting from the same seismic rates adopted by MANTIS-K, MANTIS v2.0 is intended to extend at the structural typologies, a methodology previously developed for single-structure reliability accounting for damage accumulation. Such a methodology is based on the hypothesis of Markovian evolution of structural seismic damage, i.e., the evolution of the damage due to an earthquake depends on the intensity of the earthquake and on the structural damage condition (i.e., performance level) when the earthquake occurs. Thus, accepting the same Markovian hypothesis, it was shown how, knowing the

fragility function and state-dependent fragility functions for structural typologies, together with the number of buildings in each structural typologies, the formulated methodology provides measures of forecasted losses accounting for two sources of damage accumulation, both neglected in MANTIS-K: (i) damaged accumulation due to the (possible) occurrence of more than one earthquake in the forecasting time-window; (ii) the structural damages produced by the earthquakes occurred before the computation time.

With respect to MANTIS-K, the methodology requires to substitute the fragility functions used in MANTIS-K with the state-dependent fragility functions. The same seismic rates and inventory models are used by both MANTIS-K and MANTIS v2.0 as input information, but MANTIS v2.0 is able to update the inventory models accounting for the available information about the occurred earthquakes.

The 2009 L'Aquila 2009 seismic swarm was retrospectively analysed by both the versions of the OELF system. The comparison of the results shows that by neglecting the possibility to have damage cumulation during a seismic swarm and the possibility to update the building portfolio according to the observed earthquake of the sequence leads to an underestimation of the forecasted losses, especially when the area of analysis is small and close to the epicentres of the sequence, i.e., it is supposed to be heavily damaged by the occurred shocks.

Chapter 6 – SUMMARY AND CONCLUSIONS

In this thesis the PBEE framework was adopted for the assessment of seismic risk at different time and space scales and with respect to different risk metrics.

In Chapter 2 and in Chapter 3 the seismic risk of single structures was evaluated in term of fatality rates, that is, the expected number of earthquakes (above the minimum magnitude of interest) to cause fatality. The analyzed structures come from an Italian research project, RINTC (*Rischio Implicito delle strutture progettate secondo NTC*) in which a large number of structures are designed according to Italian current building code (Chapter 2) or Italian historical building codes (Chapter 3). The fatality rates decrease with the development in time of the design technology, with the largest improvement due to the enforcement of the current code. Moreover, these rates were compared with those associated to some common death causes building occupants are also exposed to. Although this comparison must be done carefully due the fact that the fatality rates evaluation is influenced by computation methodology, it shows that the seismic risk tends to be lower than the others. These results may contribute to the discussion on the seismic safety achieved by current standards that can be considered acceptable and on the vision of the future of seismic codes, which is going towards risk-targeted design.

In Chapter 4, starting from the code-conforming structures of RINTC, the ideal seismic risk of Italy at municipality scale was evaluated, i.e., by assuming that all the residential buildings are replaced with code-conforming structures. For each municipality, the risk is quantified via failure rate, that is the mean number of mainshocks (or mainshock-aftershocks seismic sequences), that in one year, cause failure of a randomly selected building of the municipality of interest. Moreover, the expected number of failed buildings per municipality is chosen as risk metric too. The results show that the failure rates are largely different among different structural typologies and are strongly dependent on the seismic hazard level of the construction sites. In fact, the maps were reproduced by changing the hazard model with a more recent one (those adopted in the current code, MPS04, was substituted by the new MPS19) and by considering the occurrence of the seismic sequences (that is a neglected issue in the classical approach to the seismic hazard evaluation). The resulting maps evidence a non-homogeneous seismic risk in the country inherent to the current building code.

Finally, Chapter 5 deals with the operational earthquake loss forecasting, that provides a weekly seismic risk metrics. In fact, an Italian OELF system, MANTIS-K, already exist; This system evaluates at municipality scale (or for a larger geographic area) the expected number of buildings forecasted to be damaged in the week that follow the prevision. However MANTIS-K is not able to take into account for the possible damage cumulation the structures are subject to. Since this hypothesis could not be precautionary, especially during a seismic swarm, a new Italian OELF system, called MANTIS v2.0 is under-developing within the European RISE project. To face of with this issue, a methodology based on the Markovian modelling of the evolution of structural seismic damage was developed. Moreover, the possibility to have an already damaged building portfolio at time of forecast was implemented. The 2009 L'Aquila seismic swarm was retrospectively analysed by both the versions of the OELF system. The outcomes show that during a seismic swarm the forecasted losses result highly influenced to the damage cumulation. When it is neglected, it leads to an underestimation of the expected damages, especially in the area close to the epicenters of the sequence.

APPENDIX A

This Appendix discusses the way in which the conditional distribution of $Sa_{avg}(\mathbf{T})$ can be computed in two alternative cases (symbology of this section is in accordance with the rest of the paper). In the first case, the magnitude and the location of the earthquake are known and a GMPE providing the conditional distributions of the spectral accelerations associated to all the vibration periods collected in the vector \mathbf{T} is at hand. This case is the of interest for Section 5.4.1.1. In the second case, apart from magnitude and location of the (occurred earthquake), and the GMPE, the values of the spectral accelerations at three periods (indicated by the vector $\mathbf{T}^* = \{0, 0.3, 1\}$ s) are known. This case is related to Section 5.4.1.5.

It is assumed that the logarithms of the spectral ordinates at the site of interest, given magnitude, m^* , and distance (i.e., location), r^* , of the earthquake, are jointly Gaussian, that is, they follow a multivariate normal distribution. It follows that, conditional to magnitude and distance, $\ln Sa_{avg}(\mathbf{T})$ is also normally distributed and Eqs. (35) and (36) provide the conditional logarithmic mean, $E[\ln Sa_{avg}(\mathbf{T}) | m^*, r^*, \theta_q]$, and the variance, $Var[\ln Sa_{avg}(\mathbf{T})]$, of $\ln Sa_{avg}(\mathbf{T})$ for a given value of m^* , r^* and soil condition, θ_q :

$$\begin{aligned}
 & E[\ln Sa_{avg}(\mathbf{T}) | m^*, r^*, \theta_q] = \\
 & = \begin{bmatrix} \frac{1}{L} & \frac{1}{L} & \dots & \frac{1}{L} \end{bmatrix} \begin{bmatrix} E[\ln Sa(T_1) | m^*, r^*, \theta_q] \\ E[\ln Sa(T_2) | m^*, r^*, \theta_q] \\ \vdots \\ E[\ln Sa(T_L) | m^*, r^*, \theta_q] \end{bmatrix}, \quad (35)
 \end{aligned}$$

$$\begin{aligned}
& \text{Var}[\ln Sa_{avg}(\mathbf{T})] = \\
& = \begin{bmatrix} \frac{1}{L} & \frac{1}{L} & \cdots & \frac{1}{L} \end{bmatrix} \begin{bmatrix} (\sigma_1)^2 & \rho_{1,2} \cdot \sigma_1 \cdot \sigma_2 & \cdots & \rho_{1,L} \cdot \sigma_1 \cdot \sigma_L \\ \rho_{2,1} \cdot \sigma_2 \cdot \sigma_1 & (\sigma_2)^2 & \cdots & \rho_{2,L} \cdot \sigma_2 \cdot \sigma_L \\ \vdots & \vdots & \ddots & \vdots \\ \rho_{L,1} \cdot \sigma_L \cdot \sigma_1 & \rho_{L,2} \cdot \sigma_L \cdot \sigma_2 & \cdots & (\sigma_L)^2 \end{bmatrix} \begin{bmatrix} \frac{1}{L} \\ \frac{1}{L} \\ \vdots \\ \frac{1}{L} \end{bmatrix}. \quad (36)
\end{aligned}$$

In Eq. (35), $E[\ln Sa(T_l) | m^*, r^*, \theta_q]$ is the expected value of the logarithm of spectral acceleration at the period T_l as specified by the GMPE with $l=1, \dots, L$; in Eq. (36), $\rho_{h,l}$ is the spectral correlation coefficient between two spectral ordinates with $l=1, \dots, L$ and $h=1, \dots, L$ and it is given by [91]; σ_l is the standard deviation of $\ln Sa(T_l)$ as provided by the GMPE with $l=1, \dots, L$. Applying Eqs. (35) and (36), the $f_{IM|M,R,\theta_q}(im|m, R(x, y, w, z), \theta_q)$ distribution of Eq. (22) can be computed being $Sa_{avg}(\mathbf{T})$ the chosen IM .

Let us now consider that, according to data retrieved from the ShakeMap, the values of the spectra acceleration for three vibration periods, $\mathbf{T}^* = \{0, 0.3, 1\}$ s, are assumed as known. It is possible to evaluate the logarithm of the geometric mean of the pseudo-spectral accelerations, $\ln Sa_{avg}(\mathbf{T}^*) = \chi$. Eq. (28) requires the distribution of $Sa_{avg}(\mathbf{T})$ conditioned to the occurrence of a given value of m^* , r^* , θ_q and χ . Such a distribution is defined by its conditional mean, $E[\ln Sa_{avg}(\mathbf{T}) | \ln Sa_{avg}(\mathbf{T}^*) = \chi, m^*, r^*, \theta_q]$, and variance, $\text{VAR}[\ln Sa_{avg}(\mathbf{T}) | \ln Sa_{avg}(\mathbf{T}^*)]$, evaluated via Eqs. (37) and (38), respectively:

$$\begin{aligned}
& E[\ln Sa_{avg}(\mathbf{T}) | \ln Sa_{avg}(\mathbf{T}^*) = \chi, m^*, r^*, \theta_q] = E[\ln Sa_{avg}(\mathbf{T}) | m^*, r^*, \theta_q] + \\
& + \rho[\ln Sa_{avg}(\mathbf{T}), \ln Sa_{avg}(\mathbf{T}^*)] \cdot \frac{\sigma_{\ln Sa_{avg}(\mathbf{T})}}{\sigma_{\ln Sa_{avg}(\mathbf{T}^*)}} \cdot (\chi - E[\ln Sa_{avg}(\mathbf{T}^*) | m^*, r^*, \theta_q]) \quad (37)
\end{aligned}$$

$$\begin{aligned} & \text{VAR}[\ln Sa_{avg}(\mathbf{T}) | \ln Sa_{avg}(\mathbf{T}^*)] = \\ & = \text{VAR}[\ln Sa_{avg}(\mathbf{T}^*)] \cdot \left[1 - \left(\rho[\ln Sa_{avg}(\mathbf{T}), \ln Sa_{avg}(\mathbf{T}^*)] \right)^2 \right], \end{aligned} \quad (38)$$

where $E[\ln Sa_{avg}(\mathbf{T}^*) | m^*, r^*, \theta_q]$ and $\text{VAR}[\ln Sa_{avg}(\mathbf{T}^*)]$ can be evaluated as per Eqs. (35) and (36) by substituting the set of the periods in \mathbf{T} with those in \mathbf{T}^* , and $\rho[\ln Sa_{avg}(\mathbf{T}), \ln Sa_{avg}(\mathbf{T}^*)]$ is the correlation coefficient provided by Eq. (39):

$$\rho[\ln Sa_{avg}(\mathbf{T}), \ln Sa_{avg}(\mathbf{T}^*)] = \frac{\text{COV}[\ln Sa_{avg}(\mathbf{T}), \ln Sa_{avg}(\mathbf{T}^*)]}{\sqrt{\text{VAR}[\ln Sa_{avg}(\mathbf{T})] \cdot \text{VAR}[\ln Sa_{avg}(\mathbf{T}^*)]}}. \quad (39)$$

The numerator of Eq. (39) can be computed by Eq. (40) (see [97] for details):

$$\begin{aligned} & \text{COV}[\ln Sa_{avg}(\mathbf{T}), \ln Sa_{avg}(\mathbf{T}^*)] = \\ & = \begin{bmatrix} \frac{1}{L} & \frac{1}{L} & \dots & \frac{1}{L} \end{bmatrix} \begin{bmatrix} (\sigma_1)^2 & \rho_{1,2} \cdot \sigma_1 \cdot \sigma_2 & \rho_{1,3} \cdot \sigma_1 \cdot \sigma_3 \\ \rho_{2,1} \cdot \sigma_2 \cdot \sigma_1 & (\sigma_2)^2 & \rho_{2,3} \cdot \sigma_2 \cdot \sigma_3 \\ \vdots & \vdots & \vdots \\ \rho_{L,1} \cdot \sigma_L \cdot \sigma_1 & \rho_{L,2} \cdot \sigma_L \cdot \sigma_2 & \rho_{L,3} \cdot \sigma_L \cdot \sigma_3 \end{bmatrix} \begin{bmatrix} \frac{1}{3} \\ \frac{1}{3} \\ \frac{1}{3} \end{bmatrix}. \end{aligned} \quad (40)$$

Eqs. (37) from (40) allow computing the conditional distribution adopted in Eq. (28).

APPENDIX B

The adopted set of building-classes includes five different construction material, that is reinforced concrete (CR) in which the load resisting frame are infilled frame (LFINF), and rubble stone masonry (MUR-STRUB), clay brick masonry (MUR-CL99), dressed stone masonry (MUR-STDRE) or confined masonry (MCF) for which the load resisting frame are load bearing walls (LWAL). Masonry structures are non-ductile structures or low ductility structures (DNO and DUL respectively), while reinforced concrete structures were designed in absence of seismic design (CDN) or according to low code design level (CDL), that is, they are designed for lateral resistance using allowable stress design. For RC, the value of the lateral force coefficient, i.e., the fraction of the weight that was specified as the design lateral force in the seismic design code, can be 0, 5 or 10. Finally, the building-classes vary the number of the story (H) from 1 to 6.

For these building-classes RISE project provides the fundamental period and the linearized capacity curves in terms of displacement (δ) and base shear over the mass (F/m), as shown in the Figure 29.

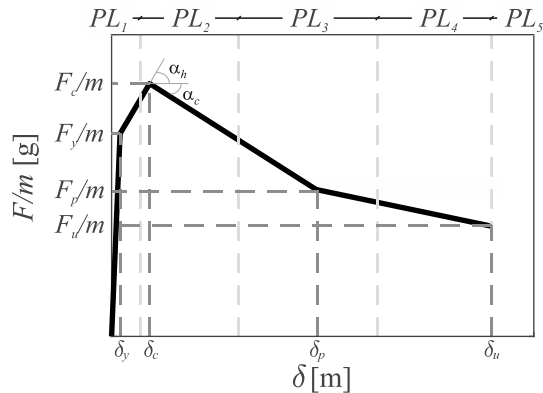


Figure 29. Example of capacity curve and definition of PLs . The subscripts y , c , p and u denote, in turn, the yielding-point, the capping-point, the residual-point and the ultimate-capacity-point.

In Table 8 the capacity curves parameters of the considered building-classes are reported. F_y and d_y are the yield base share and the yield displacement, respectively; μ_c is the capping-point ductility (i.e., the ratio between the capping-point displacement and the yielding point displacement); α_h and α_c are the hardening and the post-capping slopes, respectively; r_p is the ratio of

residual base share divided by yield base share; μ_f is the ultimate displacement capacity over the yield displacement; finally, T_y is the fundamental period.

The fragility functions and the state-dependent fragility functions (defined by the mean, η , and the standard deviation, β , of the lognormal) for each building-classes are reported in

Table 9 and Table 10, respectively.

In the tables, the taxonomy of the building-class ID is such that: i) construction material; ii) lateral load resisting frame; iii) ductility design level for the masonry structures or code design level for the reinforced concrete structures; iv) number of the stories; v) value of the lateral force coefficient expressed in percentage.

Table 8. Parameters of building-classes capacity curves.

ID building-class	F_y	δ_y	α_n	μ_c	α_c	r_p	μ_f	T_y
MUR-STRUB_ LWAL-DNO_H1	1.913	0.00030	0.18	6.71	0.00076	2.02	33.56	0.16
MUR-STRUB_ LWAL-DNO_H2	1.099	0.00060	0.14	8.40	0.00106	2.03	33.61	0.29
MUR-STRUB_ LWAL-DNO_H3	0.795	0.00089	0.15	7.85	0.00092	2.02	34.75	0.42
MUR-STRUB_ LWAL-DNO_H4	0.628	0.00119	0.14	8.40	0.00060	2.03	34.45	0.55
MUR-STRUB_ LWAL-DNO_H5	0.530	0.00149	0.14	8.06	0.00071	2.02	34.27	0.67
MUR-CL99_ LWAL-DNO_H3	0.804	0.00100	0.14	8.02	0.00094	2.02	34.10	0.44
MUR-CL99_ LWAL-DNO_H4	0.638	0.00133	0.14	8.27	0.00058	2.03	34.59	0.57
MUR-CL99_ LWAL-DNO_H5	0.540	0.00166	0.14	7.82	0.00069	2.00	34.30	0.70
MUR-STDRE_ LWAL-DNO_H4	0.667	0.00126	0.14	7.94	0.00112	2.03	34.13	0.55
MUR-STDRE_ LWAL-DNO_H5	0.559	0.00158	0.14	8.25	0.00067	2.02	34.29	0.67
MCF_LWAL- DUL_H1	4.611	0.00044	0.12	9.03	0.00073	2.02	38.37	0.12
MCF_LWAL- DUL_H2	2.305	0.00089	0.15	7.89	0.00070	2.02	38.33	0.25
MCF_LWAL- DUL_H3	1.540	0.00133	0.14	8.27	0.00087	2.02	37.59	0.37
MCF_LWAL- DUL_H4	1.158	0.00177	0.14	7.90	0.00057	2.01	37.79	0.49
MCF_LWAL- DUL_H5	0.922	0.00222	0.14	8.12	0.00071	2.02	37.89	0.62
CR_LFINF- CDN_H1_0	2.866	0.00166	0.06	5.30	-0.01781	0.67	57.52	0.15

CR_LFINF- CDN_H2_0	1.345	0.00293	0.07	4.60	-0.03034	0.82	29.29	0.29
CR_LFINF- CDN_H3_0	1.005	0.00497	0.07	4.77	-0.04592	0.85	19.73	0.44
CR_LFINF- CDN_H4_0	0.801	0.00726	0.06	4.99	-0.05877	0.88	14.82	0.60
CR_LFINF- CDN_H5_0	0.741	0.01007	0.07	4.68	-0.07305	0.91	12.23	0.73
CR_LFINF- CDN_H6_0	0.701	0.01364	0.07	4.54	-0.08767	0.93	10.31	0.88
CR_LFINF- CDL_H1_5	3.281	0.00193	0.07	4.60	-0.02577	0.70	45.96	0.15
CR_LFINF- CDL_H2_5	1.372	0.00327	0.08	4.07	-0.03492	0.79	25.42	0.31
CR_LFINF- CDL_H3_5	1.035	0.00539	0.08	3.96	-0.05687	0.79	16.43	0.45
CR_LFINF- CDL_H4_5	0.896	0.00822	0.10	3.62	-0.08606	0.84	10.88	0.60
CR_LFINF- CDL_H5_5	0.841	0.01116	0.12	3.04	-0.12993	0.84	8.11	0.72
CR_LFINF- CDL_H6_5	0.840	0.01476	0.14	2.75	-0.17942	0.87	6.19	0.83
CR_LFINF- CDL_H1_10	3.249	0.00193	0.07	4.61	-0.02495	0.70	46.47	0.15
CR_LFINF- CDL_H2_10	1.399	0.00338	0.08	4.12	-0.03683	0.79	25.72	0.31
CR_LFINF- CDL_H3_10	1.255	0.00627	0.09	3.66	-0.06469	0.80	16.40	0.44
CR_LFINF- CDL_H4_10	1.103	0.00944	0.12	3.01	-0.10194	0.82	10.58	0.58
CR_LFINF- CDL_H5_10	1.008	0.01254	0.16	2.53	-0.13685	0.80	8.87	0.70
CR_LFINF- CDL_H6_10	1.001	0.01619	0.16	2.52	-0.18343	0.85	6.19	0.80

Table 9. Parameters of fragility functions.

ID building class	Lognormal parameters	PL_2	PL_3	PL_4	PL_5
MUR- STRUB_LWAL- DNO_H1	η	-2.47	-2.04	-1.82	-1.70
	β	0.26	0.22	0.18	0.17
MUR- STRUB_LWAL- DNO_H2	η	-2.88	-2.33	-2.04	-1.85
	β	0.21	0.25	0.28	0.30
MUR- STRUB_LWAL- DNO_H3	η	-2.92	-2.27	-1.92	-1.70
	β	0.30	0.33	0.38	0.42
	η	-2.91	-2.22	-1.87	-1.66

MUR-STRUB_LWAL-DNO_H4	β	0.37	0.42	0.45	0.47
MUR-STRUB_LWAL-DNO_H5	η	-2.87	-2.17	-1.79	-1.57
	β	0.40	0.46	0.48	0.47
MUR-CL99_LWAL-DNO_H3	η	-2.86	-2.23	-1.88	-1.66
	β	0.33	0.34	0.40	0.43
MUR-CL99_LWAL-DNO_H4	η	-2.85	-2.14	-1.79	-1.58
	β	0.37	0.43	0.46	0.47
MUR-CL99_LWAL-DNO_H5	η	-2.80	-2.08	-1.71	-1.49
	β	0.41	0.46	0.47	0.48
MUR-STDRE_LWAL-DNO_H4	η	-2.87	-2.14	-1.80	-1.58
	β	0.36	0.40	0.44	0.47
MUR-STDRE_LWAL-DNO_H5	η	-2.79	-2.11	-1.74	-1.52
	β	0.41	0.46	0.47	0.47
MCF_LWAL-DUL_H1	η	-1.91	-1.52	-1.31	-1.19
	β	0.25	0.20	0.18	0.18
MCF_LWAL-DUL_H2	η	-2.23	-1.63	-1.34	-1.18
	β	0.21	0.22	0.24	0.26
MCF_LWAL-DUL_H3	η	-2.38	-1.73	-1.40	-1.18
	β	0.27	0.31	0.35	0.41
MCF_LWAL-DUL_H4	η	-2.41	-1.68	-1.31	-1.09
	β	0.34	0.38	0.43	0.46
MCF_LWAL-DUL_H5	η	-2.39	-1.64	-1.26	-1.04
	β	0.37	0.46	0.46	0.47
CR_LFINF-CDN_H1_0	η	-1.06	-0.48	-0.27	-0.12
	β	0.27	0.16	0.18	0.24
CR_LFINF-CDN_H2_0	η	-1.69	-1.04	-0.78	-0.68
	β	0.21	0.24	0.28	0.31
CR_LFINF-CDN_H3_0	η	-1.68	-1.10	-0.86	-0.78
	β	0.29	0.31	0.37	0.39
	η	-1.57	-1.12	-0.87	-0.79

CR_LFINF- CDN_H4_0	β	0.35	0.38	0.44	0.45
CR_LFINF- CDN_H5_0	η	-1.53	-1.05	-0.84	-0.76
	β	0.37	0.46	0.46	0.46
CR_LFINF- CDN_H6_0	η	-1.40	-0.99	-0.78	-0.73
	β	0.43	0.47	0.48	0.46
CR_LFINF- CDL_H1_5	η	-0.96	-0.45	-0.27	-0.11
	β	0.29	0.16	0.14	0.22
CR_LFINF- CDL_H2_5	η	-1.72	-1.05	-0.79	-0.68
	β	0.21	0.24	0.28	0.31
CR_LFINF- CDL_H3_5	η	-1.77	-1.17	-0.92	-0.84
	β	0.28	0.31	0.35	0.37
CR_LFINF- CDL_H4_5	η	-1.71	-1.24	-1.01	-0.94
	β	0.34	0.36	0.39	0.43
CR_LFINF- CDL_H5_5	η	-1.75	-1.29	-1.07	-0.98
	β	0.35	0.38	0.42	0.47
CR_LFINF- CDL_H6_5	η	-1.71	-1.28	-1.05	-1.00
	β	0.40	0.43	0.45	0.47
CR_LFINF- CDL_H1_10	η	-0.99	-0.46	-0.27	-0.10
	β	0.29	0.16	0.14	0.22
CR_LFINF- CDL_H2_10	η	-1.67	-1.03	-0.76	-0.64
	β	0.22	0.25	0.28	0.31
CR_LFINF- CDL_H3_10	η	-1.64	-1.02	-0.78	-0.65
	β	0.28	0.30	0.34	0.37
CR_LFINF- CDL_H4_10	η	-1.70	-1.12	-0.89	-0.78
	β	0.35	0.35	0.36	0.41
CR_LFINF- CDL_H5_10	η	-1.76	-1.16	-0.91	-0.78
	β	0.35	0.37	0.42	0.45
CR_LFINF- CDL_H6_10	η	-1.67	-1.19	-0.97	-0.87
	β	0.38	0.42	0.45	0.45

Table 10. Parameters of state-dependent fragility functions.

	Lognormal parameters	PL_2 PL_3	PL_2 PL_4	PL_2 PL_5	PL_3 PL_4	PL_3 PL_5	PL_4 PL_5
MUR-STRUB_LWAL-DNO_H1	η	-2.312	-1.948	-1.775	-3.168	-2.484	-3.519
	β	0.257	0.199	0.183	0.436	0.392	0.443
MUR-STRUB_LWAL-DNO_H2	η	-2.948	-2.250	-1.986	-3.321	-2.663	-3.471
	β	0.381	0.305	0.302	0.440	0.424	0.545
MUR-STRUB_LWAL-DNO_H3	η	-2.693	-2.107	-1.819	-3.125	-2.456	-3.266
	β	0.414	0.371	0.406	0.482	0.470	0.586
MUR-STRUB_LWAL-DNO_H4	η	-2.760	-2.088	-1.785	-3.038	-2.420	-3.052
	β	0.455	0.442	0.456	0.575	0.529	0.665
MUR-STRUB_LWAL-DNO_H5	η	-2.623	-1.991	-1.680	-2.915	-2.245	-2.929
	β	0.489	0.475	0.476	0.581	0.542	0.765
MUR-CL99_LWAL-DNO_H3	η	-2.709	-2.078	-1.789	-3.082	-2.415	-3.159
	β	0.440	0.388	0.418	0.485	0.484	0.575
MUR-CL99_LWAL-DNO_H4	η	-2.704	-2.012	-1.711	-2.943	-2.305	-2.986
	β	0.483	0.462	0.464	0.596	0.543	0.712
MUR-CL99_LWAL-DNO_H5	η	-2.525	-1.906	-1.588	-2.834	-2.171	-2.832
	β	0.485	0.480	0.479	0.618	0.567	0.721
MUR-STDRE_LWAL-DNO_H4	η	-2.587	-1.981	-1.690	-2.965	-2.324	-2.979
	β	0.443	0.434	0.448	0.556	0.517	0.650
MUR-STDRE_LWAL-DNO_H5	η	-2.607	-1.957	-1.637	-2.849	-2.214	-2.862
	β	0.494	0.478	0.476	0.630	0.566	0.762
MCF_LWAL-DUL_H1	η	-2.126	-1.516	-1.300	-2.736	-2.121	-2.997
	β	0.328	0.208	0.189	0.364	0.340	0.418
MCF_LWAL-DUL_H2	η	-2.025	-1.498	-1.267	-2.687	-2.022	-2.879
	β	0.273	0.255	0.265	0.422	0.434	0.559
MCF_LWAL-DUL_H3	η	-2.193	-1.586	-1.304	-2.635	-1.961	-2.767
	β	0.389	0.348	0.382	0.504	0.472	0.587
MCF_LWAL-DUL_H4	η	-2.054	-1.481	-1.191	-2.501	-1.840	-2.518
	β	0.420	0.419	0.441	0.562	0.523	0.644
MCF_LWAL-DUL_H5	η	-2.083	-1.459	-1.154	-2.407	-1.733	-2.380
	β	0.476	0.465	0.472	0.601	0.572	0.743

CR_LFINF- CDN_H1_0	η	-0.59	-0.33	-0.17	-1.28	-0.56	-1.53
	β	0.18	0.20	0.25	0.45	0.35	0.63
CR_LFINF- CDN_H2_0	η	-1.21	-0.86	-0.72	-1.81	-1.12	-1.92
	β	0.28	0.29	0.32	0.49	0.41	0.53
CR_LFINF- CDN_H3_0	η	-1.47	-1.01	-0.82	-1.90	-1.26	-2.28
	β	0.38	0.36	0.40	0.54	0.48	1.55
CR_LFINF- CDN_H4_0	η	-1.76	-1.13	-0.90	-1.99	-1.45	-2.24
	β	0.51	0.43	0.44	0.62	0.54	0.74
CR_LFINF- CDN_H5_0	η	-1.73	-1.10	-0.87	-1.96	-1.41	-2.07
	β	0.58	0.47	0.45	0.63	0.57	0.69
CR_LFINF- CDN_H6_0	η	-1.72	-1.11	-0.86	-1.91	-1.41	-2.12
	β	0.59	0.49	0.46	0.66	0.60	0.76
CR_LFINF- CDL_H1_5	η	-0.57	-0.34	-0.16	-1.34	-0.62	-1.57
	β	0.18	0.15	0.22	0.46	0.37	0.54
CR_LFINF- CDL_H2_5	η	-1.22	-0.87	-0.73	-1.87	-1.16	-2.12
	β	0.27	0.29	0.32	0.56	0.42	0.64
CR_LFINF- CDL_H3_5	η	-1.47	-1.05	-0.89	-1.95	-1.31	-2.13
	β	0.37	0.35	0.39	0.54	0.46	0.64
CR_LFINF- CDL_H4_5	η	-1.67	-1.18	-0.98	-2.06	-1.48	-2.29
	β	0.44	0.40	0.43	0.64	0.54	0.67
CR_LFINF- CDL_H5_5	η	-1.64	-1.20	-1.03	-2.04	-1.51	-2.49
	β	0.47	0.43	0.46	0.59	0.53	1.09
CR_LFINF- CDL_H6_5	η	-1.66	-1.23	-1.06	-2.01	-1.52	-2.36
	β	0.53	0.47	0.46	0.60	0.55	0.65
CR_LFINF- CDL_H1_10	η	-0.58	-0.34	-0.15	-1.32	-0.60	-1.52
	β	0.18	0.16	0.23	0.43	0.37	0.49
CR_LFINF- CDL_H2_10	η	-1.20	-0.84	-0.70	-1.80	-1.11	-2.00
	β	0.27	0.29	0.32	0.60	0.44	0.56
CR_LFINF- CDL_H3_10	η	-1.27	-0.88	-0.70	-1.79	-1.12	-1.97
	β	0.35	0.35	0.39	0.50	0.45	0.62
	η	-1.41	-1.01	-0.83	-1.85	-1.24	-1.99

CR_LFINF- CDL_H4_10	β	0.39	0.39	0.43	0.53	0.48	0.68
CR_LFINF- CDL_H5_10	η	-1.32	-0.96	-0.81	-1.86	-1.23	-2.19
	β	0.41	0.44	0.45	0.57	0.51	0.98
CR_LFINF- CDL_H6_10	η	-1.46	-1.07	-0.93	-1.89	-1.38	-2.21
	β	0.46	0.45	0.47	0.62	0.54	0.72

APPENDIX C

Figure 30 to Figure 34 report the outcomes (per municipality) of MANTIS-K system in term of percentage of buildings expected to reach PL_1 , PL_2 , PL_3 , PL_4 , and PL_4 respectively, in the week that follow the day of forecast.

Similarly, Figure 35 to Figure 38 report the results percentage of buildings expected to reach PL_1 , PL_2 , PL_3 , PL_4 , according to MANTISv2.0 system forecast. The percentage of buildings expected to collapse are represented in Figure 39.

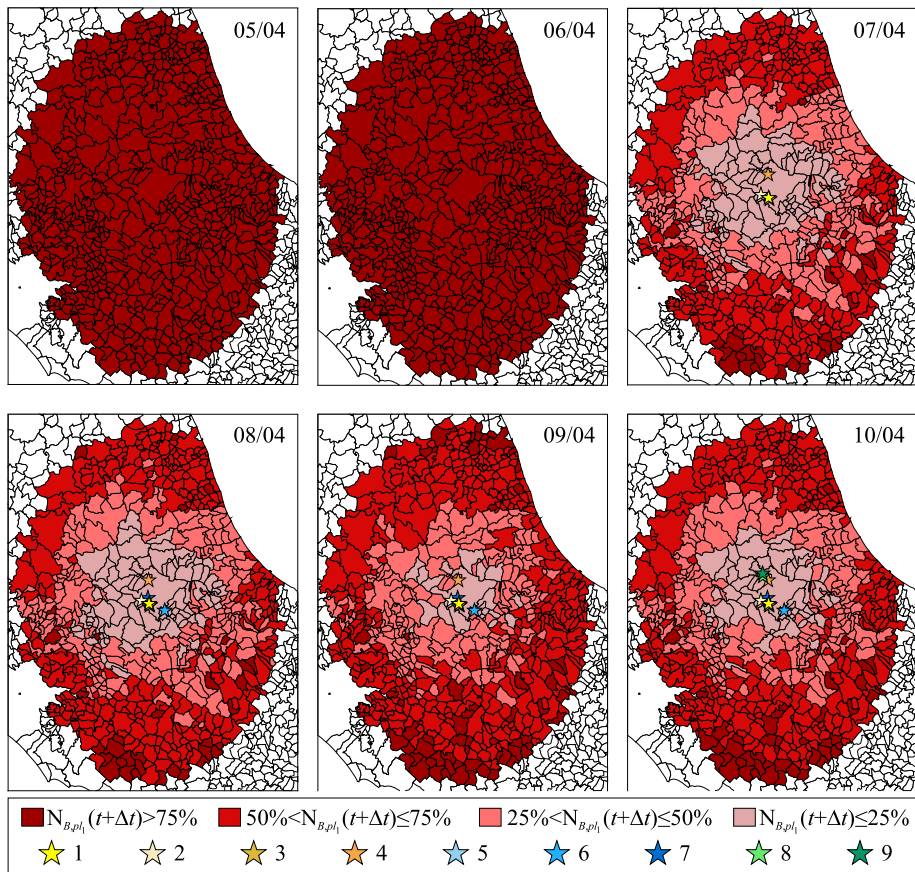


Figure 30. MANTIS K percentage of buildings expected to remain pl_1 in the week follow the day of forecast per municipality.

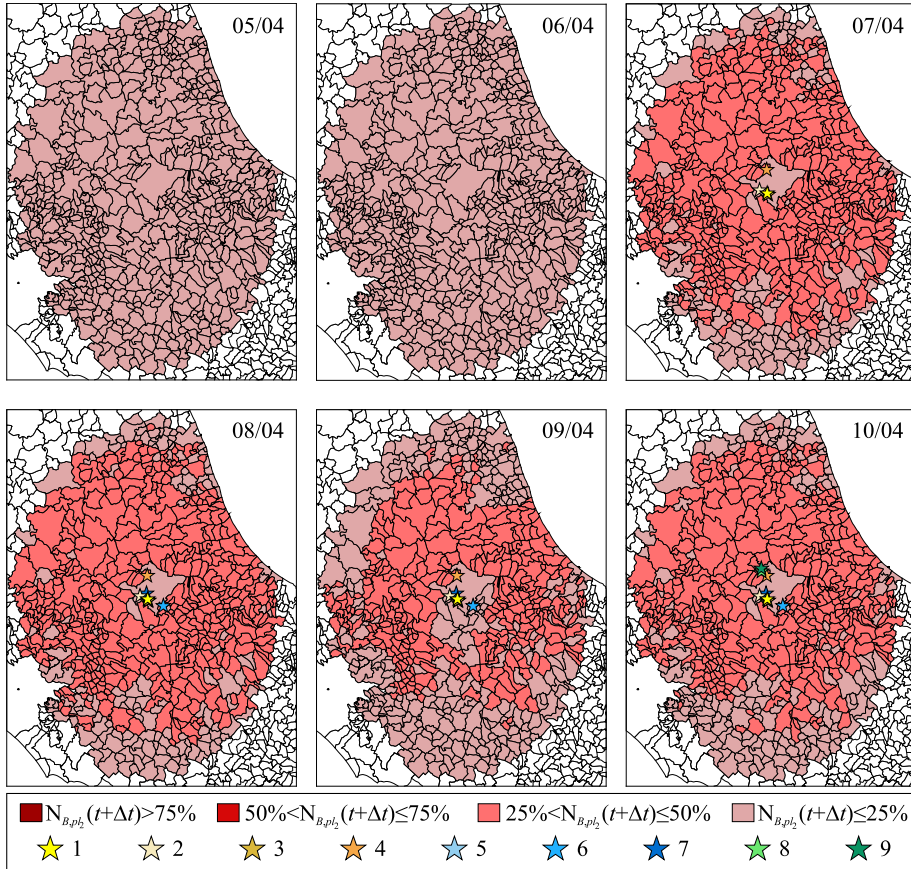


Figure 31. MANTIS-K percentage of buildings expected to reach pl_2 in the week follow the day of forecast per municipality.

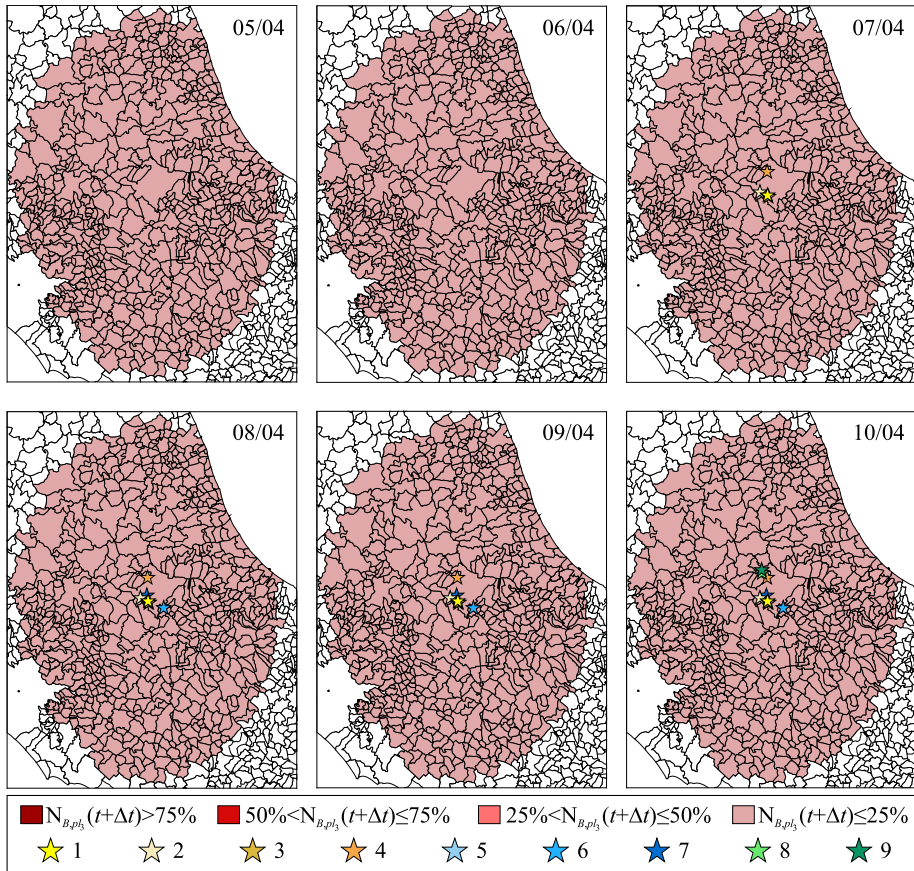


Figure 32. MANTIS K percentage of buildings expected to reach pl_3 in the week follow the day of forecast per municipality.

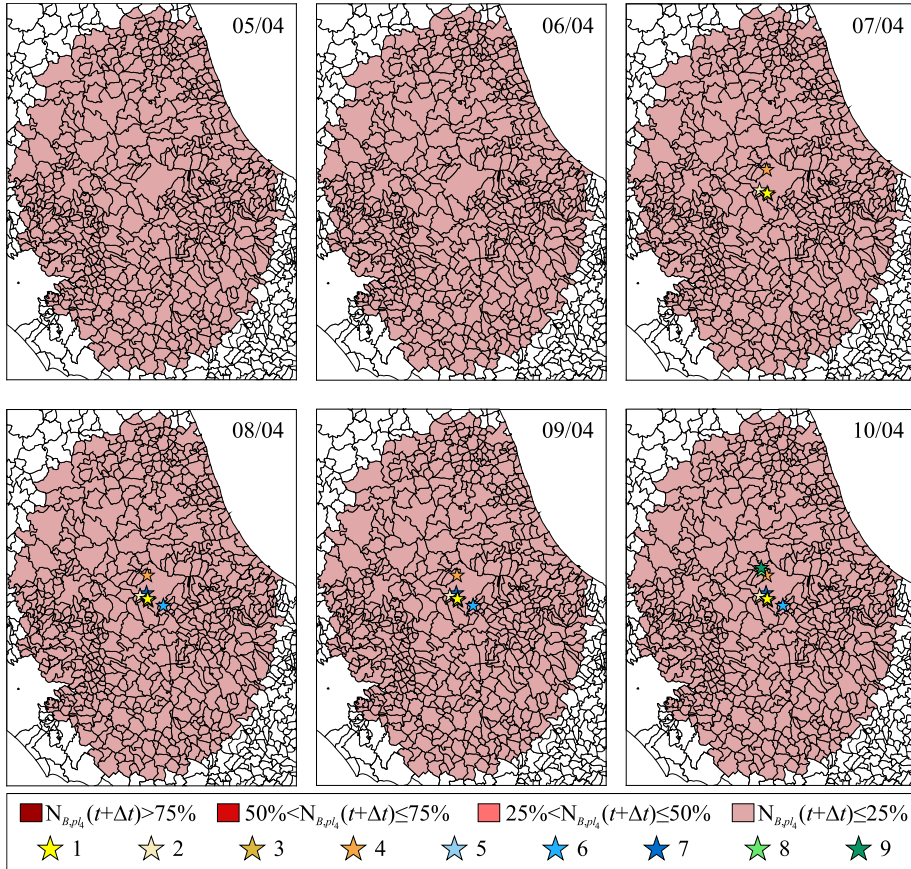


Figure 33. MANTIS K percentage of buildings expected to reach pl_4 in the week follow the day of forecast per municipality.

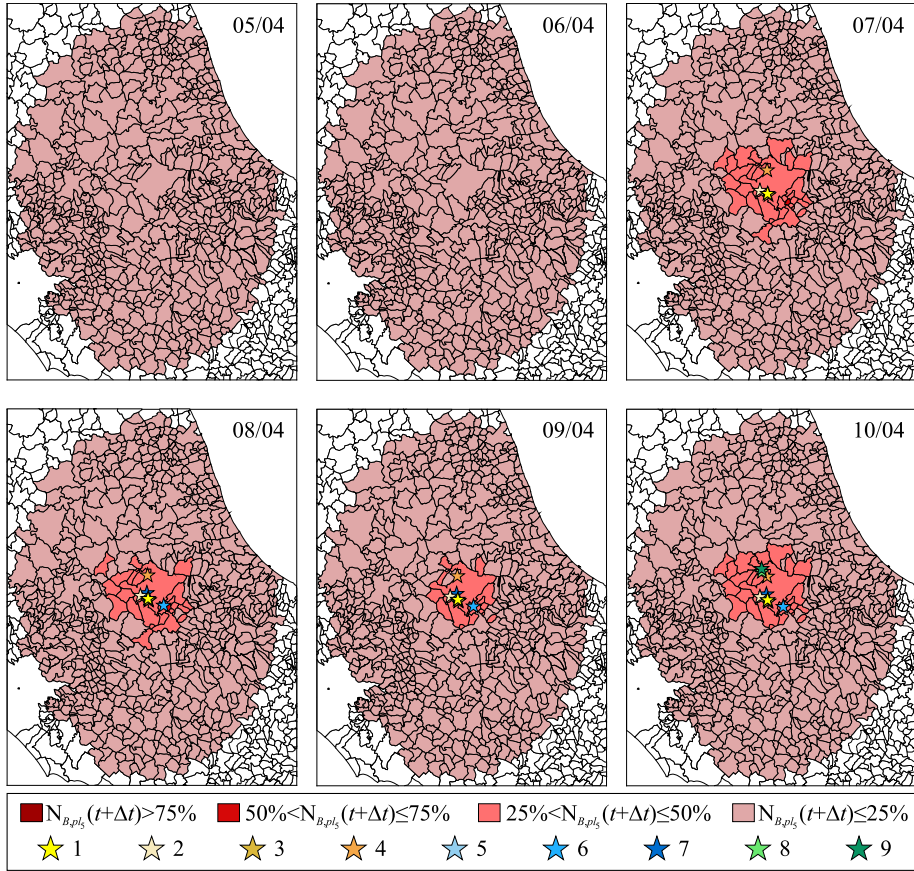


Figure 34. MANTIS K percentage of buildings expected to reach pl_5 in the week follow the day of forecast per municipality.

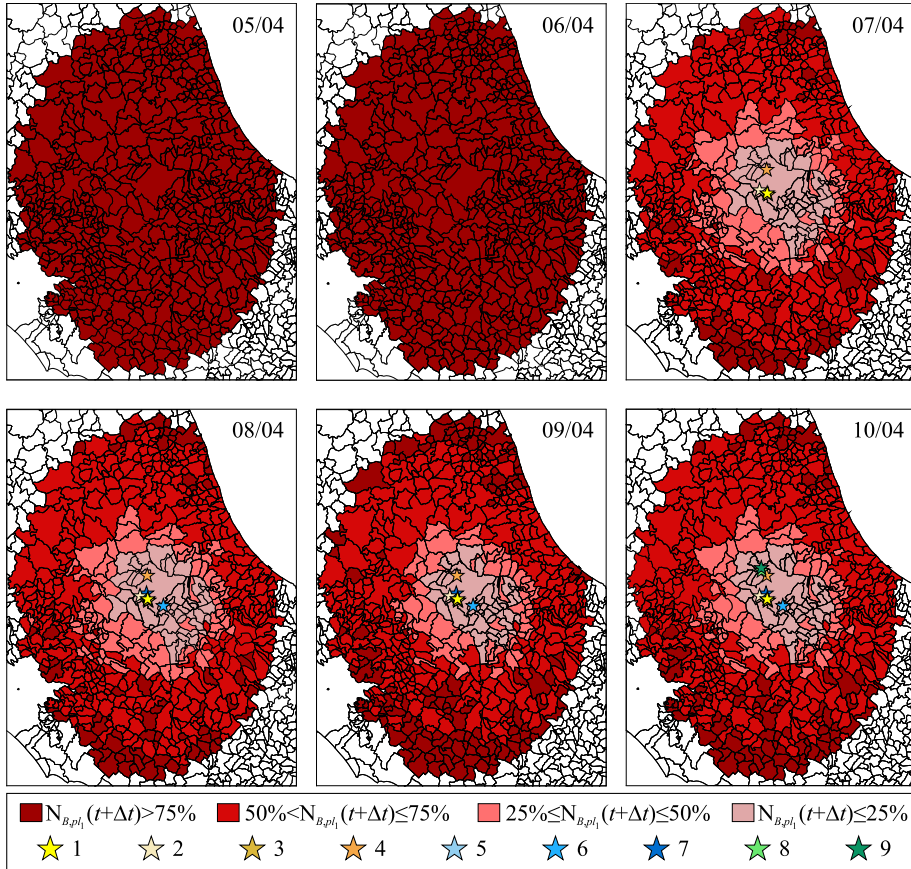


Figure 35. MANTIS V2.0 percentage of buildings expected to remain pl_1 in the week follow the day of forecast per municipality.

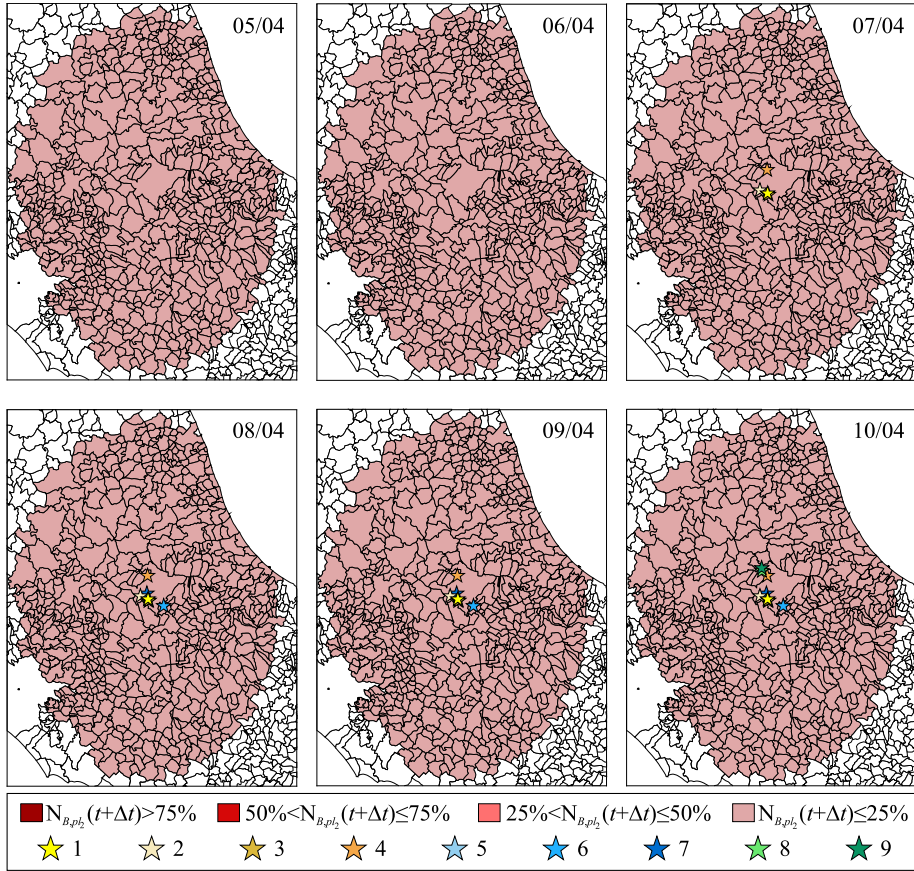


Figure 36. MANTIS V2.0 percentage of buildings expected to reach pl_2 in the week follow the day of forecast per municipality.

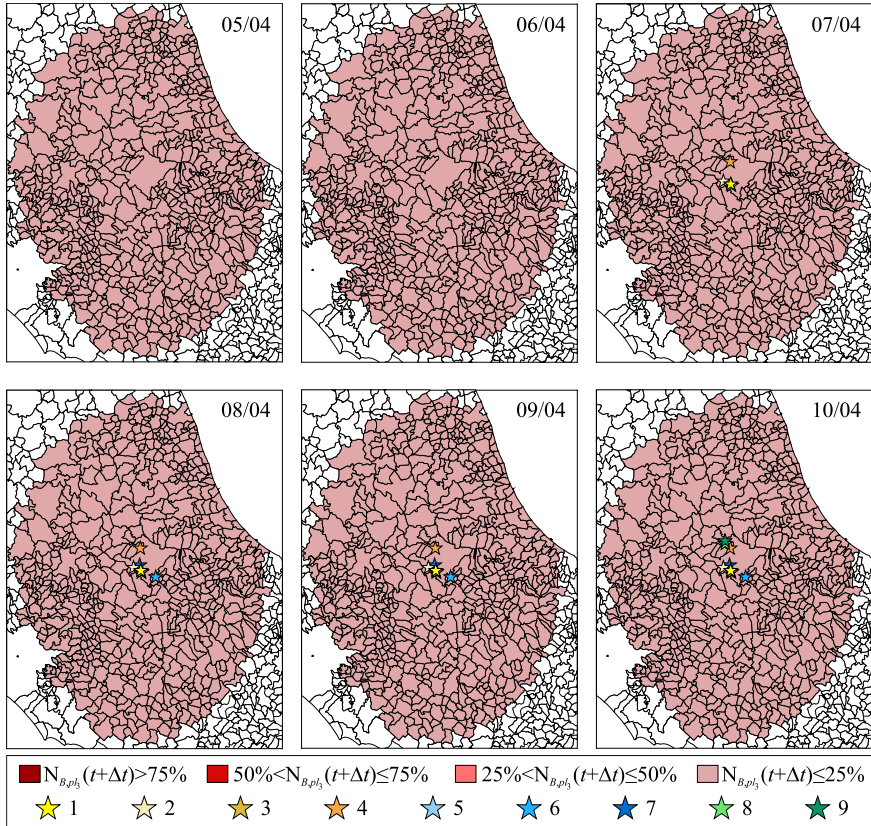


Figure 37. MANTIS V2.0 percentage of buildings expected to reach pl_3 in the week follow the day of forecast per municipality.

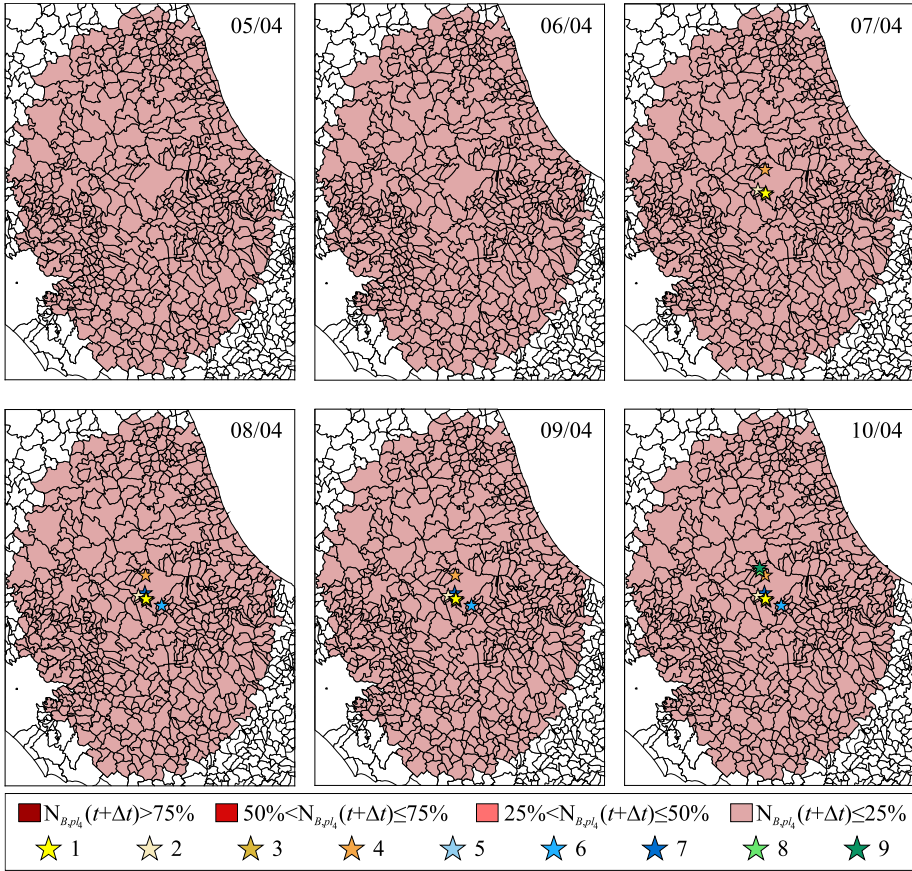


Figure 38. MANTIS V2.0 percentage of buildings expected to reach pl_4 in the week follow the day of forecast per municipality.

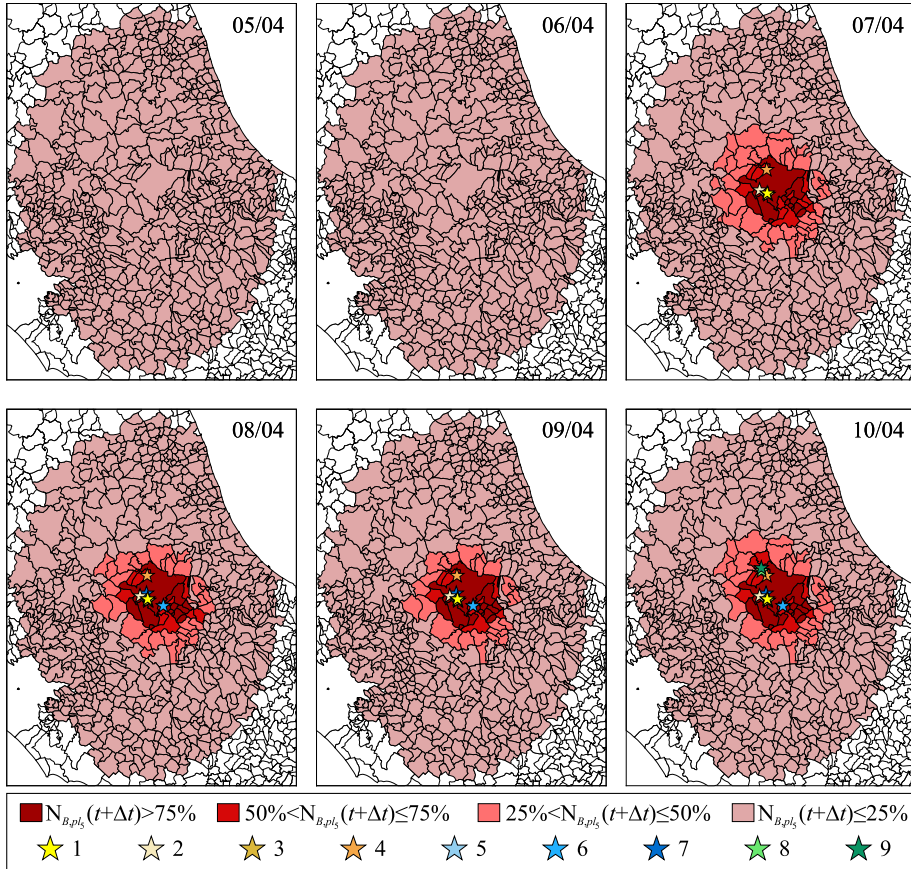


Figure 39. MANTIS V2.0 percentage of buildings expected to reach pl_5 in the week follow the day of forecast per municipality.

REFERENCES

- [1] RINTC-Workgroup. Results of the 2015-2018. The implicit risk of code-conforming structures in Italy (RINTC) project. ReLUIS Report, Rete Dei Laboratori Universitari Di Ingegneria Sismica (ReLUIS), Naples, Italy 2018:(Available at <http://www.reluis.it>).
- [2] CS.LL.PP. Norme tecniche per le costruzioni. Gazzetta Ufficiale Della Repubblica Italiana, GU 2008;29:(in Italian).
- [3] CS.LL.PP. Aggiornamento delle “Norme tecniche per le costruzioni.” Gazzetta Ufficiale Della Repubblica Italiana, GU 2018;42:(in Italian).
- [4] Iervolino I, Spillatura A, Bazzurro P. RINTC Project - Assessing the (Implicit) Seismic Risk of Code-Conforming Structures in Italy. In: Papadrakakis M, Fragiadakis M, editors. Proceedings of the 6th International Conference on Computational Methods in Structural Dynamics and Earthquake Engineering (COMPDYN 2015), 2017, p. 1545–57. <https://doi.org/10.7712/120117.5512.17282>.
- [5] Iervolino I, Spillatura A, Bazzurro P. Seismic Reliability of Code-Conforming Italian Buildings. *Journal of Earthquake Engineering* 2018;22:5–27. <https://doi.org/10.1080/13632469.2018.1540372>.
- [6] Iervolino I, Giorgio M, Cito P. The peak over the design threshold in strong earthquakes. *Bulletin of Earthquake Engineering* 2019;17:1145–61. <https://doi.org/10.1007/s10518-018-0503-9>.
- [7] Marzocchi W, Lombardi AM, Casarotti E. The establishment of an operational earthquake forecasting system in Italy. *Seismological Research Letters* 2014;85:961–9. <https://doi.org/10.1785/0220130219>.
- [8] Iervolino I, Chioccarelli E, Giorgio M, Marzocchi W, Zuccaro G, Dolce M, et al. Operational (short-term) earthquake loss forecasting in Italy. *Bulletin of the Seismological Society of America* 2015;105:2286–98. <https://doi.org/10.1785/0120140344>.
- [9] Meletti C, Galadini F, Valensise G, Stucchi M, Basili R, Barba S, et al. A seismic source zone model for the seismic hazard assessment of the Italian territory. *Tectonophysics* 2008;450:85–108. <https://doi.org/10.1016/j.tecto.2008.01.003>.

- [10] Meletti C, Marzocchi W, D’Amico V, Lanzano G, Luzi L, Martinelli F, et al. The new Italian seismic hazard model (MPS19). *Annals of Geophysics* 2021;64. <https://doi.org/10.4401/ag-8579>.
- [11] Iervolino I, Giorgio M, Polidoro B. Sequence-based probabilistic seismic hazard analysis. *Bulletin of the Seismological Society of America* 2014;104:1006–12. <https://doi.org/10.1785/0120130207>.
- [12] Iervolino I, Chioccarelli E, Suzuki A. Seismic damage accumulation in multiple mainshock-aftershock sequences. *Earthq Eng Struct Dyn* 2020;49:1007–1027. <https://doi.org/10.1002/eqe.3275>.
- [13] Romão X, Castro JM, Peirera N, Crowley H, Silva V, Martins L, et al. Project SERA. Deliverable 26.5: European physical vulnerability models. 2019.
- [14] Orlacchio M, Chioccarelli E, Baltzopoulos G, Iervolino I. State-Dependent Seismic Fragility Functions for Italian Reinforced Concrete Structures: Preliminary Results. 31th European Safety and Reliability Conference, 19-23 September 2021, Angers, France, Angers, France: 2021, p. 1591–8. https://doi.org/10.3850/978-981-18-2016-8_660-cd.
- [15] Ministero delle Infrastrutture e dei Trasporti. D.M del 17 Gennaio 2018: “Aggiornamento delle Norme tecniche per le Costruzioni.” Supplemento Ordinario Alla “Gazzetta Ufficiale,, n 42 Del 20 Febbraio 2018- Serie Generale 2018;42:1–198.
- [16] Stucchi M, Meletti C, Montaldo V, Crowley H, Calvi GM, Boschi E. Seismic hazard assessment (2003-2009) for the Italian building code. *Bulletin of the Seismological Society of America* 2011;101:1885–911. <https://doi.org/10.1785/0120100130>.
- [17] CEN EC for S. TC250/SC8/ Eurocode 8: Design Provisions for Earthquake Resistance of Structures, Part 1.1: General rules, seismic actions and rules for buildings 2004;1.
- [18] Cornell CA, Krawinkler H. Progress and Challenges in Seismic Performance Assessment. PEER Center News 2000;3:<https://apps.peer.berkeley.edu/news/2000spring/ind>.

- [19] Cito P, Iervolino I. Peak-over-threshold: Quantifying ground motion beyond design. *Earthq Eng Struct Dyn* 2020;49:458–78. <https://doi.org/10.1002/eqe.3248>.
- [20] Iervolino I, Dolce M. Foreword to the Special Issue for the RINTC (The Implicit Seismic Risk of Code-Conforming Structures) Project. *Journal of Earthquake Engineering* 2018;22:1–4. <https://doi.org/10.1080/13632469.2018.1543697>.
- [21] Manzini CF, Magenes G, Penna A, da Porto F, Camilletti D, Cattari S, et al. Masonry Italian Code-Conforming Buildings. Part 1: Case Studies and Design Methods. *Journal of Earthquake Engineering* 2018;22:54–73. <https://doi.org/10.1080/13632469.2018.1532358>.
- [22] Cattari S, Camilletti D, Lagomarsino S, Bracchi S, Rota M, Penna A. Masonry Italian Code-Conforming Buildings. Part 2: Nonlinear Modelling and Time-History Analysis. *Journal of Earthquake Engineering* 2018;22:2010–40. <https://doi.org/10.1080/13632469.2018.1541030>.
- [23] Ricci P, Manfredi V, Noto F, Terrenzi M, Petrone C, Celano F, et al. Modeling and Seismic Response Analysis of Italian Code-Conforming Reinforced Concrete Buildings. *Journal of Earthquake Engineering* 2018;22:105–39. <https://doi.org/10.1080/13632469.2018.1527733>.
- [24] Scozzese F, Terracciano G, Zona A, Della Corte G, Dall’Asta A, Landolfo R. Modeling and Seismic Response Analysis of Italian Code-Conforming Single-Storey Steel Buildings. *Journal of Earthquake Engineering* 2018;22:2104–33. <https://doi.org/10.1080/13632469.2018.1528913>.
- [25] Magliulo G, Bellotti D, Cimmino M, Nascimbene R. Modeling and Seismic Response Analysis of RC Precast Italian Code-Conforming Buildings Modeling and Seismic Response Analysis of RC Precast Italian. *Journal of Earthquake Engineering* ISSN: 2018;22:140–67. <https://doi.org/10.1080/13632469.2018.1531093>.
- [26] Cardone D, Conte N, Dall’Asta A, Di Cesare A, Flora A, Leccese G, et al. RINTC project: nonlinear analyses of Italian code-conforming base-isolated buildings for risk of collapse assessment. *Proc. of COMPDYN*

2017 – 6th ECCOMAS Thematic Conference on Computational Methods in Structural Dynamics and Earth-quake Engineering, Rhodes Island, Greece., 2017.

- [27] McGuire RK. Seismic Hazard and Risk Analysis. MNO-10. Oakland, CA: Earthquake Engineering Research Institute; 2004.
- [28] Jalayer F. Direct probabilistic seismic analysis: implementing non-linear dynamic assessments. Stanford University, 2003.
- [29] Lin T, Haselton CB, Baker JW. Conditional spectrum-based ground motion selection. Part I: Hazard consistency for risk-based assessments. *Earthq Eng Struct Dyn* 2013;42:1847–65. <https://doi.org/10.1002/eqe.2301>.
- [30] Shome N, Cornell CA. Probabilistic seismic demand analysis of nonlinear structures. Doctoral Dissertation, Stanford University, CA, 1999.
- [31] Baraschino R, Baltzopoulos G, Iervolino I. R2R-EU: Software for fragility fitting and evaluation of estimation uncertainty in seismic risk analysis. *Soil Dynamics and Earthquake Engineering* 2020;132. <https://doi.org/10.1016/j.soildyn.2020.106093>.
- [32] Chioccarelli E, Cito P, Iervolino I, Giorgio M. REASSESS V2.0: software for single- and multi-site probabilistic seismic hazard analysis. *Bulletin of Earthquake Engineering* 2019;17:1769–93. <https://doi.org/10.1007/s10518-018-00531-x>.
- [33] Stucchi M, Meletti C, Montaldo V, Crowley H, Calvi GM, Boschi E. Seismic Hazard Assessment (2003 – 2009) for the Italian Building Code. *Bulletin of the Seismological Society of America* 2011;101:1885–911. <https://doi.org/10.1785/0120100130>.
- [34] Tsang HH, Wenzel F. Setting structural safety requirement for controlling earthquake mortality risk. *Saf Sci* 2016;86:174–83. <https://doi.org/10.1016/j.ssci.2016.02.028>.
- [35] Kircher CA, Whitman R V., Holmes WT. HAZUS Earthquake Loss Estimation Methods. *Nat Hazards Rev* 2006;7:45–59. [https://doi.org/10.1061/\(asce\)1527-6988\(2006\)7:2\(45\)](https://doi.org/10.1061/(asce)1527-6988(2006)7:2(45)).

- [36] Zuccaro G, Cacace F. Seismic casualty evaluation: The Italian model, an application to the L'Aquila 2009 event. In: Spence R, So E, Scawthorn C, editors. *Human Casualties in Earthquakes: Progress in Modelling and Mitigation*, Springer, London, United Kingdom; 2011.
- [37] Grünthal G. *European Macroseismic Scale 1998*. vol. 15. 1998.
- [38] CEN. EN 1998-1: Eurocode 8 - Design of structures for earthquake resistance. Part 1: General rules, seismic actions and rules for buildings. European Committee for Standardization; 2004.
- [39] Petruzzelli F, Iervolino I. NODE: a large-scale seismic risk prioritization tool for Italy based on nominal structural performance. *Bulletin of Earthquake Engineering* 2021;19:2763–96. <https://doi.org/10.1007/s10518-021-01093-1>.
- [40] Iervolino I, Baraschino R, Spillatura A, Pacifico A. Evolution of seismic reliability of code-conforming Italian buildings. *Journal of Earthquake Engineering* n.d.:(submitted for publication).
- [41] Iervolino I, Pacifico A. Fatality rates implied by the Italian building code. *Earthq Eng Struct Dyn* 2021;50:3083–9. <https://doi.org/10.1002/eqe.3472>.
- [42] Penna A, Rota M, Bracchi S, Angiolilli M, Cattari S, Lagomarsino S. Modelling and seismic response analysis of existing URM structures. Part 1: modern buildings. *Journal of Earthquake Engineering* 2021:(in review).
- [43] Lagomarsino S, Cattari S, Angiolilli M, Bracchi S, Rota M, Penna A. Modeling and seismic response analysis of existing URM structures. Part 2: historical buildings. *Journal of Earthquake Engineering* 2021:(in review).
- [44] de Risi MT, di Domenico M, Terrenzi M, Camata G, Mollaioli F, Noto F, et al. Modelling and seismic response analysis of pre-code and low-code reinforced concrete buildings in Italy. Part I: bare frames. *Journal of Earthquake Engineering* 2021:(in review).
- [45] Bosio M, di Salvatore C, Bellotti D, Capacci L, Belleri A, Piccolo V, et al. Modelling and seismic response analysis of non-residential single-

- storey existing precast buildings in Italy. *Journal of Earthquake Engineering* 2021:(in review).
- [46] Cantisani G, della Corte G. Modelling and seismic response analysis of non-residential existing steel buildings in Italy. *Journal of Earthquake Engineering* 2021:(in review).
- [47] Jalayer F, Cornell CA. Alternative non-linear demand estimation methods for probability-based seismic assessments. *Earthq Eng Struct Dyn* 2009;38:951–72. <https://doi.org/10.1002/eqe.876>.
- [48] Spillatura A, Kohrangi M, Bazzurro P, Vamvatsikos D. Conditional spectrum record selection faithful to causative earthquake parameter distributions. *Earthq Eng Struct Dyn* 2021. <https://doi.org/10.1002/eqe.3465>.
- [49] Iervolino I, Baraschino R, Cardone D, Della Corte G, Lagomarsino S, Penna A, et al. Seismic fragility of Italian code-conforming buildings by multi-stripe dynamic analysis of three-dimensional structural models. *Journal of Earthquake Engineering* 2021:(in review).
- [50] FEMA. Multi-hazard Loss Estimation Methodology: Earthquake Model: HAZUS MR4, technical manual. 2004.
- [51] Grünthal G. European Macroseismic Scale. *Cahiers Du Centre Européen de Géodynamique et de Séismologie* 1998;15.
- [52] Task Group 3.1. *fib Bulletin* 80. 2016.
- [53] Steenbergen RDJM, Vrouwenvelder ACWM. Safety philosophy for existing structures and partial factors for traffic loads on bridges. *Heron* 2010;55:123–40.
- [54] CEN. EN 1998-2 - Eurocode 8: Design of structures for earthquake resistance - Part 2: Bridges. European Committee for Standardization, Rue de Stassart, 36 B-1050 Brussels: 2005.
- [55] Di Pasquale G, Fralleone A, Pizza AG, Serra C. Relevant changes to the Italian seismic Code from 1909 to 1975 – a synoptic table. *La Classificazione e La Normative Sismica Italiana Dal 1909 al 1984, De*

- Marco, R and Martini, MG, Istituto Poligrafico e Zecca Dello Stato, Roma 1999:(in Italian).
- [56] Di Pasquale G, Fralleone A, Pizza AGS, Serra C. Synthesis of the code evolution from the Royal decree issued after the Messina and Reggio earthquake up to the first Ministry decree issued after the law n.64/74. *La Classificazione e La Normative Sismica Italiana Dal 1909 al 1984*, De Marco, R and Martini, MG, Istituto Poligrafico e Zecca Dello Stato, Roma 1999:(in Italian).
- [57] OPCM 3274. Primi elementi in materia di criteri generali per la classificazione sismica del territorio nazionale e di normative tecniche per le costruzioni in zona sismica. *Gazzetta Ufficiale Della Repubblica Italiana*, GU 2003;105:(in Italian).
- [58] Corbane C, Hancilar U, Ehrlich D, De Groeve T. Pan-European Seismic Risk Assessment: A Proof of Concept Using the Earthquake Loss Estimation Routine (ELER). *Bulletin of Earthquake Engineering* 2017;15:1057–83. <https://doi.org/https://doi.org/10.1007/s10518-016-9993-5>.
- [59] Crowley H, Colombi M, Borzi B, Faravelli M, Onida M, Lopez M, et al. A comparison of seismic risk maps for Italy. *Bulletin of Earthquake Engineering* 2009;7:149–80. <https://doi.org/10.1007/s10518-008-9100-7>.
- [60] Crowley H, Despotaki V, Silva V, Dabbeek J, Romão X, Pereira N, et al. Model of Seismic Design Lateral Force Levels for the Existing Reinforced Concrete European Building Stock. *Bulletin of Earthquake Engineering* 2021;19:2839–2865. <https://doi.org/https://doi.org/10.1007/s10518-021-01083-3>.
- [61] Dolce M, Prota A, Borzi B, da Porto F, Lagomarsino S, Magenes G, et al. Seismic risk assessment of residential buildings in Italy. vol. 19. Springer Netherlands; 2021. <https://doi.org/10.1007/s10518-020-01009-5>.
- [62] Stucchi M, Meletti C, Montaldo V, Crowley H, Calvi GM, Boschi E. Seismic hazard assessment (2003-2009) for the Italian building code.

- Bulletin of the Seismological Society of America 2011;101:1885–911.
<https://doi.org/10.1785/0120100130>.
- [63] Iervolino I, Chioccarelli E, Giorgio M. Aftershocks’ effect on structural design actions in Italy. Bulletin of the Seismological Society of America 2018;108:2209–20. <https://doi.org/10.1785/0120170339>.
- [64] Suzuki A, Iervolino I. Seismic Fragility of Code-conforming Italian Buildings Based on SDoF Approximation. Journal of Earthquake Engineering 2019. <https://doi.org/10.1080/13632469.2019.1657989>.
- [65] Jalayer F, Cornell CA. Measuring bias in structural response caused by ground motion scaling. Earthq Eng Struct Dyn 2009;38:951–72. <https://doi.org/10.1002/eqe.876>.
- [66] Iervolino I. Assessing uncertainty in estimation of seismic response for PBEE. Earthq Eng Struct Dyn 2017;46:1711–23. <https://doi.org/10.1002/eqe.2883>.
- [67] Ragni L, Cardone D, Conte N, Dall’Asta A, Di Cesare A, Flora A, et al. Modelling and Seismic Response Analysis of Italian Code-Conforming Base-Isolated Buildings. Journal of Earthquake Engineering 2018;22:198–230. <https://doi.org/10.1080/13632469.2018.1527263>.
- [68] Ambraseys NN, Simpson KA, Bommer JJ. Prediction of horizontal response spectra in Europe. Earthq Eng Struct Dyn 1996;25:371–400. [https://doi.org/10.1002/\(SICI\)1096-9845\(199604\)25:4<371::AID-EQE550>3.0.CO;2-A](https://doi.org/10.1002/(SICI)1096-9845(199604)25:4<371::AID-EQE550>3.0.CO;2-A).
- [69] Akkar S, Bommer JJ. Empirical equations for the prediction of PGA, PGV, and spectral accelerations in Europe, the mediterranean region, and the Middle East. Seismological Research Letters 2010;81:195–206. <https://doi.org/10.1785/gssrl.81.2.195>.
- [70] Chioccarelli E, Cito P, Iervolino I, Giorgio M. REASSESS V2.0: software for single- and multi-site probabilistic seismic hazard analysis. Bulletin of Earthquake Engineering 2019;17:1769–93. <https://doi.org/10.1007/s10518-018-00531-x>.
- [71] Borzi B, Onida M, Faravelli M, Polli D, Pagano M, Quaroni D, et al. IRMA platform for the calculation of damages and risks of Italian

- residential buildings. *Bulletin of Earthquake Engineering* 2020. <https://doi.org/10.1007/s10518-020-00924-x>.
- [72] Forte G, Chioccarelli E, de Falco M, Cito P, Santo A, Iervolino I. Seismic soil classification of Italy based on surface geology and shear-wave velocity measurements. *Soil Dynamics and Earthquake Engineering* 2019;122:79–93. <https://doi.org/10.1016/j.soildyn.2019.04.002>.
- [73] Chioccarelli E, Pacifico A, Iervolino I. Italian seismic risk maps based on code-compliant design. 31th European Safety and Reliability Conference, 19-23 September 2021, Angers, France, Angers, France: 2021. https://doi.org/10.3850/978-981-18-2016-8_678-cd.
- [74] Chioccarelli E, Cito P, Visini F, Iervolino I. Sequence-based hazard analysis for Italy considering a grid seismic source model. *Annals of Geophysics* 2021;64:1–12. <https://doi.org/10.4401/ag-8586>.
- [75] Bindi D, Pacor F, Luzi L, Puglia R, Massa M, Ameri G, et al. Ground motion prediction equations derived from the Italian strong motion database. *Bulletin of Earthquake Engineering* 2011;9:1899–920. <https://doi.org/10.1007/s10518-011-9313-z>.
- [76] Beyer K, Bommer JJ. Relationship between Median Values and between Aleatory Variabilities for Different Definitions of the Horizontal Component of Motion. *Bulletin of the Seismological Society of America* 2006;96:1512–22. <https://doi.org/10.1785/0120050210>.
- [77] Crowley H, Colombi M, Borzi B, Faravelli M, Onida M, Lopez M, et al. A comparison of seismic risk maps for Italy. *Bulletin of Earthquake Engineering* 2009;7:149–80. <https://doi.org/10.1007/s10518-008-9100-7>.
- [78] Dolce M, Prota A, Borzi B, da Porto F, Lagomarsino S, Magenes G, et al. Seismic risk assessment of residential buildings in Italy. vol. 19. Springer Netherlands; 2021. <https://doi.org/10.1007/s10518-020-01009-5>.
- [79] Kitayama S, Constantinou MC. Collapse performance of seismically isolated buildings designed by the procedures of ASCE/SEI 7. *Eng*

Struct 2018;164:243–58.
<https://doi.org/10.1016/j.engstruct.2018.03.008>.

- [80] Cardone D, Perrone G, Piesco V. Developing collapse fragility curves for base-isolated buildings. *Earthq Eng Struct Dyn* 2019;48:78–102. <https://doi.org/10.1002/eqe.3126>.
- [81] Jordan TH, Chen YT, Gasparini P, Madariaga R, Main I, Marzocchi W, et al. Operational earthquake forecasting: State of knowledge and guidelines for utilization. *Annals of Geophysics* 2011;54:319–91. <https://doi.org/10.4401/ag-5350>.
- [82] Wang K, Rogers GC. Earthquake preparedness should not fluctuate on a daily or weekly basis. *Seismological Research Letters* 2014;85:569–571. <https://doi.org/https://doi.org/10.1785/0220130195>.
- [83] Chioccarelli E, Iervolino I. Comparing short-term seismic and COVID-19 fatality risks in Italy. *Seismological Research Letters* 2021;92:2382–8. <https://doi.org/10.1785/0220200368>.
- [84] Marzocchi W, Lombardi AM, Casarotti E. The establishment of an operational earthquake forecasting system in Italy. *Seismological Research Letters* 2014;85:961–9. <https://doi.org/10.1785/0220130219>.
- [85] Marzocchi W, Lombardi AM. Real-time forecasting following a damaging earthquake. *Geophys Res Lett* 2009;36:1–5. <https://doi.org/10.1029/2009GL040233>.
- [86] Iervolino I, Giorgio M, Chioccarelli E. Markovian modeling of seismic damage accumulation. *Earthq Eng Struct Dyn* 2016;45:441–61. <https://doi.org/10.1002/eqe.2668>.
- [87] Wald DJ, Quitoriano V, Heaton TH, Kanamori H, Scrivner CW, Worden CB. TriNet “ShakeMaps”: Rapid generation of peak ground motion and intensity maps for earthquakes in southern California. *Earthquake Spectra* 1999;15:537–54. <https://doi.org/10.1193/1.1586057>.
- [88] Worden CB, Thompson EM, Hearne M, Wald DJ. ShakeMap Manual Online: Technical Manual, User’s Guide, and Software Guide, 2020. <https://doi.org/10.5066/F7D21VPQ>.

- [89] Chioccarelli E, Iervolino I. Near-source seismic demand and pulse-like records: A discussion for L'Aquila earthquake. *Earthq Eng Struct Dyn* 2010;39:1039–62. <https://doi.org/10.1002/eqe>.
- [90] Gutenberg B, Richter CF. Frequency of earthquakes in California. *Bulletin of the Seismological Society of America* 1944;34:185–8. <https://doi.org/10.1785/bssa0340040185>.
- [91] Baker JW, Jayaram N. Correlation of spectral acceleration values from NGA ground motion models. *Earthquake Spectra* 2008;24:299–317. <https://doi.org/10.1193/1.2857544>.
- [92] Baker JW, Cornell CA. Spectral shape, epsilon and record selection. *Earthq Eng Struct Dyn* 2006;35:1077–95. <https://doi.org/10.1002/eqe.571>.
- [93] Villar-Vega M, Silva V, Eeri M, Crowley H, Catalina Y. Assessment of earthquake damage considering the characteristics of past events in South America. *Soil Dynamics and Earthquake Engineering* 2017;99:86–96. <https://doi.org/10.1016/j.soildyn.2017.05.004>.
- [94] Lagomarsino S, Giovinazzi S. Macroseismic and mechanical models for the vulnerability and damage assessment of current buildings. *Bulletin of Earthquake Engineering* 2006;4:415–43. <https://doi.org/10.1007/s10518-006-9024-z>.
- [95] Pacifico A, Chioccarelli E, Iervolino I. Residential code-conforming structural seismic risk maps for Italy. *Soil Dynamics and Earthquake Engineering* 2022;153:1–13. <https://doi.org/10.1016/j.soildyn.2021.107104>.
- [96] Marzocchi W, Iervolino I, Giorgio M, Falcone G. When is the probability of a large Earthquake too small? *Seismological Research Letters* 2015;86:1674–8. <https://doi.org/10.1785/0220150129>.
- [97] Iervolino I. *Dinamica delle strutture e ingegneria sismica. Principi e applicazioni*. Hoepli; 2021.